Schweizerische Eidgenossenschaft
Confédération suisse
Confederazione Svizzera
Confederaziun svizra

Federal Department of the Environment, Transport, Energy and Communications DETEC

Swiss Federal Office of Energy SFOE
Energy Research and Cleantech Division

Final report dated 15 March 2023

Monitored pilot test of an innovative single-end fault locator named CH-7000, based on the electromagnetic time-reversed theory.

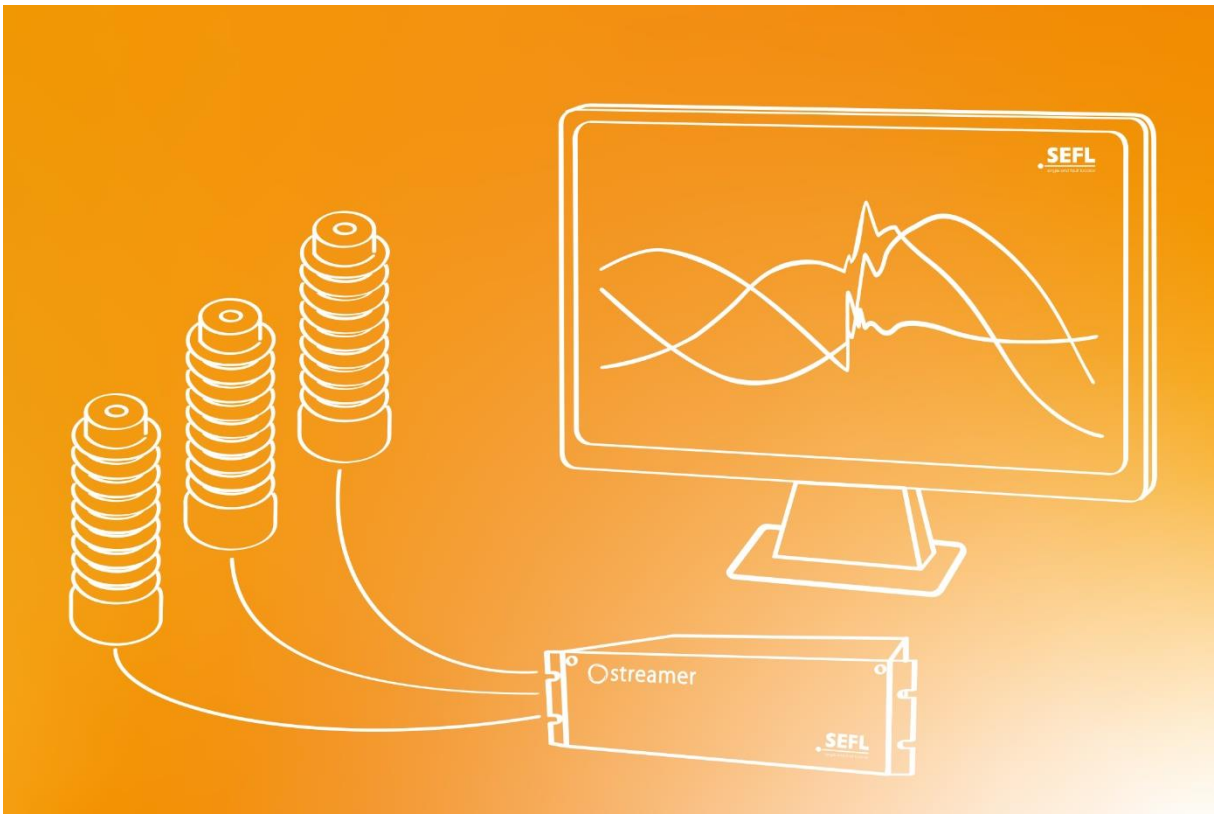

Source: Streamer Electric AG

Date: 15 March 2023

Location: Bern

Publisher:
Swiss Federal Office of Energy SFOE
Energy Research and Cleantech
CH-3003 Bern
www.bfe.admin.ch

Subsidy recipients:

Streamer Electric AG
Masanserstrasse 4, CH-7000, Chur
www.streamer-electric.com

Ecole Polytechnique Fédérale de Lausanne
EPFL-SCI-STI-FR, Station 11, 1015 Lausanne
www.epfl.ch

Groupe E AG
Route de Morat 135, 1763 Granges-Paccot
www.groupe-e.ch

Authors:
Polina Gonina, Streamer Electric AG, polina.gonina@streamer-electric.com
Dmitriy Belko, Streamer Electric AG, dmitry.belko@streamer-electric.com
Farhad Rachidi, Ecole Polytechnique Fédérale de Lausanne, farhad.rachidi@epfl.ch
Yves Fritsché, Groupe E AG, yves.fritsche@groupe-e.ch

SFOE project coordinators:
Dr. Karin Söderström, karin.soederstroem@bfe.admin.ch
Dr. Michael Moser, michael.moser@bfe.admin.ch

SFOE contract number: SI/502059-01

Zusammenfassung

Das Projekt befasst sich mit der Entwicklung und Pilotierung eines neuartigen Fehlerorters für elektrische Verteilnetze bis 38 kV. Das Gerät nutzt einen einzigen Messpunkt und eignet sich für Netze mit verteilten Erzeugungseinheiten aus erneuerbaren Quellen. Ziel des Projekts ist es, den bestehenden Prototypen durch die Entwicklung intelligenter Funktionen zu verbessern, um seine Integration in die modernen und digitalen Umspannwerke zu ermöglichen.

Im Rahmen des Projekts wurde die Funktionalität der Software deutlich verbessert. Die Fehlerorter-Software wurde um die komplexere Version mit neuen intelligenten Funktionen erweitert. Jetzt ist der Fehlerorter in ein modernes Umspannwerk integriert, erkennt das Vorhandensein des Fehlers und klassifiziert die auf der Leitung auftretenden Ereignisse: Störungen, Phase-Erde-Fehler, Kurzschlussfehler. Wichtig sowohl für das System als auch für das Versorgungsunternehmen, wo es installiert ist – die Fehlerortungsergebnisse werden in ihr SCADA-System integriert, und der Fehlerorter erhält den Schaltstatus von SCADA, um die tatsächliche Netzwerkmodellkonfiguration zu aktualisieren. Für den Austausch der Leitungsdaten wurde die Anbindung an die Cloud-Datenbank des Versorgers mit Netzparametern entwickelt. Darüber hinaus wurde die Systemarchitektur während des Projekts geändert: Zwei Einheiten des Systems (Erfassungs- und Ausarbeitungseinheiten) wurden auf zwei verschiedene Standorte aufgeteilt und über das Internet verbunden.

Die Leistungsfähigkeit der Entwicklung wurde in einer Monitoringphase untersucht und anhand von Feldversuchen an einem Verteilnetz in der Region Freiburg evaluiert. Der Pilottest wurde durchgeführt, um die Fähigkeit des Geräts zu bewerten, Fehler (verschraubte und ohmsche Leiter-Erde-Fehler) zu lokalisieren. Betrachtet wurde ein Netz im Raum Fribourg mit drei Abgängen, die von der gleichen Primärunterstation versorgt werden. Für jede Zuleitung wurde eine Fehlerstelle ausgewählt und es wurden zwei Arten von Fehlern gemacht, einer mit und einer ohne Widerstand, die jeweils 2 Sekunden dauerten.

Die Art von Fehlern, die künstlich auf der überwachten Leitung erzeugt wurden, d. h. Phase-Erde mit kleinem Fehlerstrom zur Erde, wird mit instabiler Genauigkeit identifiziert. Als vielversprechender Ansatz für mehr Stabilität erwies sich die Methode, das mathematische Modell der Leitung zu kalibrieren, das im Fehlerortungsalgorithmus verwendet wird. Im Rahmen des Projekts wurde der zusätzliche Pilotversuch an einem realen Mittelspannungsnetz konzipiert, der die Einspeisung eines Spannungspulses auf die Leitung zur Weiterverarbeitung der erfassten Daten im Leitungsmodell beinhaltete.

Résumé

Le projet porte sur le développement et les essais pilotes d'un nouveau localisateur de défauts pour les réseaux de distribution électrique jusqu'à 38 kV. L'appareil utilise un seul point de mesure et convient aux réseaux avec des unités de production décentralisées à partir de sources renouvelables. L'objectif du projet est d'améliorer le prototype existant en développant des fonctions intelligentes pour permettre son intégration dans les sous-stations électriques modernes et numériques.

Dans le cadre du projet, la fonctionnalité du logiciel a été considérablement améliorée. Le logiciel de localisation des défauts s'est étendu à la version, qui est plus complexe avec de nouvelles fonctionnalités intelligentes. Désormais, le localisateur de défauts est intégré dans une sous-station électrique moderne, détectant la présence du défaut et classant les événements survenant sur la ligne : perturbations, défauts phase-terre, défauts de court-circuit. Important à la fois pour le système et l'utilitaire, là où il est installé - les résultats de localisation des défauts sont intégrés dans leur système SCADA ainsi que l'état du commutateur du SCADA est reçu par le localisateur de défauts pour mettre à jour la configuration réelle du modèle de réseau. La connexion à la base de données cloud de l'utilitaire contenant les paramètres réseau a été développée afin d'échanger les données de la ligne. De plus, l'architecture du système a été modifiée au cours du projet : deux unités du système (unités d'acquisition et d'élaboration) ont été réparties sur deux sites différents et connectées via Internet.

Les performances du développement ont été examinées lors d'une phase de monitoring et évaluées grâce à des tests de terrain sur un réseau de distribution dans la région de Fribourg. Le test pilote a été réalisé pour évaluer la capacité de l'appareil à localiser les défauts (défauts ligne-terre boulonnés et résistifs). Un réseau dans la région de Fribourg avec trois départs alimentés par le même poste primaire a été considéré. Pour chaque départ, une localisation de défaut a été sélectionnée, et deux types de défauts ont été réalisés, un avec et un sans résistance, d'une durée de 2 secondes chacun.

Le type de défauts créés artificiellement sur la ligne surveillée, c'est-à-dire phase-terre avec un faible courant de défaut à la terre, est identifié avec une précision instable. L'approche prometteuse pour obtenir plus de stabilité s'est avérée être la méthode de calibrage du modèle mathématique de la ligne utilisée dans l'algorithme de localisation des défauts. Dans le cadre du projet, le test pilote supplémentaire sur un réseau moyenne tension réel a été conçu, qui comprenait l'injection d'une impulsion de tension sur la ligne pour un traitement ultérieur des données enregistrées dans le modèle de ligne.

Summary

The project deals with the development and pilot testing of a novel fault locator for electrical distribution networks up to 38 kV. The device uses a single measuring point and is suitable for networks with distributed generation units from renewable sources. The objective of the project is to improve the existing prototype by developing smart functions to allow its integration in the modern and digital electrical substations.

Within the framework of the project, the functionality of the software was significantly improved. The fault locator software has extended to the version, which is a more complex one with new smart features. Now the fault locator is integrated into a modern electrical substation, detecting the presence of the fault and classifying the events occurring on the line: disturbances, phase-to-ground faults, short-circuit faults. Important both for the system and the utility, where it is installed – the fault location results are integrated into their SCADA system as well as the switch status from SCADA is received by the fault locator for updating the actual network model configuration. The connection to the utility's cloud database containing network parameters has been developed in order to exchange the line data. Furthermore, the system architecture has been changed during the project: two units of the system (acquisition and elaboration units) were split into two different locations and connected through internet.

The performance of the development was examined during a monitoring phase and evaluated thanks to field tests on a distribution network in the Freiburg region. The pilot test has been performed to assess the capability of the device to locate faults (bolted and resistive line-to-ground faults). A network in the area of Fribourg with three feeders supplied by the same primary substation was considered. For each feeder, a fault location had been selected, and two type of faults have been made, one with and one without resistance, lasting 2 seconds each.

The type of faults that were artificially created on the monitored line, i.e. phase-to-ground with small fault current to ground is identified with unstable accuracy. The promising approach to get more stability turned out to be the method of calibrating the mathematical model of the line that used in the fault location algorithm. Within the project, the additional pilot test on a real medium voltage network were devised, which included injection of a voltage pulse to the line for further processing of the recorded data in the line model.

Main findings

- The development and implementation into the fault locator software of a smart triggering strategy is based on two steps: the first step aims at identifying the events with high-frequency content, i.e. faults and disturbances, the second step aims at classifying the measured event as a fault or a disturbance. The prototype correctly distinguished the events during monitoring phase and detected the presence of all the faults during the live tests.
- The development of a function to classify the type of faults and identify the faulty feeder.
- The development of a specific software function devoted to the communication with the SCADA system to integrate the results of the fault location and receive the real-time status of the switches along the line to infer the real-time topology.
- The development of a local relational database on the elaboration unit and linked to the fault locator software. This database contains the main data structure for the whole software. The development of the strategy to connect the fault locator to the database of the utility to automatically input the needed data into the fault locator system.
- The development of a methodology and its integration to the software to improve the accuracy of short-circuit faults localization. The methodology has proven to be successful during the years of different installations: 6 short-circuits occurred in the monitoring networks were detected with more precise accuracy, where in 2 cases the fault location error was only 100 m and in 4 cases the error was 200-600 m against 800-4700 m for the conventional method. Now the method is implemented in the fault locator software.
- Finding the principal limitation in accuracy of fault localization and carrying out pilot tests on the line with the injection of a simple signal into the line as one of the strategies to calibrate the line model. The main findings of these tests was that in the mathematical model the total capacitance of the overhead line is less than in reality. Also according to the test results, the same patterns voltage response spectrograms for each injection site have been found in the experimental and computational data. However, not identical correspondence of calculations and measurements indicates some shortcomings of the mathematical model, which leads to a finite error in determining the fault location. Even though the work done on the model has not yet given us a unified strategy for building the model and answering the question of which critical parameter was missing in the model, the data obtained during the pilot tests with the application of a voltage pulse turned out to be very useful. Eventually, we continue to extract data from the tests also for the analysis, which are already outside the scope of the project, however it gives us better understanding of the transient phenomena in the network.

Contents

Abbreviations

AI: Artificial Intelligence

CB: Circuit Breaker

DAQ: Data Acquisition

DG: Distributed Generation

DSO: Distributor System Operator

EMTR: Electromagnetic Time Reversal

FCSE: Fault Current Signal Energy

FI: Fault Indicator

FFT: Fast Fourier Transform

GFL: Guessed Fault Location

HMI: Human Machine Interface

HV: High Voltage

MV: Medium Voltage

MCCS: Maximum of the cross-correlation sequence

OHL: Overhead Line

PMU: Phasor Measurements Units

SCADA: Supervisory Control and Data Acquisition

SEFL: Single-End Fault Locator

SEU: System Elaboration Unit

TR: Time Reversal

1 Introduction

1.1 Background information and current situation

Context

Nowadays the structure, operation, and control of electrical power grids are going through fast and important changes. In the 1990s, the privatization and liberalization process led to intense competition, and growing attention to cost reduction, calling for cost-effective operation and stricter power quality requirements. Meanwhile, the liberalization entailed the loss of vertical integration between the stages of the electricity chain. This, along with the evolution towards more sustainable electrical systems, has led to the presence of smaller and distributed generators connected at various voltage levels. There is no doubt that power distribution systems will benefit from these developments, but at the same time, new technical challenges are certainly emerging and need to be addressed. Some of these are the occurrence of bidirectional power flows, the handling of possible line congestions, as well as protection system failures. Within this context, the integration of renewables into existing grids is motivating changes in the grid operation and topology.

In this context, reliable and efficient fault detection and location functionalities are increasingly required to match power quality constraints. In this regard, when a fault occurs in an electrical power network, the faulty element is disconnected from the rest of the grid as fast as possible by a set of automatic protective relay devices. The aim is to minimize damage and avoid dangerous situations for the system stability. Following the relay operation, it is also important to pinpoint the precise fault position. Indeed, power supply restoration can be faster if the location of the fault is either known or can be estimated with satisfactory accuracy. The estimation of the fault position, with the highest possible accuracy, is known as *fault location*.

The project proposal focuses on the application of an innovative fault locating method for distribution networks up to 38 kV.

Existing challenges

Majority of fault location devices are designed to operate on lines with a wide voltage range of 6-750 kV, have found application mainly in voltage classes of 110 kV and higher. In distribution networks of 6-35 kV, their use is extremely limited, since they have significant weakness, primarily related to the difficulty of recognizing the phase-to-ground current due to their small value in ungrounded networks. Another huge challenge in distribution lines is identifying of a fault location on the branching areas on the line and recognizing not only the distance to the fault location, but also the correct branch where the event occurred.

The major advantages of an accurate fault locating procedure are as follows ([1],[2]):

- faster power restoration;
- improvement of system availability, performance, and power quality;
- reduction of time spent by maintenance crews searching for the fault point (reduction of costs for the utility and improved power quality for the end user);
- detection and location of transient faults allows the assessment of minor damages which might not be easily visible on inspection;
- improvement in disturbance diagnostics by identifying temporary faults and detecting weak spots.

Nowadays, the fault location, as a function, can be implemented in i) microprocessor-based protective relays, ii) digital fault recorders, iii) stand-alone fault locators, and iv) off-line post-fault analysis programs [1].
Since the 1950s, most of the research on fault location has been focused on transmission lines (e.g. [3], [4]). This is due to the appreciable impact of faults in transmission grids on the security of supply and the long time required to physically inspect faulty lines.
Only later, identifying the fault location in sub-transmission and distribution networks has also attracted attention because of the increasing emphasis on quality and reliability of supply: an accurate fault location procedure becomes therefore important as it minimizes the inconveniences caused to the affected users. Thus, the fault location functionality is considered as one of the first functions to be integrated into modern distribution networks [1].
Despite a large amount of research carried out and several solutions available on the market, locating faults in electrical power distribution networks still represents a challenge due to several aspects:

1. Medium voltage (MV) networks may be multi-terminal, with branches and loops.
2. Furthermore, distribution networks are usually inhomogeneous (i.e., distribution feeders have different Resistance/Reactance ratios because they are composed of different types of conductors). In this regard, in terms of equivalent representation, cable sections cause additional difficulties compared to overhead lines.
3. Possible errors are also due to loads, which are often unbalanced and variable (the compensation of their effect is therefore difficult).
4. The fault location accuracy is also affected by the fault impedances and the measurement errors associated with the measurement transformers (which is significant in the case of small values of voltage during the fault). Besides, the presence of Distributed Generation (DG) can largely impair the accuracy of fault location procedures developed for passive distribution networks.

As a result, the accuracy of existing fault locating methods is still affected by several factors, such as pre-fault system conditions, fault impedance, communication link accuracy (in the case of multi-end methods), and measurement noise. Moreover, the low-cost and widely spread impedance-based fault location methods are not suitable for active distribution networks. Indeed, the nodal infeed from distributed generators induces errors in the computed distance to the fault. As a result, the sophisticated traveling wave-based methods (which consider high-frequency voltage or current signals) will thus be preferred to locate faults in these networks.

Current status of technology

As reported in the previous section, the fault location problem in transmission and distribution lines has been a topic of investigation since the 1950-s and numerous fault location methods have been proposed in the literature. The various fault location procedures can be classified into the categories reported in what follows.

1. Manual method.

One-by-one shutdown of the sections (with open circuit breaker at the beginning of the feeder) until the faulted section is found. Then, the maintenance crew inspects the identified section to fix the problem. In case of an absence of more advanced solutions, this method is still used by utilities for fault localization.

2. Fault Circuit Indicators.

A fault circuit indicator is a device that provides visual or remote indication of the presence of the fault on a given section of the electric power system. The operating principle consists of sensing the change in the electromagnetic field and the threshold is set relative to that change. There are two types of Fault Indicators (FIs) available on the market: the 1st type is based on voltage and the sensing unit is usually placed on the pole below the three conductors; the 2nd type is more advanced and universal in terms of

suitability for the installation. FIs of the 2nd type can be installed on the lines with two or more circuits on a single pole since the sensing units are based on the current, i.e. they are represented as current transformers with an open core. The sensing units are complemented with the communication unit, which is responsible for data transfer to a remote server for analysis and reporting. The FIs are easy to install on the live line and therefore line disconnection is not required (i.e., no energy supply interruption for customers). In term of installation, it is recommended to equip the network with the FIs at the key points or at inaccessible parts of the line to separate the line into pieces and make the fault investigation process easier with low investments.

The major disadvantage of using fault indicators are:

- The accuracy of the fault location depends on the quantity of the devices installed along the line: the more devices, the higher the accuracy, the higher the cost;
- The battery power supply is sensitive to the 3G/4G network coverage and the ambient temperature below zero degrees;
- High maintenance expenses related to the batteries' replacement process;
- They cannot be used for the networks with the bidirectional power flows, i.e. networks with distributed generation.

3. Phasor-based solutions, installed at the substations.

These methods rely on the calculated impedance of the faulty line to identify the fault location by measuring the steady-state voltage and the current phasors. Using ad-hoc algorithms, the total impedance of the circuit is determined and compared with the line-impedance of the line. The distance to the guessed fault location is determined based on the calculated line impedance.
Despite the logical transparency of the solutions, their accuracy is affected by the fault resistance, branches, configuration of the line, load flow unbalance, and the presence of distributed generation units. Indeed, the continuous growth of DG presence will jeopardize the applicability of traditional phasor-based fault localization solutions. Moreover, these traditional methods cannot be implemented for the HVDC transmission systems, which are one of the essential elements of modern power systems.

4. Traveling wave-based methods

These methods rely on the analysis of the high-frequency components of the fault-originated transient signals which are little influenced by the fault impedance. Traveling wave-based fault location methods analyze different features of the traveling waves and utilize various techniques to identify the fault location. One of the first adopted techniques is based on the cross-correlation between the forward and backward traveling waves. The main drawback of such a method is the discrimination of the traveling waves originated due to the fault point from reflections originated at remote ends of the line. Moreover, the accuracy of this method is mainly dependent on the sampling window. The arrival time-based methods identify the fault location by assessing the arrival time of the traveling waves at one or several terminals of the line. Indeed, more measurement points can usually guarantee better accuracy. However, significant investment in technical implementation is required. Some traveling wave-based devices use time measurements and needs two measurement points to achieve sufficient accuracy (double-end fault locator): the time between the arrivals of the waves of these two systems indicates the location of the guessed fault location. Double-end fault locators have the disadvantage of significant investments for the technical implementation. Reliability depends on the correct operation of devices from two ends of the line and the communication channels. Also the accuracy of fault location directly depends on the high-accuracy synchronization of devices on both ends of the line.

Despite the superior performance of the traveling-based methods compared to phasor-based methods, their accuracy is affected by different factors such as:

- Assessment of the number of observation points versus the number of possible multiple fault location units. In a nutshell, to avoid uncertainty, the branchy or inhomogeneous network should be separated into homogeneous pieces and, at every terminal of these pieces, the fault location unit should be installed.
- Demand for precise time stamping for methods requiring several synchronized metering stations.
- Loss of GPS signal impacting fault accuracy.
- A requirement of a large bandwidth recording systems.

5. Knowledge-based approaches – artificial intelligence methods.

It is known that research efforts have been devoted to the use of knowledge-based fault location methods. Expert systems identify the most probable fault location using the available information regarding the network status (e.g., the state of switches, unpowered user complaints, etc.). Artificial neural networks and fuzzy logic have been widely studied for fault location problems. It is, however, worth mentioning that extensive training for such methods limits their application as well as the demand for data of the highest quality.

1.2 Purpose of the project

As said, the project deals with the development and pilot testing of a fault locator for electrical distribution networks up to 38 kV. The objective of the project is to improve the existing prototype by developing smart functions to allow its integration in modern and digital electrical substations. Specifically, the project aims at: developing an advanced triggering system to identify the presence of a fault; integrating the result into the SCADA system of the utility; and developing the connection and interface with the customer's database for data exchange. In addition, the aim is to further improve the accuracy of the localization. The performance of the development will be examined during a monitoring phase and evaluated thanks to field tests on a distribution network in the Freiburg region (Switzerland).

Contribution of the project to the current challenges

To overcome the limitation of current solutions, as a strategic move, Streamer decided to develop a smart single-end fault locator (SEFL) based on the electromagnetic time reversal (EMTR) theory.

Considerable attention has been devoted by researchers to methods based on the EMTR theory. The latter constitute a subgroup of the traveling wave-based methods since they consider the high-frequency voltage or current transients originated by the fault occurrence. As this is an emerging technique for fault location in power networks, further theoretical refinements and practical considerations are still needed in view of a successful implementation.

The EMTR-based technique proposed in [5] features the following advantages with respect to classical methods:

1) the EMTR method applies to inhomogeneous feeders (i.e., mixed overhead and cable lines);

2) it is based on single-end measurements and therefore, complex communication links or synchronization between multiple observation points are not needed;

3) the method is theoretically characterized by a high location accuracy (±100 m can be possible).

1.3 Objectives

Objects to be achieved by the project

Based on the *stand-alone* single-end fault locator (SEFL) available at the beginning of the project (Nov. 2020), whose only function is to apply EMTR method for fault localization on the line, this project aims at developing a *smart* SEFL, named CH-7000, able to be integrated into the modern digital electrical substations, and contribute to the power grid automation. This will allow meeting the market's needs and deliver a unique and competitive solution to DSOs.

The specific goals of the projects are as follows:

1. The development of an ad-hoc triggering strategy to detect the presence of faults and, once detected, distinguish between lightning-originated events and faults. The integration of signal outputs from the protection system at the substation to the SEFL. This goal is addressed in WP1.
2. The design and the implementation of a specific software function devoted to the communication with the SCADA system to integrate the SEFL results of the fault location. This goal is addressed in WP2.
3. The development of the strategy to connect the SEFL to the Groupe E database to automatically input the needed data into the SEFL system. This goal is addressed in WP3.
4. Improvement of the accuracy of the fault location results (to ±100 m). This goal will be addressed in WP4.

The monitoring phase (i.e., WP5) and the pilot test (i.e., WP6) will serve as an evaluation of the project goals.

Anticipated findings

In short, the project should lead to the following findings:

1. WP1: The development of an ad-hoc triggering strategy to detect the presence of the fault and its implementation into the SEFL software.
2. WP1: The development of a Matlab tool to analyse the waveforms recorded by the SEFL software, by using several time-domain and frequency-domain features.
3. WP1: The development of a methodology to distinguish faults and disturbances.
4. WP1: The study of a possible methodology to distinguish faults and lightning-originated event.
5. WP1: The development of a function to classify the type of faults and identify the faulty feeder.
6. WP2: The design of a specific software function devoted to the communication with the SCADA system to integrate the SEFL results of the fault location.
7. WP2: The development of the software function devoted to the communication with the SCADA system to receive the real-time topology of the network by SEFL.
8. WP3: The development of the strategy to connect the SEFL to the Groupe E database to automatically input the needed data into the SEFL system.
9. WP4: The development of a methodology to improve the accuracy of phase-to-phase faults.
10. WP4: The development of another metric different from suggested fault current signal energy to identify the location of the fault.

11. WP4: The development of an interactive dashboard to analyze the fault location results based on different metrics.
12. WP4: The development of the function to calculate the line model containing different types of line and cable data models in the SEFL software.
13. WP4: The refinement of the mathematical model features in order to improve the efficiency of fault location.
14. WP5 and WP6: The developed functions should be evaluated and adjusted during Monitoring phase and Pilot test.

2 Description of facility

In this project, we suggest to locate faults, by using the EMTR theory. Before describing the facility in Section Activity carried out3.2 (i.e., fault locator hardware installed at Groupe E), Section 2.1 recalls in brief the EMTR theory and its application to the fault location problem.

For the sake of clarity, we also recall that the objective of the technology under development is twofold:

1. Measure and record high-frequency transient signals at the primary substation, providing date and time of the event and distinguishing and faults and other types of events;
2. By analyzing the mentioned high-frequency transients caused by faults, the device should be able to pinpoint the most likely fault location.

The inputs of the fault-locating system are:

a) Three-phase voltage measurements, acquired by using the data acquisition system, whose specifications are summarized in Table 1 (described in Section 3.2.1);
b) Network data reported in Table 2 to build the electrical model of the grid in a simulation software EMTP-RV[1] (described in Section 3.2.2).

2.1 The EMTR-based algorithm [5]

To explain the time-reversal (TR) process, let us consider the evolution of a physical quantity f(t) as a function of time in a system, from time $t = 0$ up to time $t = T$ (*direct time*). The TR process describes a transformation whereby the previous behavior of the system from $t = 0$ to T is reproduced in the future, namely from $t = T$ to $2T$ (*reversed time*). This is obtained by imposing appropriate initial conditions on the original system so that it begins to retrace its previous states. In this case, the system is called *time-reversal invariant*.

Mathematically, TR invariance can be checked by verifying that the equations describing the physical phenomenon remain unchanged by applying the TR operator (i.e., $t \rightarrow -t$). In other words, a system is TR invariant with respect to a physical quantity if, given a solution $f(t)$ of its underlying equations, the TR function $g(t)$:

$$g(t) = f(-t + T)$$

is also a solution.

[1] EMTP-RV is a well-known software for simulation and analysis of power systems, especially for the simulation of electromagnetic and electromechanical transients. This software is used to build the electrical network model and to run electromagnetic transient simulations.

By making reference to the transmission line theory, the equations describing the voltage wave propagation along a multi-conductor, lossless transmission line are TR invariant. In particular, the voltage wave equation reads:

$$\frac{\partial^2}{\partial x^2}\mathrm{U(x,t)} - L'\mathrm{C}'\frac{\partial^2}{\partial t^2}\mathrm{U(x,t)} = 0$$

where $U(x,t)$ is the vector of the conductors' voltages at time t and position x, and L' and C' are respectively the matrices of the line per-unit-length inductance and capacitance. By applying the TR operator to the latter equation we obtain:

$$\frac{\partial^2}{\partial x^2}\mathrm{U(x,-t)} - L'\mathrm{C}'\frac{\partial^2}{\partial t^2}\mathrm{U(x,-t)} = 0.$$

Thanks to the second-order time derivative, if U(x, t) is a solution of the wave equation, U(x,−t) is a solution as well. This implies that the voltage wave equation is time-reversal invariant.
Thanks to the reversibility in time of the voltage wave equations, the EMTR theory can be successfully applied to the problem of fault location to estimate the place where the fault was originated.
In the case of a fault event, the physical quantity to observe can be the voltage over a given time window *T* (e.g., one period that is *T =20* ms). A fault occurring in the grid can be seen as a step function source triggered by the fault event. The fault-generated step wave propagates along the line and is reflected at the line extremities (e.g., power transformers or loads). An observation point (e.g., the primary substation) at which voltage waveforms are measured will observe a superposition of waves that are traveling along the various lines and branches of the network. Once the transient voltages are measured, we apply the TR process (Figure 1) to let the system (i.e. the electrical grid) retrace its previous states and let us know where the event (i.e. the fault) was generated.

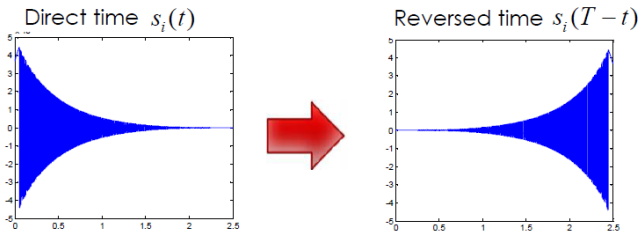

Figure 1: Time reversal process

Briefly, the method is based on four steps:

1. Measurement step (direct time): measure of the fault-generated transients (e.g., the voltage transient $v_0(t)$) at observation point of the network;
2. Guessed fault locations (GFLs) definition: a set of GFLs is defined;
3. Simulation steps (reverse time): the recorded fault-originated transient signal is time-reversed, i.e. $v_0(t) \rightarrow v_0(-t+T)$In the simulated grid model, the observation point is replaced by a source imposing the time-reversed transient, $\rightarrow v_0(-t+T)$. This step involves numerical simulations to take into account the network parameters and topology. The number of simulations is equal to the number of GFLs. For each simulation, at the GFL, a conductor-to-ground short-circuit connection has to be placed.
4. Signal energies' computation: computation of the signal energy, Ei, associated with the current flowing through each GFL, i.e. flowing through each transverse branch representing the

conductor-to-ground short-circuit connection. The maximum of the calculated signal energies identifies the most probable fault location.

The next section describes the system operating algorithm.

2.2 Implementation of the algorithm under development

The main steps of the fault location platform under development are summarized in what follows.

1. *Measurements and data acquisition*. Three high-frequency sensors are installed at the busbar to continuously measure the three-phase voltages at the primary substation. Voltage data is sampled and is continuously recorded by the data acquisition system (see Section 3.2.1).
2. *Smart trigger*. In order to discern fault-originated electromagnetic transients, an ad-hoc triggering system is developed (in the framework of this project) for the SEFL software.
3. *Signal filtering*. Once the fault-originated voltage transients are identified, the low-frequency components (e.g., 50 Hz) are removed by using suitable filtering techniques.
4. *Fault location platform*. The filtered signals can now be used by the SEFL software to implement the fault locating algorithm based on the time-reversal theory, following the steps described in the previous paragraph. A third-party simulation software, named EMTP-RV, is used to build the network model of the distribution network and perform electromagnetic transient simulations in the reversed time. To this end, an industrial PC with high-computational capacity and speed is used to obtain the results in just a few minutes. The connection to the utility database developed in the framework of this project allows the user to have an up-to-date network model. Additionally, thanks to the connection with the utility's SCADA to be develop in the framework of this project, the real-time topology (i.e., real-time status of the switches) can be inferred.
5. *Result*. The most likely fault location is calculated, identified by the maximum of the current-signal energy and then send it to the SCADA system. The local HMI displays relevant data to the user, allows the user to update settings, and sends the commands to the data acquisition system.

The measurement equipment description is integrated into Section 3 below.

3 Procedures and methodology

3.1 Description of general procedure within the project

The project consists of seven work packages (i.e., WP1 ÷ WP7), plus an additional work package, WP0, which deals with project management. The hierarchical organization and the involvement of each project partner per work package are reported in Figure 2, while Figure 3 recalls the work packages content and shows their interaction.

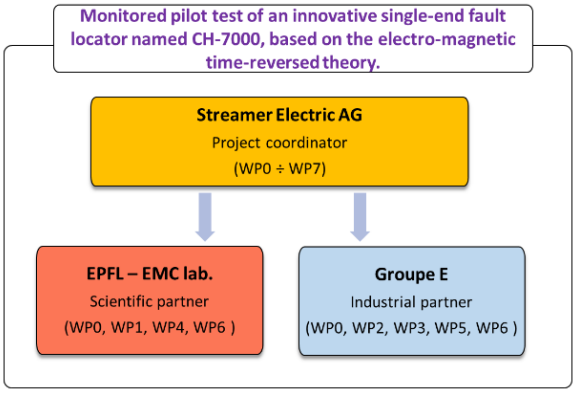

Figure 2: Hierarchical organization of the project

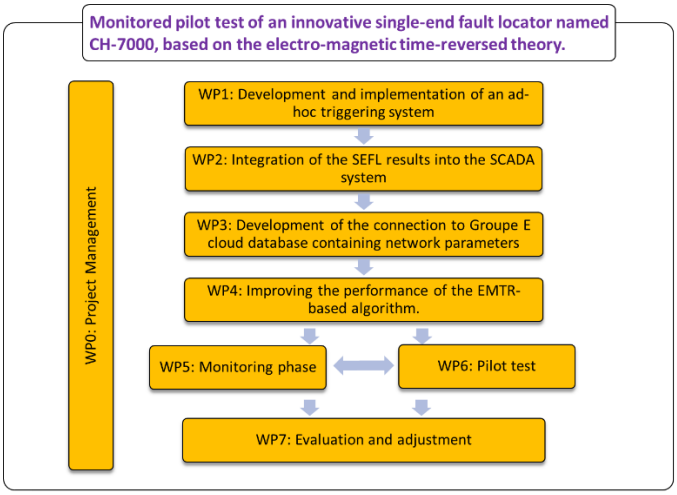

Figure 3: Project structure and work packages

3.2 Activity carried out

3.2.1 Measurement set-up installed at Groupe E

The Data Acquisition System (DAQ) is installed only at the MV side of one of Groupe E primary substations and does not require any other equipment installed along the line. The DAQ is composed of the following main components:

1. Three sensors, one per phase, are installed at the busbar at the primary substation to measure the three-phase voltages (Figure 4). Voltage data is sampled and is continuously recorded by the data acquisition system.

Figure 4: Voltage sensors installed at the busbars

The sensors are manufactured by G&W Electric, a global leader in electric power equipment since 1905. The sensors are high-frequency electronic voltage sensors of two types: for indoor up to 24 kV (Figure 5, a) or outdoor up to 38 kV (Figure 5, b) use. For the installation at Groupe E, sensors 24 kV indoor versions are used.

a) b)

Figure 5: High-frequency electronic voltage sensors
a) for indoor use b) for outdoor use

The devices incorporate the following functions:

- Voltage transducer (electric field sensing technology), which is not in contact with the busbars;
- Post insulator.

Even though the main frequency components of the voltage-originated transients are in the range of kHz, the sensors' bandwidth is large (up to 4.5 MHz, 3 dB attenuation) to guarantee the versatility of the solution for different types of networks.

2. The data acquisition system: analog-to-digital converter (ADC) and controller, is placed in a server rack located at the primary substation (see Figure 6).

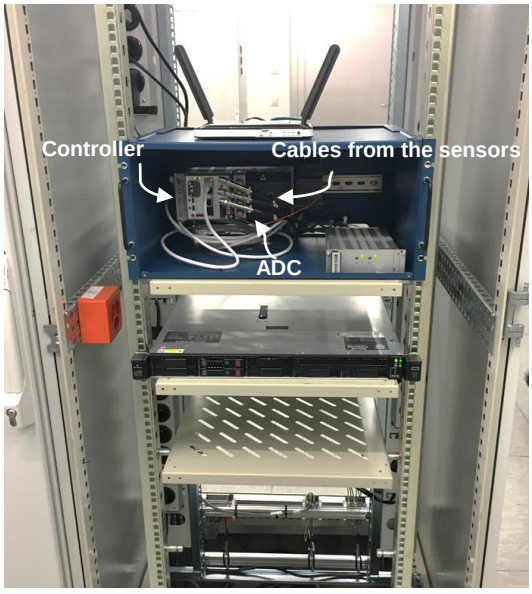

Figure 6: Data acquisition system

To sample the measured signals from the sensors, a 14-bit ADC or, in other words, digitizer for measurements up to 20 MS/second per channel is used. The supplier of the ADC is the NI 9775 module manufactured by National Instruments, a reliable producer of high-quality automated test equipment and virtual instrumentation software.

A rugged controller (National Instruments cRIO-9040) containing both a real-time processor and FPGA (field-programmable gate array), where the FPGA is directly connected to the ADC. The ADC and the controller are reported in Figure 7 and Figure 8 respectively.

Figure 7: NI 9775, 4-channel digitizer

Figure 8: cRIO-9040 controller

Once the event is detected by the DAQ system, fault data is transferred to a high-performance server to i) post-process data, ii) implement the EMTR-based algorithm, and iii) run simulations to have the result of the fault location. It was decided that there would be one server per installation for pilot tests. For the commercial product, when the number of installations is supposed to increase, one server, so-called central server, can be used for several SEFL units, that will reduce the cost for each installation. The high-performance server can be located at the primary substation or at the data center of the utility. The latter option was developed in the framework of this SFOE project (see Section 4.1.2.3 for the details). Streamer and Groupe E decided to use a server located at Groupe E's data center.
The technical characteristics of measurement set-up is presented in Table 1.

Table 1: Data acquisition system specification

Voltage transducers	Rated voltage	Indoor installation: up to 24 kV
		Outdoor installation: up to 38 kV
	Secondary voltage, U_{pn}	5 V
	Nominal frequency	DC, 50 Hz or 60 Hz
	3 dB Bandwidth	20 Hz – 4.5 MHz
	Creepage distance	Indoor installation: 375 mm
		Outdoor installation: 740 mm
	Weight	Indoor installation: 1.6 kg
		Outdoor installation: 3.0 kg
	Power supply	230 V
Data acquisition system	Sampling rate	20 MHz
	Signal to Noise Ratio SNR	68 dB
	ADC resolution	14 bits
	Power supply	230 V
	Dimensions	Indoor installation: 4U of 19'' rack
		Outdoor installation (climate controlled): 12 U of 19'' rack

3.2.2 Line modelling in EMTP-RV

One of the key components in the fault locator system and the algorithm is the creation of a network model – a digital twin of the power line where SEFL is installed. As mentioned in Section 2 the monitored line is modeled via electromagnetic transient program EMTP-RV where a line is represented by equivalent circuit parameters. In Figure 9 the example of a network model with 3 feeders from the substation is presented. The model is based on the line data provided by the utility which is the information about topology and composition of the line (example of the requested information is presented in

Table 2). The original data from the utility is taken from the data base of the utility, but in case of doubts, the controversial data can be verified and observed on site by Streamer. Further, the data is converted by the software to the electrical parameters, namely resistance, capacitance, inductance, conductivity of the line, as well as the transient wave travel time. There are different approaches (or models) for the parameters calculation in EMTP-RV: constant parameter (CP) and frequency dependent (FD) models. The CP model assumes that the line parameters are constant, and they are calculated at a user-supplied model frequency. The constant parameter model is the basic line and cable model used in transient studies. Its main advantage is computational speed, but typically provides less optimal and accurate results and can become inaccurate for transients with wide dispersion of frequencies. The FD model class provides an accurate representation of the distributed nature of all the line parameters and capable of accounting for the frequency dependency of line parameters.

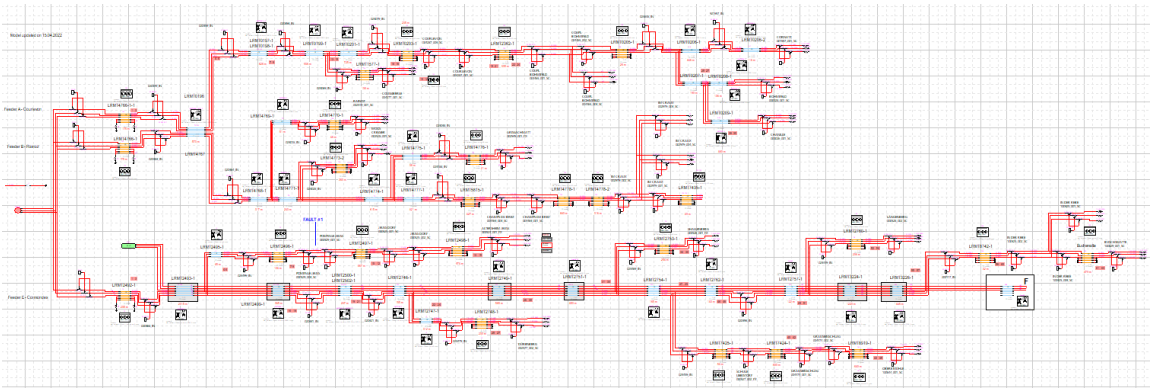

Figure 9: Example of line model of 3 feeders in EMTP-RV

Table 2: Network data provided by DSO

Requested data
General information
Network topology
Overhead lines
Length (m)
Height of conductors (m)
Optional: Sag of mid-span
DC Resistance of the conductor (Ohm/km)
Geometrical configuration
Conductor diameter (mm)
Conductor material

Ground resistivity (Ohm·m)
Cable lines
Length (m)
Conductor diameter (mm)
Conductor material
Insulation thickness (mm)
Insulation material
Sheath thickness (mm)
Sheath material
Cable depth (m)
Ground resistivity (Ohm·m)
Cable configuration

The next subsections describe the activities carried out so far, with reference to the work-packages illustrated in Section 3.1.

3.2.3 WP1: triggering system

The selected methodology for the smart triggering strategy is based on two main steps:

1. The first step aims at identifying the events with high-frequency content, i.e. faults and disturbances. The chosen principle is based on the signal derivative.
2. The second step aims at classifying the measured event as a fault or a disturbance. The chosen principle is based on the measured signal integral.

The correctness of this approach was tested by using 170 disturbances recorded on the monitoring units, 112 fault events recorded during past pilot tests, and 60 events recorded by the monitoring units.

Step 1: first derivative triggering condition

In normal grid operation, the instantaneous voltage $v(t)$ measured at the sensing point as a function of time t reads:

$$v(t) = A \cdot sin(\omega t)$$

where *A* is the amplitude of the sine function, and ω is the angular velocity, i.e. $\omega = 2 \cdot \pi \cdot f$, where *f* is the system frequency ($f = 50\ Hz$ in Europe).

The derivative of the instantaneous voltage *v(t)* is:

$$\frac{dv(t)}{dt} = A \cdot \omega \cdot \cos(\omega t)$$

And therefore:

$$dv(t) = A \cdot \omega \cdot \cos(\omega t) \cdot dt$$

As $-1 \leq \cos(\omega t) \leq 1$, it follows that:

$$|dv(t)| \leq A \cdot \omega \cdot 1 \cdot dt = A \cdot \omega \cdot dt \qquad (1)$$

In our application, the instantaneous voltage is measured over a given time window T, and then sampled with a time step Δt. Therefore it is composed of discrete samples V_i, $i \in [1,..,N]$, where $N = {}^{T}/_{\Delta t}$. For a discrete signal, inequality (1) becomes:

$$|\Delta V| \leq A \cdot \omega \cdot \Delta t$$

In case of non-sinusoidal high-frequency signals, (1) does not hold anymore. As example, Figure 10 reports the case of a classical fault where $|\Delta V| \geq A \cdot \omega \cdot \Delta t$ after the fault occurrence.

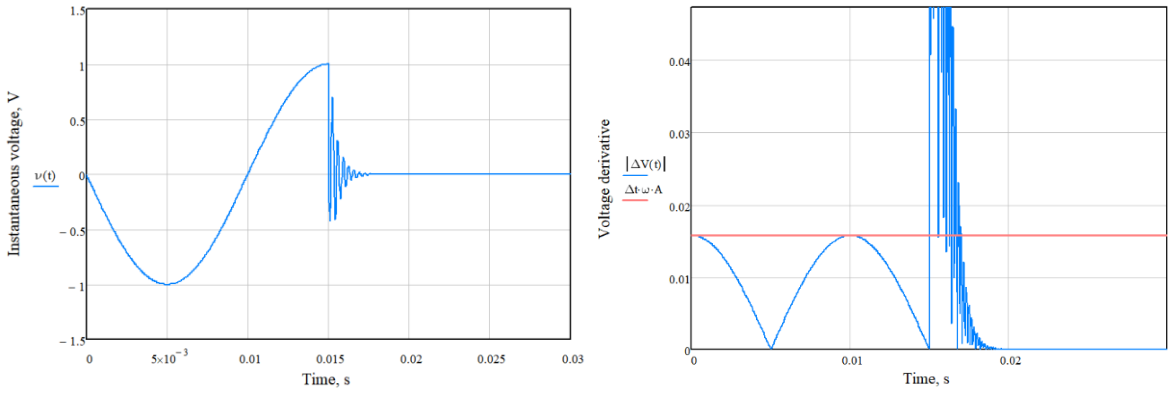

Figure 10: Typical waveform of a line-to-ground fault (left side) and its derivative (right side).

Given the above, the first triggering condition was set to:

$$|\Delta V| \geq k_n \cdot A \cdot \omega \cdot \Delta t \qquad (2)$$

Where k_n is an experimental coefficient that takes into account the measurement noise.

In summary, this condition (2) aims at identifying all the event with fast transients (i.e. high-frequency signals) and is based on the fact that, in normal grid operation, the measured voltage is a sinusoidal function, whose derivative is bounded by -A·ω·Δt and +A·ω·Δt. As shown, this mathematical condition is not met in case of fast transients.

Step 2: second integral condition

We consider here the instantaneous voltage $v(t) = A \cdot sin(\omega t)$ during normal grid operation and the area subtended by the function over a generic time window, whose length is equal to the period T as reported in Figure 11.

As known, the area subtended by the sine over the first half period, S_1, is equivalent to the area subtended by the function over the second half period, S_2:

$$S_1 = \int_{to-\frac{T}{2}}^{t_0} |v(t)|\, dt = \int_{to}^{to+\frac{T}{2}} |v(t)|\, dt = S_2$$

On the other hand, in case of an event triggered at the generic time t_0, the two areas do not have the same value anymore. As an example, we report in Figure 12 two faults measured during a past test campaign at Groupe E: on the right side we report the case of a line-to-ground fault occurred close to the zero-crossing, while on the right side the case of an arc fault. For such events $S_1 \neq S_2$.

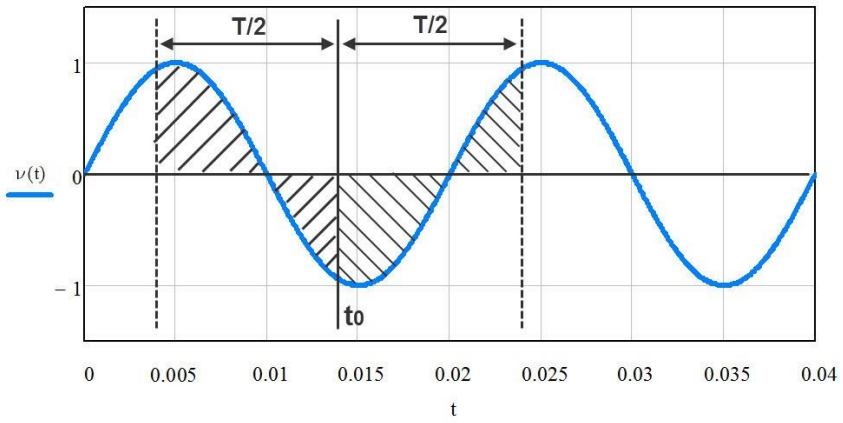

Figure 11: Instantaneous voltage $v(t) = A \cdot sin(\omega t)$ during normal grid operation and the area subtended by the function over a period T.

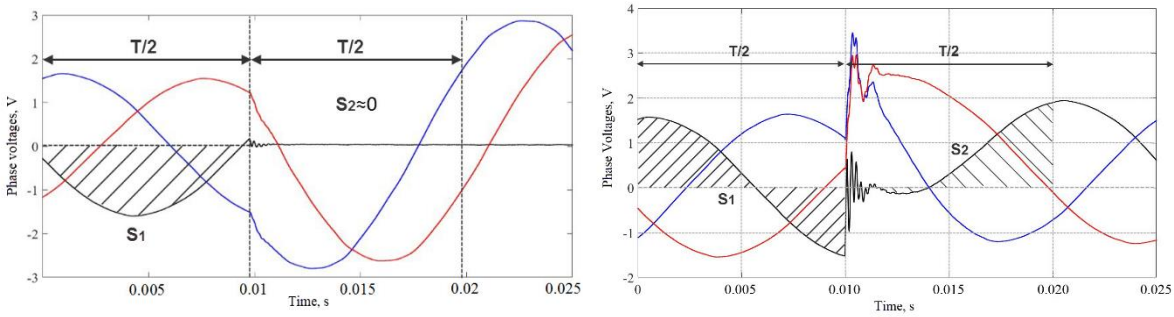

Figure 12: Areas before and after the fault occurrance

By looking at Figure 12, the area before the triggered event S_1 can be calculated as:

$$S_1 = \int_{to-\frac{T}{2}}^{t_0} |v(t)|\, dt = \int_{to-\frac{T}{2}}^{\frac{T}{2}} A \cdot sin(\omega t)\, dt + \int_{\frac{T}{2}}^{to} (-A \cdot sin(\omega t))\, dt = \frac{A}{\omega} \cdot [-\cos(\omega t)]\Big|_{to-\frac{T}{2}}^{\frac{T}{2}} + \frac{A}{\omega} \cdot [\cos(\omega t)]\Big|_{\frac{T}{2}}^{to}$$

The angular velocity can be written as $\omega = 2 \cdot \pi \cdot f = \frac{2\pi}{T}$ and thus:

$$S_1 = \frac{AT}{2\pi} \cdot \left[\left[-\cos\left(\frac{2\pi}{T} t\right) \right]\Big|_{to-\frac{T}{2}}^{\frac{T}{2}} + \cos\left(\frac{2\pi}{T} t\right)\Big|_{\frac{T}{2}}^{to} \right] =$$

$$= \frac{AT}{2\pi} \left[-\cos\left(\frac{2\pi}{T} \cdot \frac{T}{2}\right) + \cos\left(\frac{2\pi}{T} \cdot to - \frac{2\pi}{T} \cdot \frac{T}{2}\right) + \cos\left(\frac{2\pi}{T} to\right) - \cos\left(\frac{2\pi}{T} \frac{T}{2}\right) \right] =$$

$$= \frac{AT}{2\pi} \left[-\cos(\pi) - \cos\left(\frac{2\pi}{T} \cdot to\right) + \cos\left(\frac{2\pi}{T} to\right) - \cos(\pi) \right] = \frac{AT}{2\pi} [1 + 1] = \frac{AT}{\pi}$$

The area after the triggered event, S_2, can be calculated in the same way as:

$$S_2 = \int_{to}^{t_0+\frac{T}{2}} |v(t)|\,dt = \int_{to}^{T} (-A\cdot\ sin\left(\frac{2\pi}{T}t\right))\,dt\ + \int_{T}^{t_0+\frac{T}{2}} A\cdot\ sin\left(\frac{2\pi}{T}t\right)dt =$$

$$= \frac{AT}{2\pi}\cdot\left[\cos\left(\frac{2\pi}{T}t\right)\Big|_{to}^{T} + \left[-\cos\left(\frac{2\pi}{T}t\right)\right]\Big|_{T}^{t_0+\frac{T}{2}}\right] =$$

$$= \frac{AT}{2\pi}\left[\cos\left(\frac{2\pi}{T}\cdot T\right) - \cos\left(\frac{2\pi}{T}\cdot to\right) - \cos\left(\frac{2\pi}{T}to + \frac{2\pi}{T}\frac{T}{2}\right) + \cos\left(\frac{2\pi}{T}T\right)\right]$$

$$= \frac{AT}{2\pi}\left[\cos(2\pi) - \cos\left(\frac{2\pi}{T}\cdot to\right) + \cos\left(\frac{2\pi}{T}\cdot to\right) + \cos(2\pi)\right] = \frac{AT}{2\pi}[1+1] = \frac{AT}{\pi}$$

As a result:

$$S_1 = S_2 = \frac{A\cdot T}{\pi}$$

Generally, we can take any T_{area} before the triggered event and after, if T_{area} is multiple of half period:

$$S = \int_{to-T_{area}}^{t_0} |v(t)|\,dt = \int_{to}^{to+T_{area}} |v(t)|\,dt\ = \frac{2AT_{area}}{\pi},\ T_{area} = n\cdot\frac{T}{2}, n = 1,2,3\ldots$$

Given the above, the integral condition was set to:

$$S_2 \le k_s \cdot S_1 \qquad (3)$$

Where k_s is an experimental coefficient that takes into the sensitivity of the principle.

In summary, after triggering the event (first derivative triggering condition), condition (3) aims at identifying only the faults among all the events that are measured at step 1. Condition (3) is based on the fact that, in normal grid operation, the measured voltage is a sinusoidal function and the area subtended by the sine over the first half period is equivalent to the area subtended by the function over the second half period. As shown, this mathematical condition is not met in case of faults.

3.2.4 WP1: lightning-related event classification

Electromagnetic transients occurring in power distribution networks can be of different origins. Internal transients are usually due to device switching, e.g. capacitor bank switching, circuit breaker operation, load startup and disconnect. External transients include lightning strikes, accidents, etc. Lightning transients can also be categorized into two subcategory, namely direct lightning and indirect lightning. Direct lightning transients are generated when lightning strikes one of the line conductors, while indirect lightning results from a lightning discharge occurring nearby the line, the electromagnetic field of which inducing overvoltages along the line. For the case of distribution networks, because of the relatively modest height of the line conductors, most of the lightning events are indirect.

The main difference between fault- and lightning-generated transients can be inferred from their waveform characteristics and frequency content. Typically, lightning-originated waveforms are characterized by faster rise times, shorter durations and higher frequency contents. Figure 13a shows, as an example, a lightning-induced transient signal that lasted several tens of microseconds. Its rise time was a few microseconds.

Fault-originated signals are in general characterized by longer durations and rise times. Figure 13b presents an example of a fault-originated transient, the duration of which is about 800 microseconds while its rise time is about 100 microseconds. Faults- and lightning-generated transients can be distinguished from their waveform characteristics and frequency content. Typically, lightning-originated

waveforms are characterized by faster rise times, shorter durations and higher frequency contents, compared with fault-originated transients.

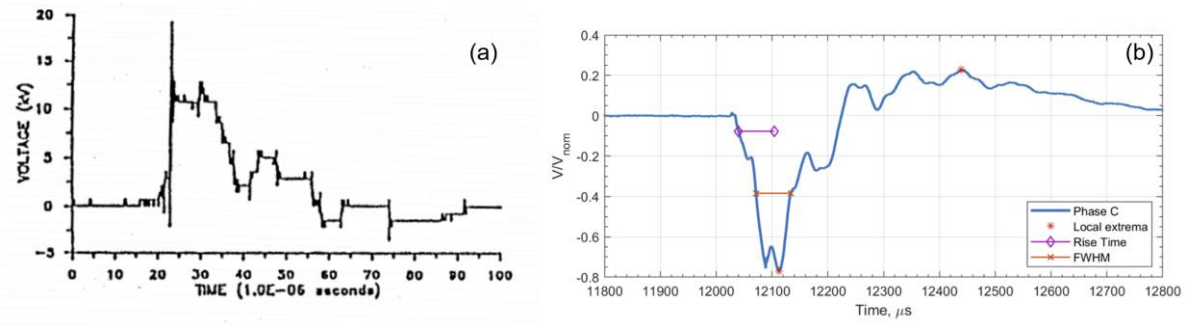

Figure 13: Voltage transient waveforms for lightning- (a) and fault- (b) originated events (taken from [9] and our monitoring dataset, respectively)

Examining transients that are induced by indirect lightning strikes at different locations with respect to the line and the measurement point, one can observe that they vary from case to. Moreover, parameters of the lightning discharge (peak current, waveform characteristics, return stroke speed, etc.) may vary as well. This variability makes the task of transient classification even more complex. However, some characteristics cannot be seen from the waveform directly, e.g. the signal energy which is an integral quantity. They could potentially serve as a key to distinguish different classes of transients as well. In this regard, we assume that comprehensive characterization of the waveforms by using parameters related to both time and frequency domain could provide a basis for the targeted classification.
In the following subsections, we describe a set of time-domain and frequency-domain parameters that can be used to characterize transient waveforms. These parameters have been used in the past to describe the characteristics of other types of waveforms, such as intentional electromagnetic interference sources ([6], [7]).

Time-domain parameters

- Peak Amplitude

The peak amplitude of a waveform R_{max} is defined as the maximum value of the signal $R(t)$ during its rise. For a pulse-like function, it corresponds to its absolute maximum value:

$$R_{max} = \max(|R(t)|)$$

- Time to peak

The time to peak is defined as the time it takes the waveform to achieve its maximum amplitude, starting from a zero-amplitude level:

$$\Delta t_{max} = t|_{R(t)=R_{max}} - \max(t|_{R(t)\approx 0})$$

- Peak derivative

The peak derivative is calculated as the maximum derivative of the waveform before reaching its peak amplitude:

$$\left(\frac{dR}{dt}\right)_{max} = \max\left(\frac{dR}{dt}\right),\ t < t|_{R(t)=R_{max}}$$

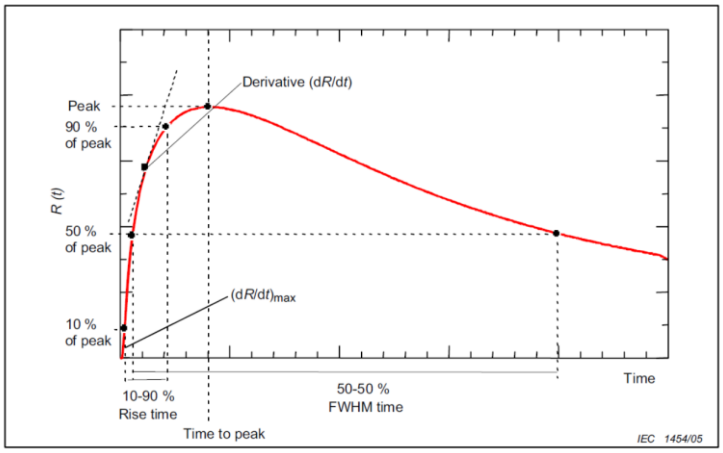

Figure 14: Illustrative plot of a monopolar pulse and its waveform attributes (from [6])

- 10-90% rise time

The 10-90% rise time is defined as the time it takes the waveform to increase from 10% to 90% of its peak amplitude, during its rising period:

$$\Delta t_{10-90} = t|_{R(t)=0.9R_{max}} - t|_{R(t)=0.1R_{max}},\ t < t|_{R(t)=R_{max}}$$

- Maximum rate of rise

The maximum rate of rise of an impulse signal can be defined as the ratio of its peak amplitude and its peak derivative:

$$t_{mr} = \frac{R_{max}}{\left(dR/dt\right)_{max}}$$

- Alternative evaluation of the rise time

The 10-90% rise time metric is applicable mostly for monopolar pulses. If the network under consideration has a complex topology, the transient exhibits multiple superimposed pulses due to the back and forth reflections of the wave (Figure 15) and therefore, it is not always possible to define a unique rise time for each waveform.
To overcome this problem, an alternative equation was considered to identify the local maxima and minima of the waveform, and the characteristic rise time of each waveform was estimated according to the following definition ([7])

$$t_{mr} = \frac{R_{max}}{\left(dR_2/dt\right)_{max}}$$

where $\left(dR_2/dt\right)_{max}$ corresponds to the maximum derivative near the peak current location.

- Full-width-at-half-magnitude (FWHM)

The FWHM represents the time elapsed between the instant when the waveform reaches 50% of R_{max} during its rising period and the instant when it decays to 50% of R_{max} during its falling period:

$$\Delta t_{10-90} = t|_{R(t)=0.5R_{max}\&\left(dR/dt\right)>0} - t|_{R(t)=0.5R_{max}\&\left(dR/dt\right)<0}$$

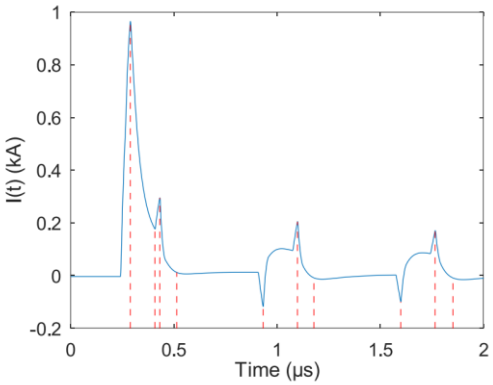

Figure 15: Example of a waveform characterized by multiple pulses

- Pulse width (PW)

The characteristic PW of each waveform was defined as the FWHM of an equivalent decaying exponential exhibiting the same rectified impulse as the induced current waveforms:

$$PW = -\ln(0.5)\frac{\int|R(t)|dt}{R_{max}}$$

- Peak absolute impulse

$$N_3 = \left|\int_0^t R(t)dt\right|_{max}$$

- Rectified total impulse

$$N_4 = \int_0^\infty |R(t)|dt$$

- Square root of action integral

$$N_5 = \left\{\int_0^\infty |R(t)|^2 dt\right\}^{\frac{1}{2}}.$$

- Signal energy

$$E = \int_0^\infty |R(t)|^2 dt.$$

Frequency-domain waveform parameters

- Peak spectral amplitude

The peak spectral amplitude corresponds to the maximum amplitude of the frequency spectrum of the waveform:

$$R_{max}(f) = \max(|R(f)|)$$

- Center frequency

The center frequency corresponds to the frequency at which $R_{\max}(f)$ is evaluated:

$$f_0 = f|_{|R(f)|=R_{\max(f)}}$$

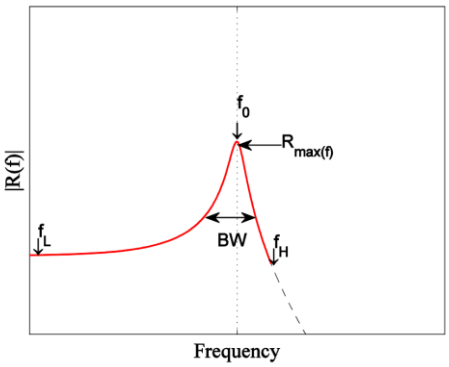

Figure 16: Frequency-domain parameters

- Band-ratio and bandwidth

By definition,

$$br = {f_H}/{f_L}$$

where the low- and high- frequency limits, f_L and f_H are defined as the smallest interval in which 90% of the energy is contained .
The interval between f_L and f_H is sometimes referred to as 90% energy bandwidth:

$$BW_{90} = f_H - f_L.$$

3.2.5 WP1: connection to protection system

Groupe-E protective strategy

This section briefly reports the protective strategy of MV networks at Groupe E.

Each feeder is individually protected by a three-phase circuit breaker (CB). Furthermore, a shunt circuit breaker is installed at the primary substation used to maintain the continuity of supply during a single line-to ground fault (potentially +56% considering also permanent faults). The shunt breaker is a simple circuit-breaker with single phase closing and tripping mechanism, which solidly connects the faulty phase to the substation ground, after the fault occurrence. The main idea and advantage is that, when the shunt operates, the fault voltage is stabilized and limited to a low residual value, and the capacitive current is drained back to the substation and the arc is quenched [8].

Regarding the specific protective functions used to identify the fault condition, Groupe E's strategy foresees the use of the ANSI 50 (i.e., instantaneous overcurrent) for short-circuits and the ANSI 67N (i.e., neutral directional overcurrent) for ground faults. Furthermore, the signals containing the information on the operation of the shunt circuit breaker is also available.

Interaction between the SEFL and the protection system

The protection system of the primary substation where the SEFL is installed can provide the fault locator with useful information and therefore we decided to connect the fault locator with the output of the protective relays. Indeed:

1. The information provided by the protection system can confirm the actual occurrence of the event to distinguish permanent faults and transient faults;
2. The protection system can identify the faulty line when the SEFL supervises more than one feeder, i.e. the fault locator is installed on a busbar that supplies several lines. This would improve the accuracy of the fault location algorithm and, at the same time, reduce the number of needed simulations;

3. The protective functions can indicate what type of fault has occurred (e.g., short-circuit or ground fault) and run the suitable fault locating algorithm (see also Section 3.2.8).

With reference to the first point, the idea was to use the information from the circuit breaker operation (any protective function) to confirm the actual occurrence of the fault and send the result of the fault locating algorithm only if the circuit breaker operated. This was done to consider the request of Groupe E who is not interested in knowing the occurrence of transient faults, but only permanent faults. This is also the case of many other utilities. Furthermore, such information would double-check the internal algorithm of the fault locator dealing with the identification of faults described in Section 3.2.3.

Regarding the second point, Table 3 shows that tripping and operation signals are available individually for each feeder and make it possible to identify the faulty feeder among the ones supplied by the same busbar. The use of such information makes it possible to search for the fault in the electrical model only along the faulty line, reducing not only the number of simulations, but also the probability of error (as it would be impossible to locate the fault on the wrong feeder).

Referring to the third point, Table 3 shows that tripping signals are available and make it possible to distinguish ground faults and short-circuits, using the logic reported in Figure 17. In case of ground faults, the conventional EMTR-based method [5] will be run. In case of short-circuit an ad-hoc method for phase faults will be used (see Section 3.2.8), which provide higher accuracy. More specifically, the logic of the appropriate method selection is shown at the top of Figure 17: if the overcurrent function ANSI 50 of any feeder tripped and, at the same time, none of the shunts operated, we consider the fault as a “short-circuit” and implements the method described in Section 3.2.8; contra-wise, if ANSI 50 has not tripped, the SEFL calculates the fault location by using the conventional EMTR-based method [5].

The bottom of the figure represents the logic of the permanent fault confirmation. Here we check both the faulty feeder and fault’s permanence by using the information about the circuit breaker and the shunt circuit breaker operation.

It is worth mentioning that, if such information is not available, the type of faults can be determined by considering the Fortescue components. To this end, we decided to include the Fortescue components’ calculation in the fault-locating algorithm. More than 70 measurements were tested in order to check this approach’s correctness.

Table 3: Protective functions and available signals at Groupe E

Protective function	**Available signals**	
ANSI 67N (neutral directional overcurrent)	- Protective function tripping - Circuit breaker operation	Each feeder has this protective function.
ANSI 50 (instantaneous overcurrent)	- Protective function tripping - Circuit breaker operation	Each feeder has this protective function.
Shunt circuit breaker (for arc quenching)	- Shunt circuit breaker operation	Each substation has a shunt circuit breaker.

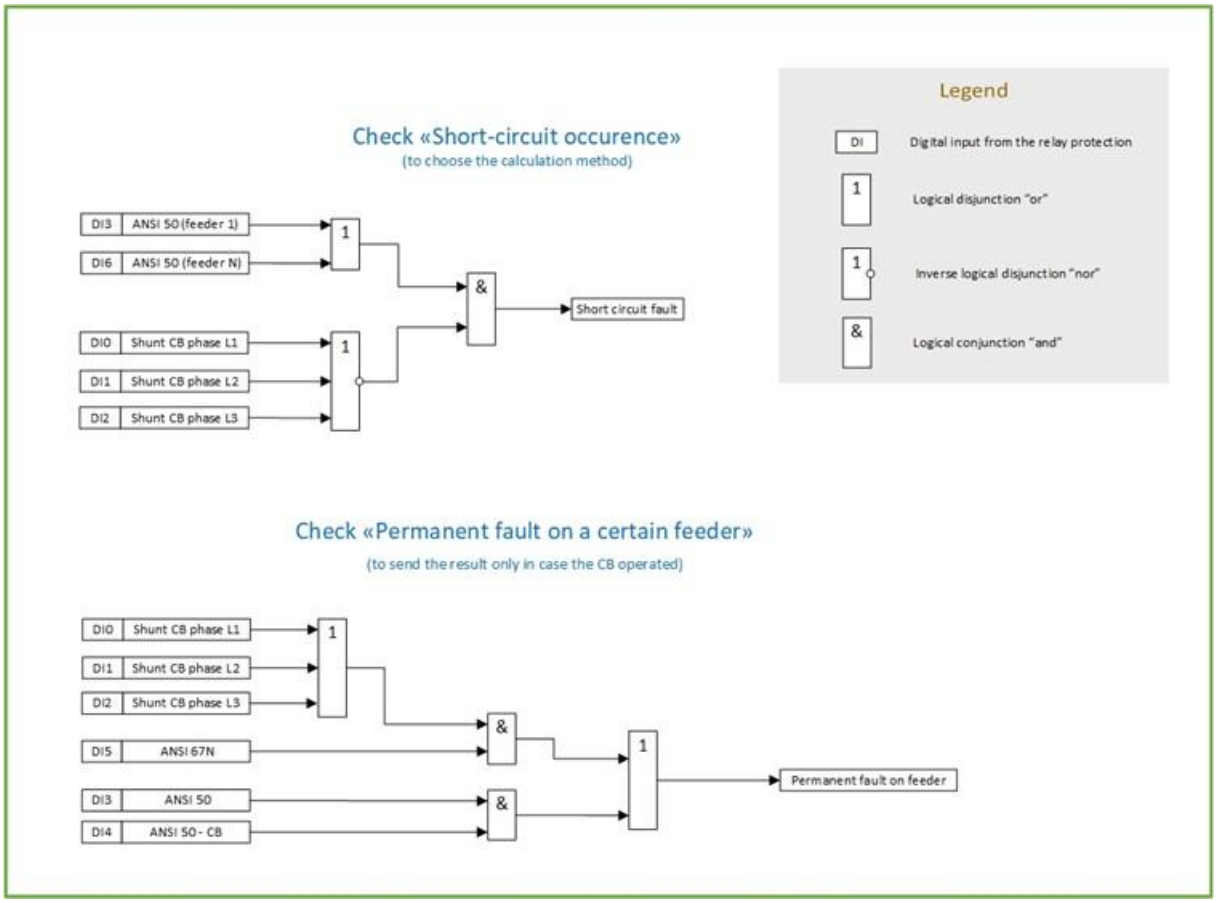

Figure 17: Logic to be implemented when connecting the protection system to the SEFL

3.2.6 WP2: connection to SCADA

Before starting this project (Nov. 2020), the user could check the fault location result by checking the SEFL software installed on the SEFL unit at the electrical substation. If an internet connection was available and allowed, the user could connect to the stand-alone device and check for the result remotely.

An essential step toward the development of a smart device is the integration of the fault location results into the SCADA (Supervisory Control and Data Acquisition) system. Indeed, as indicated by Groupe E, the result should be ideally gathered in real-time by the utility's SCADA system, generally accepted as a means of real-time monitoring and control of electric power systems. This would also avoid that sensitive information would be access from an external internet connection.

The objective of this work package was therefore to design a specific software function devoted to the communication with the SCADA system to integrate the SEFL result. The design considered:

- The compliance with at least one of the most common electrical standards to guarantee interoperability and security.
- That the result must be provided according to the nomenclature provided by the utility.
- That the SCADA system should be also able to send the real-time status of the switches along the line to infer the real-time topology to the SEFL system. The latter point is quite innovative, as usually the SCADA is meant only to receive and collect info, and not to communicate it to an outside device.

This work package turned out to be by far the most difficult part of the project in terms of organisation (different departments with different competences at both Streamer and Groupe E were involved), timing, and execution.
The main outcome of this WP is that the software architecture of SEFL has been radically changed.

First of all, for security reasons, SEFL has to be split into two physical locations (Figure 18):

- The controller and the DAQ (named SEFL Acquisition Unit) is placed in the substation. It is not possible to directly access to it remotely anymore;
- The computation unit (named SEFL Elaboration Unit) is placed at Groupe E's data center and is the fault locator 'heart': it is connected to the SEFL Acquisition Unit, the SCADA, and the utility's databases. By using a safe channel[2], an external user (like Streamer) can access it for maintenance purposes.

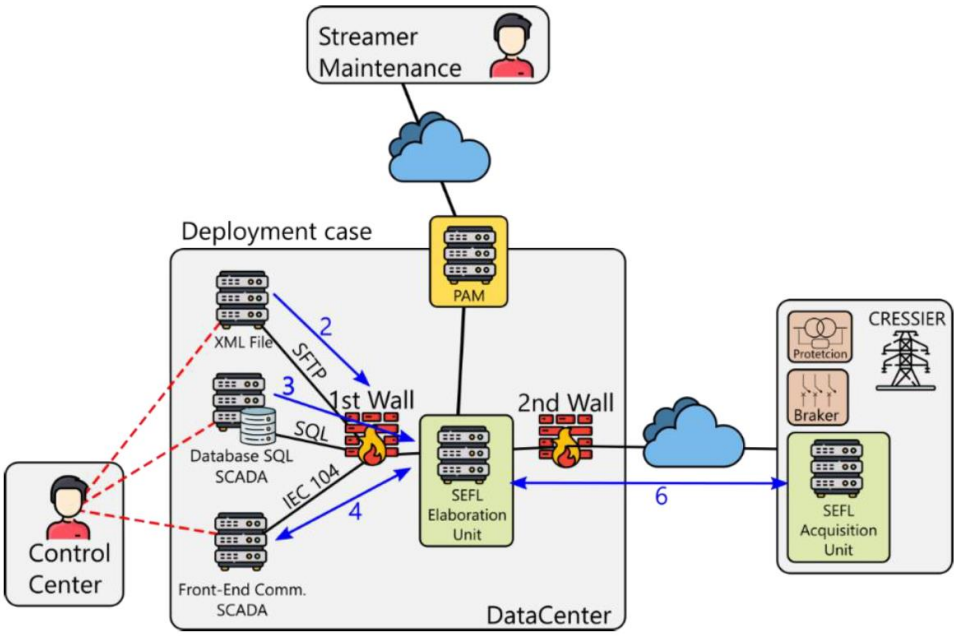

Figure 18: Architecture of the SEFL

Despite its complexity compared to the planned solution, we believe that this system architecture will be suitable for many utilities worldwide and therefore, even if the separation into two physical locations was not planned in the framework of this project (we had seen it as a further step), we decided to proceed and implement it.

Regarding the connection with the SCADA, as a standard, Groupe E selected the IEC 60870-5-104, which is widely use in Europe, China and several other countries and provides network access for IEC 60870-5-101 based on TCP/IP, which can be used for telecontrol tasks among control centers and substations.

The SCADA is a client of the SEFL Server and is responsible for establishing communication with the SEFL Server. The list of signals for information exchange between the SCADA and the SEFL Elaboration Unit (Table 4) is based on the SCADA operability list, and, as said, is bidirectional.

[2] At the moment, Streamer has access to the SEFL Elaboration Unit by using a site-to-site VPN tunnel.

Table 4: Data exchange SEFL-SCADA

Source	Type of signal	Description
SEFL	Monitoring, simple signal with time stamp, digital value	General SEFL alarm (operating problem)
SEFL	Monitoring, simple signal with time stamp, digital value	Detection of a fault on a given line
SEFL	Measurement, floating point (short), analogue value	Result of the fault location: Cable or Overhead line ID
SEFL	Measurement, floating point (short), analogue value	Result of the fault location: distance to the fault
SCADA	Control, simple command, digital value	Tripping of ANSI 67N on a given line
SCADA	Control, simple command, digital value	CB operation due to ANSI 67N on a given line
SCADA	Control, simple command, digital value	Tripping of ANSI 51 on a given line
SCADA	Control, simple command, digital value	CB operation due to ANSI 51 on a given line
SCADA	Control, simple command, digital value	CB operation due to ANSI 51 on a given line
SCADA	Control, double command, digital value	Shunt circuit breaker status on a given substation

It was also decided to access the status of the switches along the line to infer the real-time topology by using Groupe E's SQL database, which contains the real-time status of the switches along the MV lines updated every minute. Among others, the following information are extracted from the database and used:

- Switch ID;
- Switch name;
- Line name;
- Time stamp;
- Current switch status (to infer the real-time topology);
- Default switch status (to check the topology of the grid in normal operation).

It was decided that the SEFL software checks for updates in the Groupe E SQL database:

- every time that there is an event recorded by the SEFL acquisition unit;
- every *minute*; where *minute* is a given time in minute settable by the user.

Every time the switch status is updated, the event logger in the SEFL software stores this information. The EMTP-RV file describing the network topology, containing also the network topology with the switches along the line is updated accordingly and automatically.

3.2.7 WP3: connection to database

Innovative utilities, like Groupe E, have created data repositories of the distribution network stored in a database. The data stored in the database are updated due to physical changes in the grid (e.g. replacement of an overhead line section with an underground cable).

In this work package, the aim was to develop an automatic tool to connect the SEFL to the utility's database and input the needed data into our system. Specifically, the following steps were taken into account:

a) Create a local database (i.e., on the SEFL hardware) containing the needed data to build the EMTP-RV model (e.g., section length, conductor cross-section, etc…);
b) Create a connection with Groupe E database;
c) Weekly comparison of the difference between the actual and the previous database to update the local database accordingly;
d) Create a local tool able to organize and calculate the data according to data attributes needed by EMTP-RV subroutines.

The main activity of this work package dealt with the creation of an organized relational database in MySQL linked to the SEFL software, which can be used in the future for all utilities and contains the main data structure for the whole SEFL software (not limited to this work package). This was the first step of a more generic task that includes the creation of a more comprehensive database with also network data, following the steps a) – d) mentioned above.

In the case of Groupe E, the electrical features of the network are stored in a XML file, which contains detailed information about lines, branches, brakers, switches, fuses, loads, transformers, etc.. Each object contains all the information needed to infer the network topology. It was decided that access to this file is done using SFTP, in order to read the relevant data and to update the file if any change occurred.

3.2.8 WP4: improving the performance of the EMTR-based algorithm

In order to improve the accuracy, three approaches were used:

- The development of phase-to-phase and three-phase methodology
- The development of maximum cross-correlation sequence (MCCS) metric
- The study of line model refinement (replacement for the approach of machine learning)

<u>Phase-to-phase and three-phase methodology</u>

A different fault-locating approach was developed to locate short-circuits. Compared to the conventional EMTR-based methodology described in [5], two aspects were modified and adapted:

1. The definition of the guessed fault location (GFL);
2. The calculation of the energy of the fault current signals at each GFL;

depending on the type of faults, as mentioned in Section 3.2.5.

Regarding the definition of the set of guessed fault locations (first aspect), in this case, we define a set of guessed fault locations, but then we also group the guessed fault locations by 2 (if the fault is a phase-to-phase faults) or by 3 (if the fault is a three-phase fault). Figure 19 reports the three different situations.

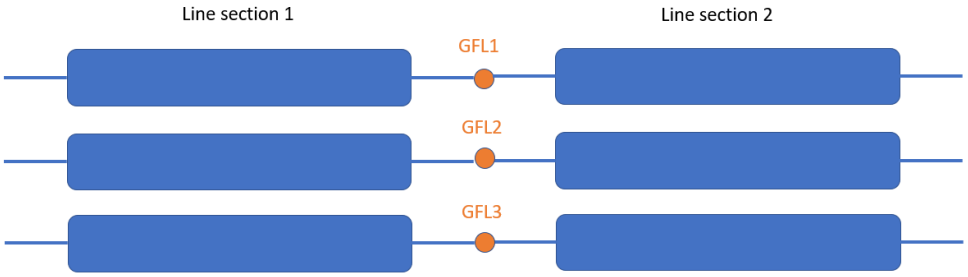

For line-to-ground faults -- we define three fault locations: GFL1, GFL2, GFL3.

For phase-to-phase faults -- we define three fault locations combinations: GFL1 – GFL2, GFL2 – GFL3, GFL3 – GFL1

For phase-to-phase faults -- we define one fault locations combination: GFL1 – GFL2 – GFL3.

Figure 19: Definition of guessed fault location

Regarding the calculation of the signal energy of the fault current associate at each guessed fault location (second aspect), Figure 20 shows the procedure used to calculate the signal energy of the original method, which can still be used for line-to-ground faults.

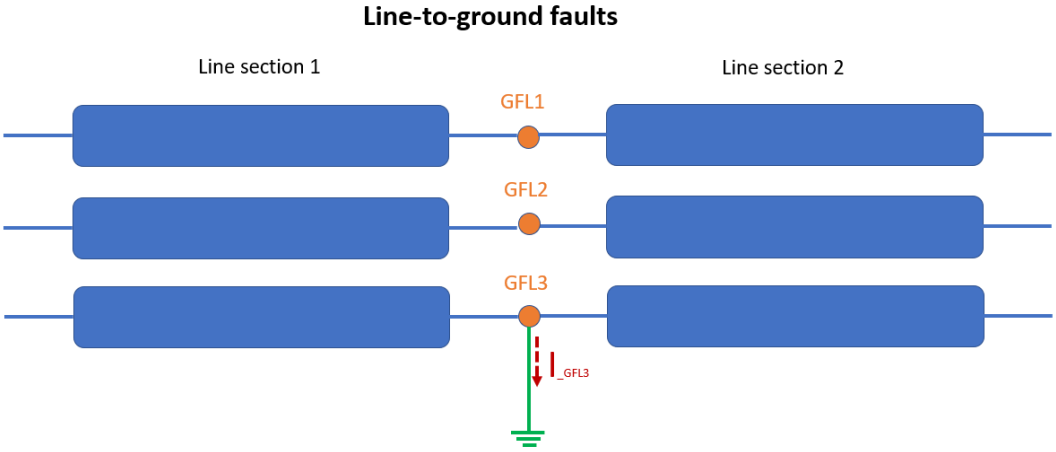

For each guessed fault location:

1. We create a connection to ground (here done only for GFL3, for the sake of simplicity) represented here by the green line.
2. We calculate the current flowing though ground $I_{\_GFL3}$, here represented by the red arrow.
3. We calculate the signal current energy.

Figure 20: EMTR procedure for line-to-ground faults.

In this case, instead of calculating the signal energy associate to each guessed fault location, we calculate the signal energy of the current flowing through ground through the two (if the fault is a phase-to-phase fault) or three (if the fault is a three-phase fault) guessed fault locations as defined in Figure 19. The next figures report the different situations: Figure 21 shows the procedure for phase-to-phase faults, while Figure 22 illustrates the one for three-phase faults.

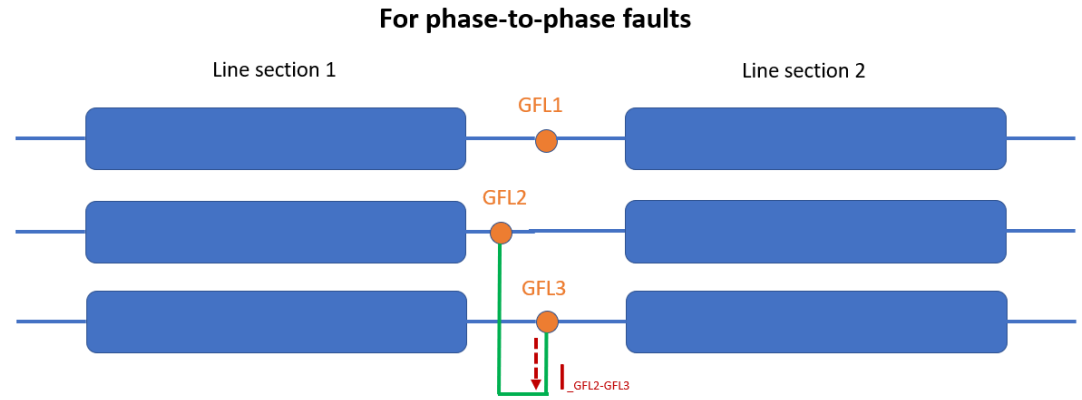

For each guessed fault location:

1. We create a connection between two phases without the connection to the ground (here done only for GFL2 - GFL3, for the sake of simplicity) represented here by the green line.
2. We calculate the current flowing though the connection $I_{GFL2\text{-}GFL3}$, here represented by the red arrow.
3. We calculate the signal current energy.

Figure 21: EMTR procedure for phase-to-phase faults

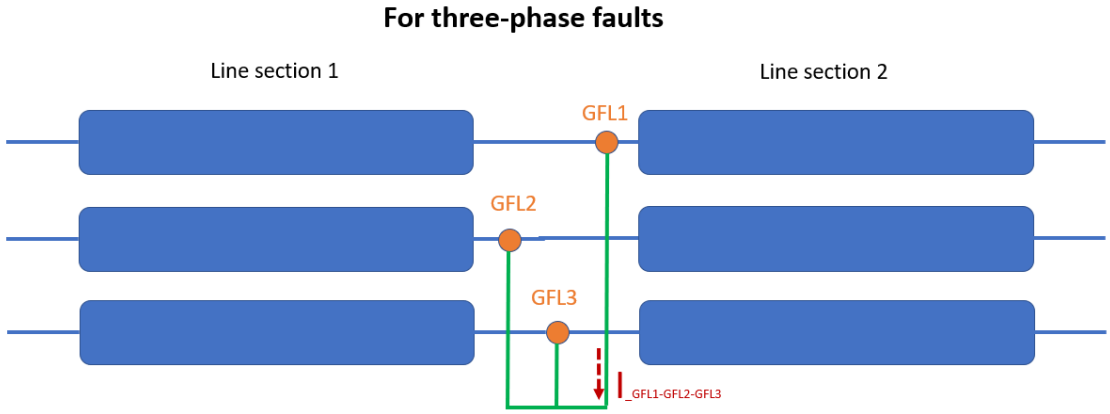

For each guessed fault location:

1. We create a connection between three phases without the connection to the ground, represented here by the green line.
2. We calculate the current flowing though the connection $I_{GFL1\text{-}GFL2\text{-}GFL3}$, here represented by the red arrow.
3. We calculate the signal current energy.

Figure 22: EMTR procedure for three-phase faults.

There were several natural faults during the monitoring phase of the line operated by the Russian DSO, including phase-to-phase faults. Thanks to this, we had a possibility to compare the new fault-locating approach with EMTR-method for short-circuit faults calculations and estimate its advantages for such events. As an example, in the case of a phase-to-phase fault got during monitoring stage due to tree

branches on the line, “short-circuit method” gave the fault location error 250 m, when conventional EMTR-method for this type of fault showed 1050 m.

Maximum cross-correlation sequence method

As described in Section 2.1, the main steps of the EMTR-based fault location methods can be summarized as follows:

i. The forward-propagation stage or direct time. In this step, the fault-originated transients are measured at a single observation point.

ii. The backward-propagation stage or reverse time. In this step, the measured transients are time-reversed and back-injected by simulation into a numerical model of the target power network.

iii. The fault location is identified using an appropriate criterion or metric which quantifies the refocusing of the backward-propagated waves.

EMTR-based fault location metrics

Various metrics have been proposed to quantify the time-reversed transients refocusing at the original fault location. Razzaghi *et al.* proposed in 2013 the metric of fault current signal energy (FCSE) which allows to identify the fault location by examining the maximum energy of the fault branch current [5]. He *et al.* proposed the fault current signal peak amplitude as an alternative metric to deal with situations where fault-induced transients are limited by a low signal-to-noise ratio [10]. A theoretical study was presented to infer the correlation between the transfer functions formulated in the direct and reversed times, respectively [11]. Taking advantage of the similarity between the back-injected time-reversed transients and the fault current signal, a metric named the maximum of cross-correlation sequences was proposed in [12], [13]. The direct-time transfer function in [11] and [13] is defined as the ratio of fault-originated transients [denoted by $V_0^{\mathrm{DT}}(t)$] to the fault current. The input and output of the reversed-time transfer function are the time-reversed copy of $V_0^{\mathrm{DT}}(t)$ and its induced fault current observed at a guessed fault location, respectively. Besides, Zhang *et al.* introduced the concept of the so-called mirror lines, according to which the fault location is identified by a set of root mean square (RMS) metrics, such as the RMS value of the fault current signal that is constructed by assuming the targeted line lossless [14]. Inspired by emerging studies of time-reversal in mismatched or changing media (e.g., [15]), the concept of lumped mismatched media was recently introduced to fault location, resulting in two novel metrics, namely the bounded phase [16] and the mirrored minimum energy [17].

The maximum of the cross-correlation sequence (MCCS) metric

It is proved that there exists a similarity characteristic in the process of applying the EMTR technique to locating faults in power networks. The similarity characteristic demonstrates that the fault current at the fault location exclusively behaves as a quasi-scaled copy of the time-reversed back-injected transient voltage [13]. Based on the similarity characteristic, a metric named the maximum of the cross-correlation sequence (MCCS) was proposed. The metric is the cross-correlation between the back-injected voltage signal and the fault current signal simulated at the guessed fault locations to quantify the level of similarity and to identify the true fault location [13].

The step-by-step procedure of implementing the MCCS metric is summarized in a pseudo-algorithm presented as follows.

Pseudo-algorithm of EMTR-MCCS metric

Input:	network topology, parameters, and guessed fault locations $\boldsymbol{x_{\mathbb{G}}}$
	fault-originated transients $\boldsymbol{V_0^{DT}(t)}$, $\boldsymbol{t \in [0, T]}$
	time-reversed copy of $\boldsymbol{V_0^{DT}(t)}$, namely $\boldsymbol{V_0^{TR} = V_0^{DT}(-t + T)}$,
for	each *a priori* $\boldsymbol{x_g \in x_{\mathbb{G}}}$, do
	1: simulate the fault current $\boldsymbol{I^{RT}(x_g, t)}$ using network model and $\boldsymbol{V_0^{TR}(t)}$
	2: compute the MCCS metric
	$$\boldsymbol{R^m(x_g) = \max\left\{\sum_{k=0}^{K} V_0^{TR}[(k+l)\cdot \Delta t]\cdot I^{RT}(x_g, t)\right\}}$$
	$\boldsymbol{K = T/\Delta t,\ l = 0, \pm 1, \pm 2, \ldots, \pm(K-1)}$
end	$\boldsymbol{x_{f,estimated} = \arg|_{x_{\mathbb{G}}} \max[R^m(x_{\mathbb{G}})]}$
Output:	$\boldsymbol{x_{f,estimated}}$

The MCCS metric assesses the time-domain similarity between $\boldsymbol{V_0^{TR}(t)}$ and $\boldsymbol{I^{RT}(x_g, t)}$ in the time scale of the duration of the back-injected transients, namely $\boldsymbol{T}$. In other words, the MCCS metric requires simulating the fault current signal only in the duration of $\boldsymbol{T}$, as opposed to the fault current signal amplitude or energy metrics (e.g., [5], [16]) requiring the observation of the full waveform of $\boldsymbol{I^{RT}(x_g, t)}$, whose duration is generally twice as long as $\boldsymbol{T}$. As a result, the MCCS metric provides an advantage over the classic metrics in terms of computation efficiency. More specifically, it reduces the simulation time consumption *per* guessed fault location and, thus, benefits a faster response in identifying fault occurrences.

Machine learning approach

Initially, one of the approaches to improve the accuracy of fault location was applying artificial intelligence (AI) to the problem of fault localization on the line. In order to realize the idea, the following method had been chosen: to generate fault events by using numerical simulations in a digital line model. Starting with the application of AI models in direct time model we would verify its performance and consider an option to extend the approach by combining it with the technique used in the current algorithm of the system.

However, the accuracy of the line modelling is the key basis for any algorithm and approach. It was decided that we test different ways of modelling in order to find the most accurate one and be sure that the error in fault location coming from line modelling is small as possible. It means that the model is supposed to be improved aiming it to not be the main source of errors in the fault location accuracy and we reduce the impact of this component to the total accuracy. In order to move in the direction of the model refinement, we came up with the study that includes pilot tests on the line using a pulse generator. By injecting a signal of a certain shape from the generator into a real line and repeating the same in the digital model, we change the parameters and properties in the line model, achieving the maximum match between the responses of the injected pulses in both cases (see Section 4.2). Having achieved the maximum match in the reflectograms, we thereby make the model more accurate and close to the real one. Thus, the work is focused on line model calibration and described in Section «Network model refinement» below.

Network model refinement

In order to study the accuracy of the mathematical model of the line, tests with the voltage pulse generator were carried out on the real line.

Objectives of the pilot test: injection of 8/20 μs voltage pulse with amplitude 8-10 kV to the different locations of the real line. Spreading and reflecting along the line, the injected pulse is recorded and measured by sensors G&W ALTEA CVS-24-O-HF installed at the primary substation.

Purpose of the pilot test:

- measure reflectograms (waveforms) of the signal that contain the information about the reflections of the pulse from line sections with different electromagnetic properties, as well as about the speed and attenuation of the test pulse;
- simulate a pulse with similar characteristics and at the same injection location in the digital line model and obtain the corresponding reflectograms;
- analyze the received data and compare reflectograms in order to refine the digital model of the line, i.e. the line parameters and the line modeling method.

Despite the fact that the experiment was not conducted on the Groupe E line, but on another overhead line, it will allow us to evaluate the accuracy of mathematical models in the EMTP-RV, which are used to build any lines.

The tested line is considered as simple, that is good for the tests: the total line length is 11 km with 3 considering branches, composed with only overhead conductors of the same type and different line cross-section. The line has the disconnectors installed along the line, which was used as a tool of line configuration change. Thus, two sets of disconnectors placed on the line were used to create two different line configurations:

- line section 3.7 km length;
- line section 7 km length.

Pulse voltage generator 10 kV (PG-10)

The mobile PG-10 was assembled according to the Marx generator circuit and tested in the Streamer's own laboratory (Figure 23). The PG-10 is charged by 220 V AC voltage and gives a voltage pulse of 8/20 μs (Figure 24), it has outputs for the connection to the overhead line wire and a remote control panel for safe operation.

The 8/20 pulse has been chosen as the test pulse for the following reasons. For quality recording of the waveform response, the length of the injected pulse should not be too long to avoid a noticeable overlap of reflections on the final voltage. The pulse length should not be too short, so that it does not lead to a strong attenuation of the pulse. Preliminary calculations on the model showed that the 8/20 pulse is well suited for the original problem. Moreover, the 8/20 pulse is known as a test pulse and is not questioned by grid companies.

Figure 23: Mobile voltage pulse generator in the durable box

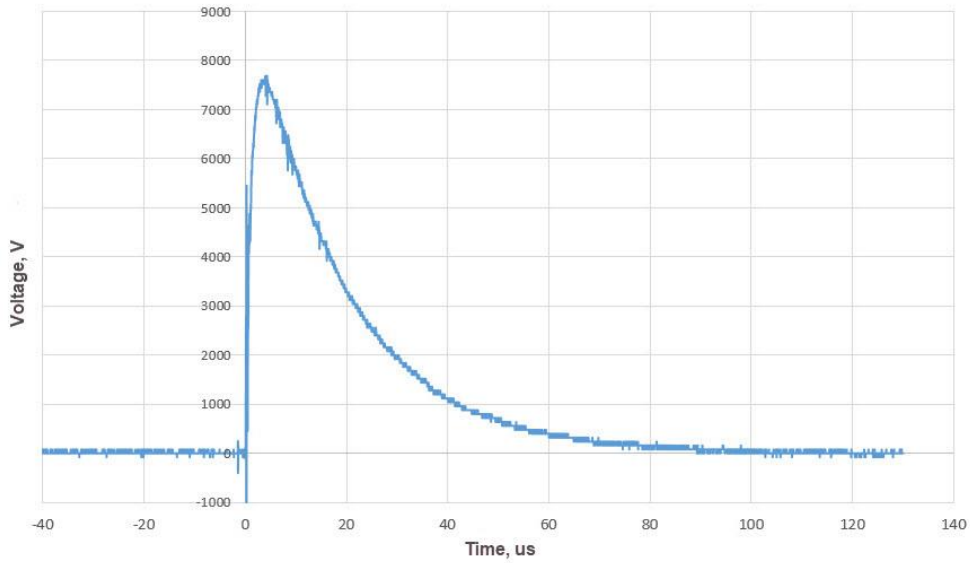

Figure 24: Voltage pulse 8/20 µs

Line configuration and test program

The schematic of the experimental line and the locations where the pulse generator was connected are shown in Figure 25.

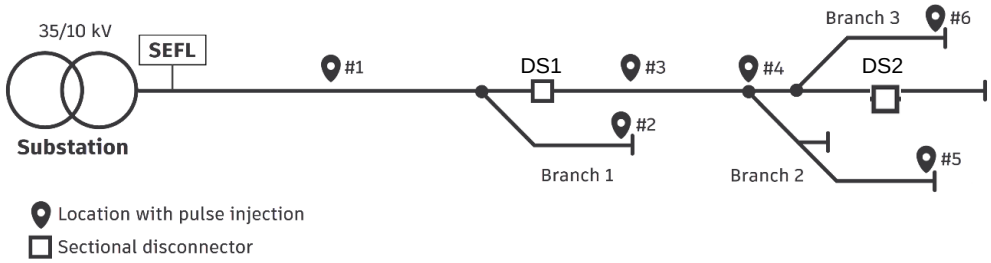

Figure 25: OHL diagram with test locations

The test program consisted of 6 injection points, each with 3-4 experiments for the reliability of measurements (Table 5). For experiments #1-2 a part of the line was separated by a disconnector DS1, so for these experiments, the response oscillograms were recorded on the line section with the length 3.7 km. For the experiments #3-6 the line configuration was created by opening the disconnector DS2 forming a section with the 8.8 km length.

Table 5: Experimental tests with the pulse generator

#	Point of injection	Number of injections	Distance of the injection point from the substation	Full section length
# 1	Pole 28	4	1526 m	3705 m
# 2	Branch 1 (025)	3	3279 m	3705 m
# 3	Pole 75	4	4475 m	8787 m
# 4	Pole 92	4	5575 m	8787 m
# 5	Branch 2 (061)	4	6355 m	8787 m
# 6	Branch 3 (070)	3	6280 m	8787 m

Figure 26 shows a photo from the tests: the process of connecting the PG-10 terminals to one of the phases of the 10 kV overhead line for experiments #3 and #5.

Figure 26: Photo from the test sites: connection of the pulse generator to the overhead line.

The description of the results obtained during the pilot test with the voltage pulse generator and further analysis is presented in Section 4.2 WP4: Improving the accuracy of the fault location

3.2.9 WP5: monitoring phase

As foreseen by the project schedule, in the second year of the project, there was a monitoring phase: the prototype is monitored on a daily base to collect possible issues on software and hardware to check the correct behaviour of the software developed in WP1÷ WP4. If a fault occurs, Groupe E will also share the automatic report issued by its control centre to check the SEFL result of the fault location.

First, the SEFL system was installed at Groupe E primary substation. The installed equipment is described in Section 3.2.1. The software developed and updated during the previous work packages is installed on the SEFL prototype.

Once per week, Streamer connected remotely by the software TeamViewer to the prototype to follow next behaviour:

- The SCADA system should be able to send the real-time status of the switches along the line to infer the real-time topology;
- SEFL should be able to communicate the result of the information regarding the fault location if a fault occurs;
- Once a change occurs in Groupe E cloud database, SEFL should be able to update and/or calculate the data used to build the network model in the EMTP-RV software environment daily.
- Connect the SEFL to the Groupe E database to automatically input the needed data into the SEFL system.

3.2.10 WP6: pilot test

Again, to assess the performance of the prototype under operation two test campaigns were carried out at known network. The test network is operated with isolated neutral system with shunt circuit-breaker at 18 kV substation. The fault locator was placed at the substation, where voltage sensors were situated at the busbar connected with three feeders and supplied by the same transformer in the primary substation. The feeders are non-homogeneous and 33% of the total line length is composed of underground cables.

The first pilot test was the field test and carried out on Groupe E's grid, creating single-phase-to-ground faults. During this pilot test voltage waveforms of the artificial faults were measured and recorded by SEFL.

The second pilot test was aimed to test the new functionalities implemented in the software and the approaches of the accuracy improvements. Thanks to the monitoring phase and the first pilot test, mostly software functionalities were tested during this second pilot. Another measure of the prototype performance such as applying of methods of accuracy improvement to the faults can be achieved thanks to the offline simulations in the software. In order to meet the objectives of the second pilot test, Streamer and Groupe E agreed to take advantage of continuous monitoring on the line and use the recorded waveforms from the first pilot test data.

First pilot test

Phase-to-ground faults are realized by using a 24-kV ABB medium voltage circuit-breaker to create direct contact between the phase and the ground, allowing the line current to flow from the phase to ground. The duration of the fault is set by Groupe E at 2 seconds.

As most of the faults are resistive faults, a resistor is added in series. The resistor consists of a base electrode at the bottom of the mold and two peripheral copper rings (Figure 27). The resistor is filled with a mix of salt and water. The value of the resistance is given by the way in which the base electrode and the peripheral electrodes are connected (e.g., in series or parallel) and the amount of salt melted in the water. The values of the resistances are described below in the tables.

Figure 27: The resistor is used for a fault creation

The first pilot test was carried out in the beginning of the monitoring phase. There were three configurations of the line during the pilot test: first configuration with all three feeders connected to the busbar at the same time and two configurations with only one feeder connected to the busbar, i.e. circuit breakers of other two feeders were opened at the time of faults. The faults were created at 3086 m, 2500 m and 1668 m from the substation for each configuration respectively. Table 6 shows different line configurations and organized faults on them with the following characteristics.

Table 6: Topology and fault information for a line configuration

Topology	Location and distance from the substation	Test number	Fault type	Resistance
3 feeders : Feeder E Cormondes + Feeder A Courlevon + Feeder B Rainoz	Feeder E Cormondes 3086 m	# E_1	Phase-to-ground	$R = 0\,\Omega$
		# E_2	Resistive phase-to-ground	$R \approx 34\,\Omega$
		# E_3	Resistive phase-to-ground	$R \approx 68\,\Omega$
Feeder A Courlevon	Feeder A Courlevon 2500 m	# A_1	Phase-to-ground	$R = 0\,\Omega$
		# A_2	Resistive phase-to-ground	$R \approx 34\,\Omega$
		# A_3	Resistive phase-to-ground	$R \approx 68\,\Omega$
Feeder B Rainoz	Feeder B Rainoz 1668 m	# B_1	Phase-to-ground	$R = 0\,\Omega$
		# B_2	Resistive phase-to-ground	$R \approx 34\,\Omega$
		# B_3	Resistive phase-to-ground	$R \approx 68\,\Omega$

In order to describe the fault location procedure in the SEFL system, the main steps of the fault location platform are presented:

1. *Measurements* by high-frequency voltage sensors and data acquisition.
2. *Smart trigger.* The triggering system implemented into the software has registered high-frequency transients caused by faults. The waveform of three-phase voltages measured at

Cressier substation busbar at the moment of phase-to-ground fault is presented in Figure 28. As the single phase-to-ground fault originated in the network with isolated neutral system, the voltages action was as foreseen: voltage of faulty (or grounded) phase dropped to zero and voltages of two others phases increased to the square root of 3 from nominal values ($\sqrt{3}V_n$).

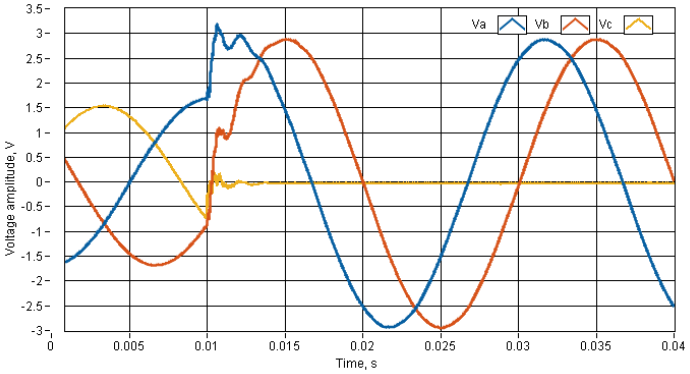

Figure 28: Three-phase voltage transient waveform at the moment of fault during test #E_1 (R=0 Ω)

3. *Signal filtering.* Once the voltage waveform is identified and recorded, the transient part of the waveform is taken for further post-processing. Usually 2 seconds duration of the transient part is used in the algorithm. The low-frequency components are removed from the curve by using fourth-order high-pass Butterworth filter. The filtered signals can now be used by the SEFL software to implement the fault locating algorithm based on the time-reversal theory, following the steps described in the previous paragraph. The filtered signals are time-reversed following EMTR-theory. The example of reversed and filtered signal is shown in Figure 29.

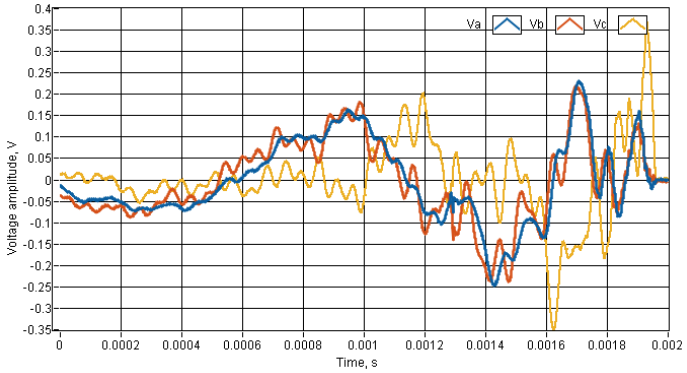

Figure 29: Three-phase voltage transient waveform at the moment of fault during test #E_1 (R=0 Ω)

4. *Fault location result*. When the voltage transient of a fault is processed, the algorithm makes simulations by using third-party software EMTP-RV and calculates the energy of the current signal. The highest signal energy indicates the fault location. Figure 30 shows the signal energy

graph for Test #E_1, where the highest signal energy belongs to GFL #18 but the fault was organized at GFL #12. The fault location error here is 1200 m.

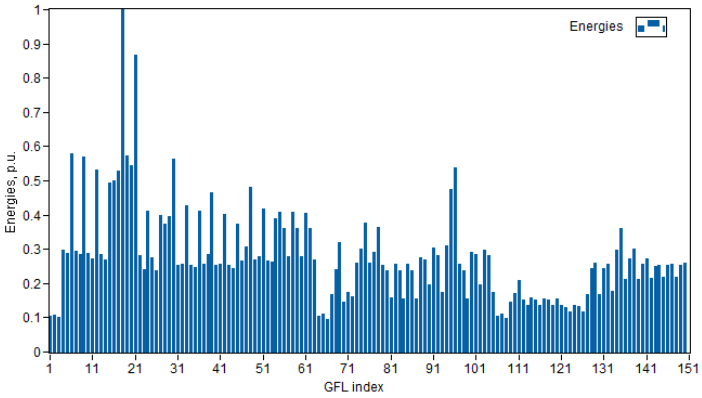

Figure 30: Signal energy graph for Test #E_1

The table with the results of fault location for all tested cases along with the results of the second pilot test are presented in Table 11 the Section 4.2.

Second pilot test

As mentioned above, the second pilot test is planned in order to test the implemented functionalities of the software and the approaches of the accuracy improvements. Therefore, we apply and process previously recorded data as a fault event and test updated SEFL software and subsystems integration.

Information exchange with the SCADA

Two fault cases measured during the first pilot test were used for the testing of the functionality to communicate the result to SCADA system. For the realization of the connection between SEFL and SCADA systems at Groupe E the correspondence table between SEFL's nomenclature and Groupe E's line sections was created. In the process of the development, it was agreed that the result must be provided according to the nomenclature provided by Groupe E and it should be the name of line sections in a form "LRMTXXXX_X". In most cases one "SEFL" name corresponds two names of Groupe E, i.e. SEFL name (e.g. 01_006A) is located between "LRMT2499-1" and "LRMT2500-1", as shown in Figure 31.

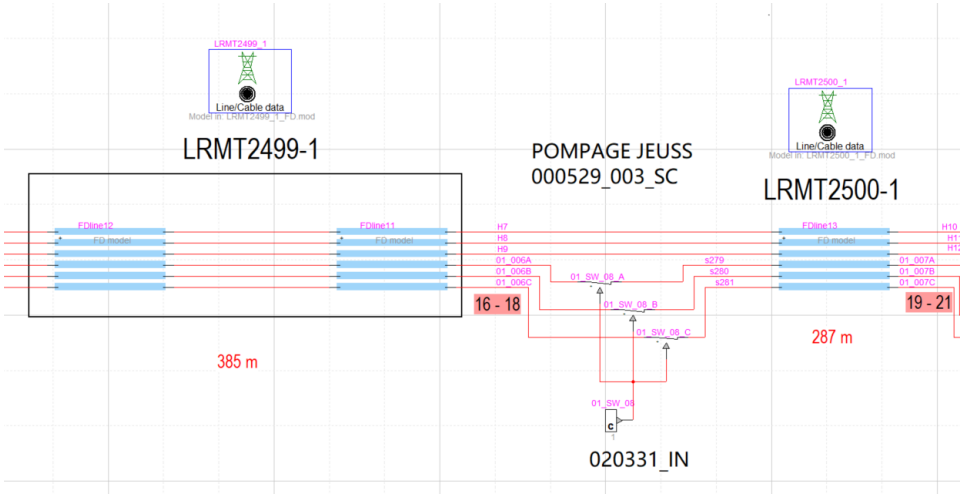

Figure 31: Sections LRMT2499-1 and LRMT2500 in Groupe E line model

Table 7 shows a fragment of the correspondence table between names of SEFL and Groupe E for the indication of a fault location on the line.

Table 7: SEFL and Groupe E names for the designation of a fault location on the line

Test number	SEFL's name	Groupe E's name	Groupe E's name
# E_1	01_006C	LRMT2499_1	LRMT2500_1
# B_1	03_006A	LRMT4373_2	-

The first test case is the one with the configuration of 3 feeders model and the single-phase-to-ground fault uploaded as a simulation of a real fault occurred on the line.

1. SEFL platform.
    - The file with the fault measurements from the test #E_1 was uploaded to the platform for the reproducing the real fault and calculation of the fault location result.
    - The model is three feeders connected to the busbar at the substation at the same time.
    - Cormondes - the faulty feeder.
    - The fault location platform with the result calculated (marked in red rectangular) is presented in Figure 32.

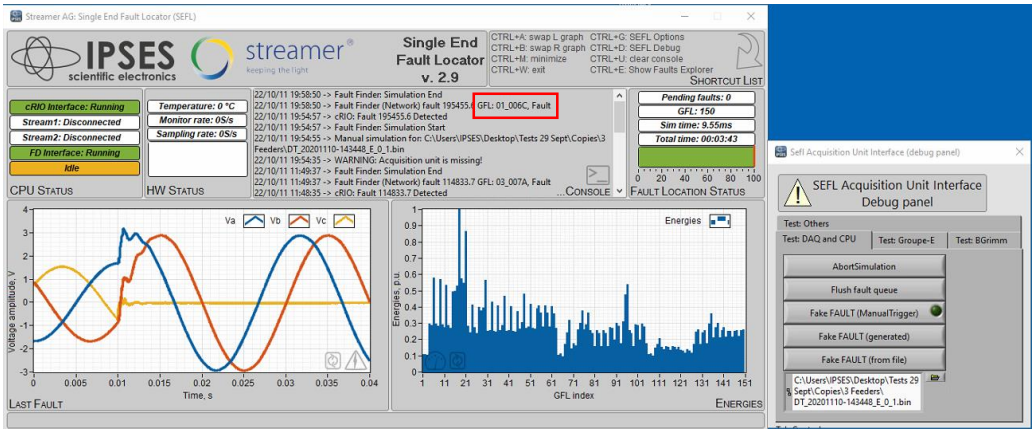

Figure 32: Fault location platform SEFL with the calculated result for the test #E_1

2. HMI of SCADA system.

    On the side of Groupe E the correctness of data transferring to SCADA and its visualization was checked.

    In Figure 33 the SCADA HMI is presented, where the following elements refer to the fault:

    a. The name of the faulty feeder (Cormondes) at top of the window.

    b. As soon as the signal arrives the SCADA platform, the indication "AL" turns into red color (left corner of the window).

    c. The name of faulty line section is displayed in the left corner of the HMI according to the correspondences between SEFL and Groupe E's names (Table 7).

    d. Since a line topology is available in SCADA system, the fault location is also specified by cross mark directly at the feeder.

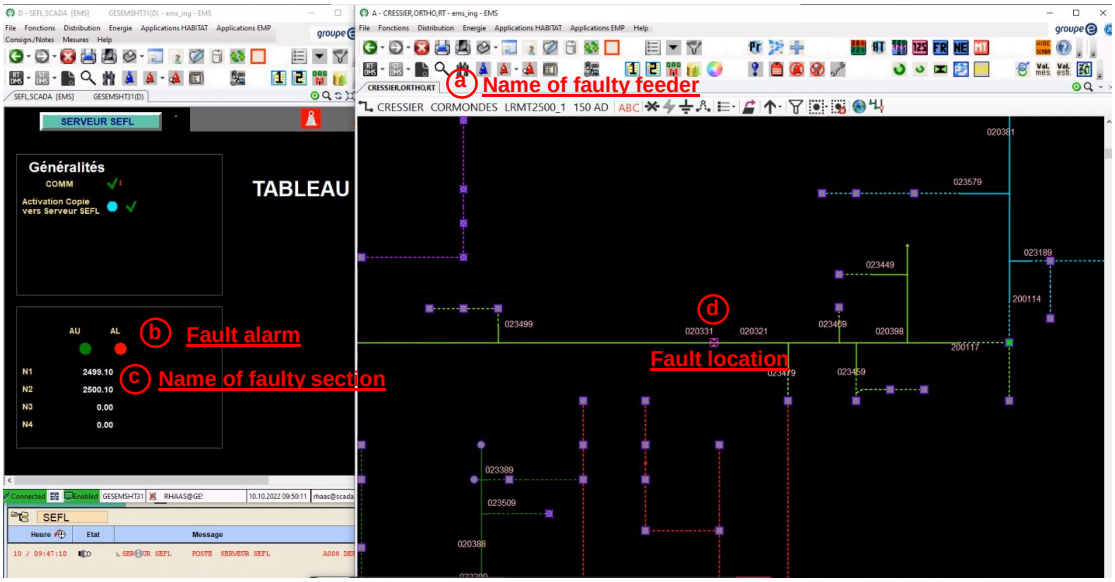

Figure 33: SCADA interface of Groupe E for the test #E_1

Another simulated test case was the single-phase-to-ground fault #B_1, when one feeder was connected to the busbar and the circuit breakers of other two feeders were disconnected.

1. SEFL platform.
    - The file with the fault measurements from the test #B_1 was uploaded to the platform for the reproducing the real fault and calculation of the fault location result.
    - The line configuration is one feeder connected to the busbar at the substation.
    - Rainoz - the faulty feeder.
    - In Figure 34 the fault location platform with the result calculated is presented (marked in red rectangular).

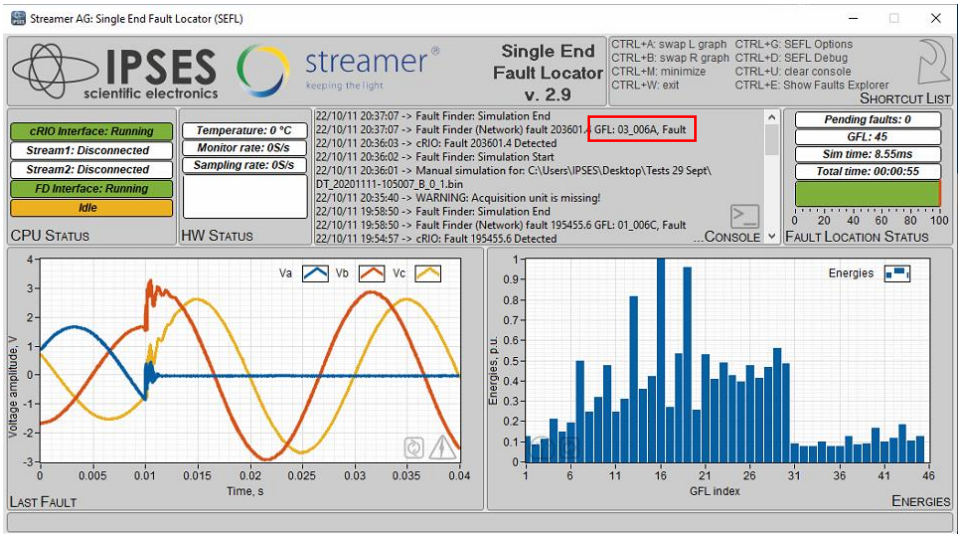

Figure 34: Fault location platform SEFL with the calculated result for the test #B_1

2. HMI of SCADA system.

   The fault alarm and message with the location of fault are sent to the SCADA system. The Figure 35 shows the SCADA interface of the fault event.

   a. The name of the faulty feeder (Rainoz) at top of the window

   b. As soon as the signal arrives the SCADA platform, the indication “AL” turns into red color (left corner of the window).

   c. The fault location is displayed in the left corner of the HMI according to the correspondence Table 6 between SEFL and Groupe E’s names. As the fault location is in the end of the feeder’s branch, the name of line section is only one.

   d. The location is also specified by cross mark directly at the feeder.

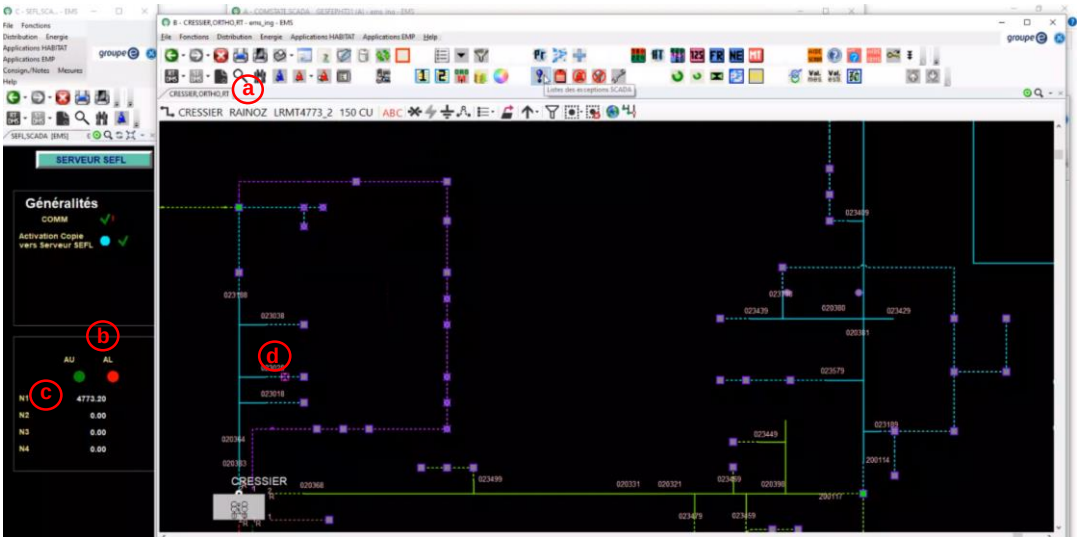

Figure 35: SCADA interface of Groupe E for the test #B_1

Real-time grid topology from the SCADA

The SCADA system should be able to send the real-time status of the switches along the line to infer the real-time topology to the SEFL system. This is necessary to update the network model at the time of the fault occurrence and use the actual one for the fault location calculation. In order to match the names of switches located along the network and the ones used in the SEFL model, the correspondence table was created. The fragment of the table is shown in Figure 36, where comma-separated names of Groupe E and SEFL are presented.

1	UtilitySwitchID, NetlistSwitchID
2	020368_IN, 01_SW_01
3	023499_IN, 01_SW_02
4	000529_003_SC, 01_SW_03
5	000529_001_SC, 01_SW_04
6	000525_001_SC, 01_SW_05
7	000525_002_SC, 01_SW_06
8	000524_001_FX, 01_SW_07
9	020331_IN, 01_SW_08
10	020321_IN, 01_SW_09
11	023479_IN, 01_SW_10

59	CB-CRESSIER-018_DJ-C08_DJ, 01_SW_28
60	CB-CRESSIER-018_DJ-C07_DJ, 02_CB
61	CB-CRESSIER-018_DJ-C09_DJ, 03_CB

Figure 36: Fragment of the correspondence table for switches on the line

Once a switch changes its position in network, the SEFL elaboration unit uses the correspondences to actualize this in the line model as well as in the log store. To try this functionality during pilot test, the

circuit breaker of the feeder Cormondes was currently opened. This change is visible in the console of the software (shown in red rectangular in Figure 37) and saved respectively.

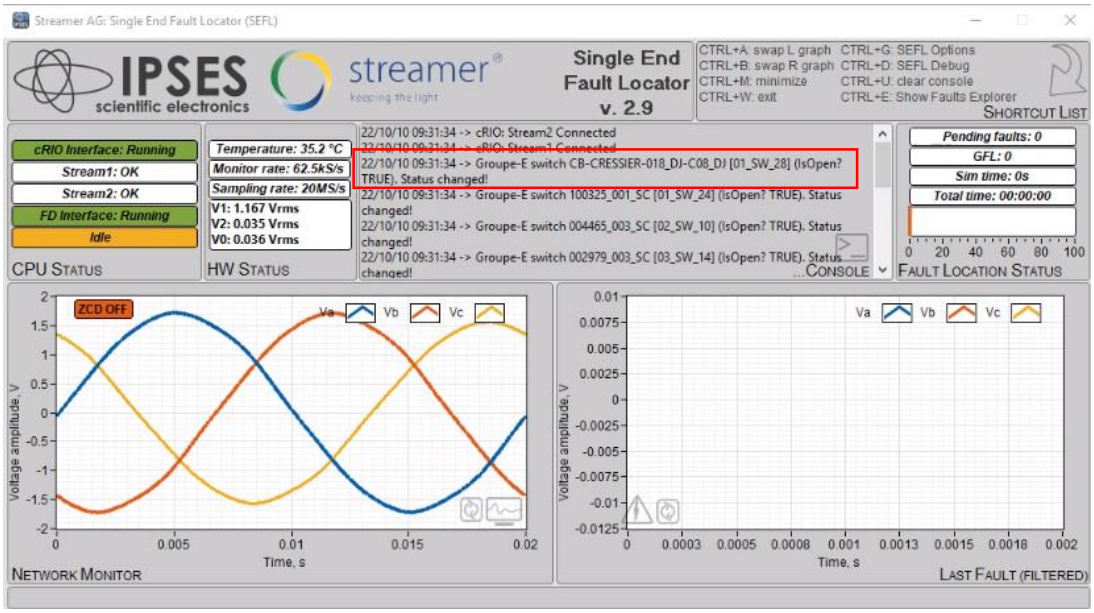

Figure 37: SEFL software interface where the updated status of the switch 01_SW_28 is presented n the console

3.2.11 WP7: evaluation and adjustment

In order to evaluate, improve developed functionalities and achieve a software operation without errors and bugs, the updated software was monitored during WP5 and WP6, as well as post-release tested. During monitoring period various types of adjustments and improvements were done related to different functionalities. Main revisions are presented in Table 8.

Table 8: Adjustments of the SEFL software during monitoring phase

#	WP#	Functionality	Issue	Cause/comment	Solution
1	WP2	Feeder Selector	Wrong model used for calculations: three feeders were calculated instead of only faulty feeder.	The feeder selector functionality was disabled (human factor).	To implement the option panel in the main software window with the information about switched off/on functions.
2	WP1 WP2	Trigger and Feeder Selector	Failure of time synchronization with NTP server.	NTP server was unreachable.	To get an access to NTP server inside of the utility network (Groupe E).
3	WP4	Calculation of Fault location result	Some signal energies (what is the result of fault location) are not calculated.	The third-party program EMTP-RV that participate in calculations, crashed at some iterations of signal energy calculation.	Implementing of a function to retry calculation if .mda file is not created.
4	WP2	SCADA	The message about fault in SCADA was cleared after 90 seconds. After the cleanup the system should wait other 90s to notify a message.	This leads to a delay in the notification about fault.	To get the system ready to send the second message after first message cleared in 90 seconds.
5	WP1	Additional module: Second busbar/ Current measurement	In case when the module is not used in the installation the user needs to load the same network models to both cells.	Time consuming and high error probability.	To make the function optional.
6	WP1	Pending faults	When multiple recordings of an event occur in a row, some of them can be missed while transferring from acquisition unit to elaboration unit.	The improvement of SEFL software performance.	To develop options with pending faults that are awaiting processing.

4 Results and discussion

Section 4.1 and Section 4.2 describe the results and evaluation of the project goals of WP1 – WP4. Section 4.1 describes the results related to the new functionalities integrated to the SEFL software and that were initially applied. Section 4.2 outlines the results and research findings related to fault location accuracy. The monitoring phase (i.e., WP5) and the pilot test (i.e., WP6) serve as an evaluation of the project goals and will be *italicized* in the description below.

4.1 Development and implementation of the SEFL software

The SEFL Elaboration Unit (SEU) developed so far, based on the activities described in Section 3 , consists of an application running the FPGA, the real-time target, and the server. It is developed in LabVIEW environment, MySQL and .NET, and composed of more than 800 files over the three programs. In the framework of this project, the following software parts were developed:

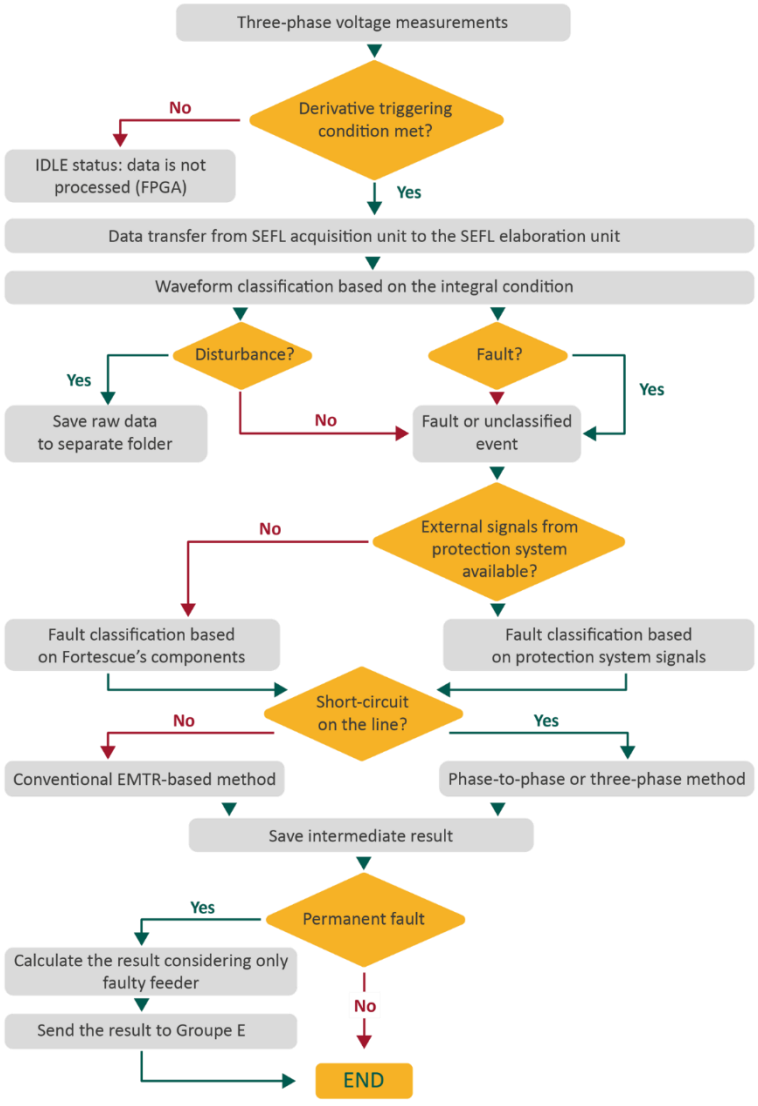

Figure 38: Flow chart of with the logic of the main algorithm to be implemented into the SEFL software

In particular, the System Elaboration Unit provides the following functions:

- Providing a user interface with a control dashboard;
- Managing the control settings and parameters;
- Keeping track of data stored in the application's shared memory (databases, incoming network data, etc);
- Managing the control and the communication with the DAQ (controller Compact RIO) subsystem;
- Controlling the fault finder subsystem and manage system resources when running the simulations that are used in the fault location module.

The software parts developed in the framework of this project are reported in Figure 39.

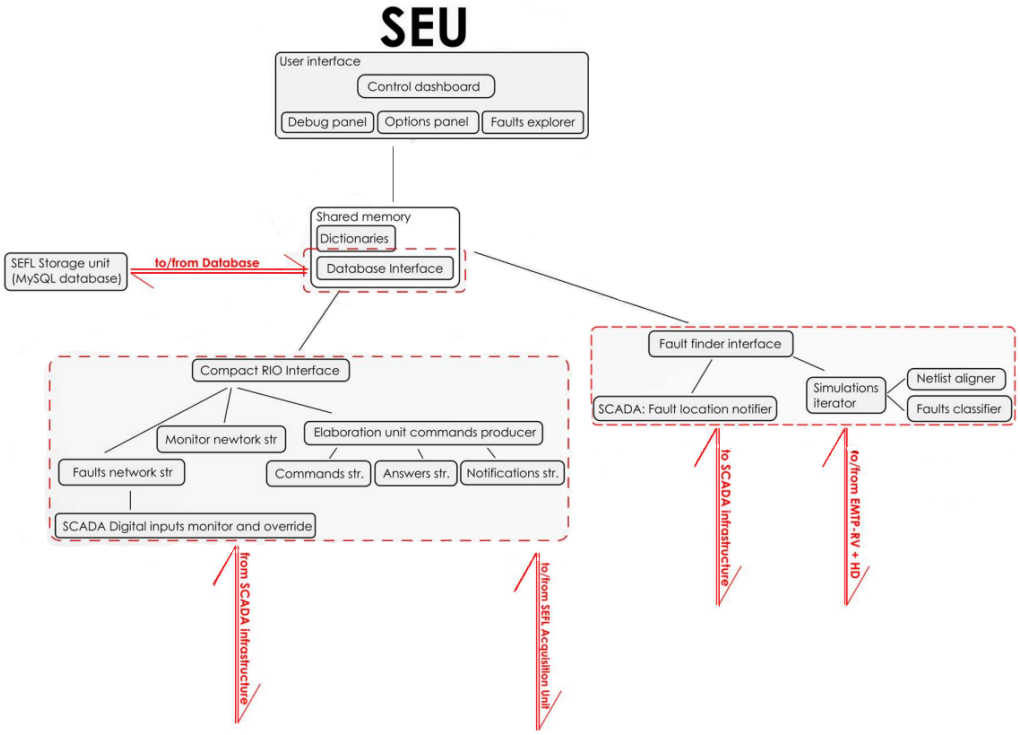

Figure 39: SEU logic blocks and communication links

4.1.1 WP1: Development and implementation of an ad-hoc triggering system

4.1.1.1 Triggering system

Based on the methodology proposed in Section 3.2.3 (step 1 – derivative condition), a new triggering system for the analog voltages was developed in the LabVIEW environment for FPGA and integrated into the SEFL software. Now the software has two triggering methods: standard and derivative, and a user can choose the desired one from the User Interface of the SEFL software.

Pilot test: 24/24 organized faults on the line were detected correctly.

The second integral condition is able to discern the faults from the disturbances inherent in lines (e.g., switching of inductive loads, circuit breaker and shunt operations, etc). For now, all types of events are recorded for further analysis and development, however the classification can be followed from the event log during monitoring phase (e.g. in Figure 40).

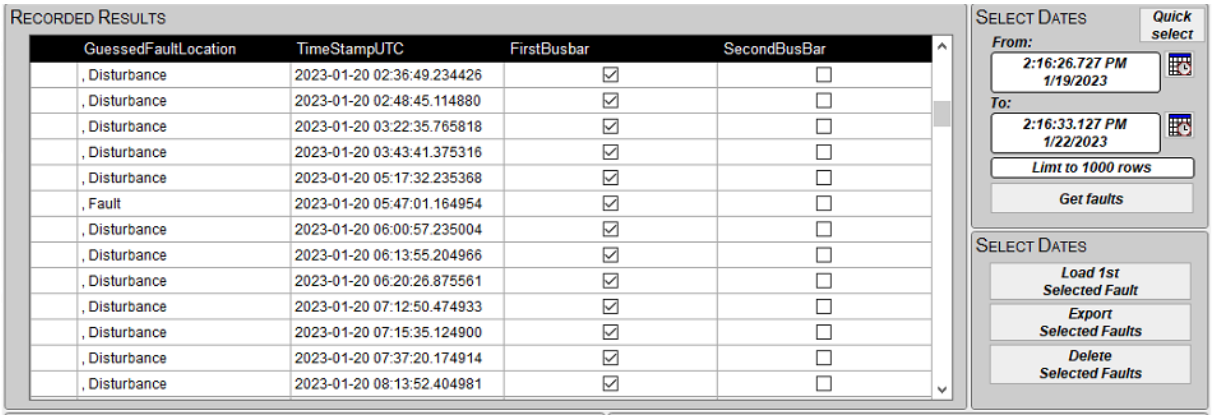

Figure 40: Event log in SEFL software

Pilot test: on the second pilot test with offline simulations, when the development of the function was finalized, all events were detected correctly, as shown in the event log in Figure 41.

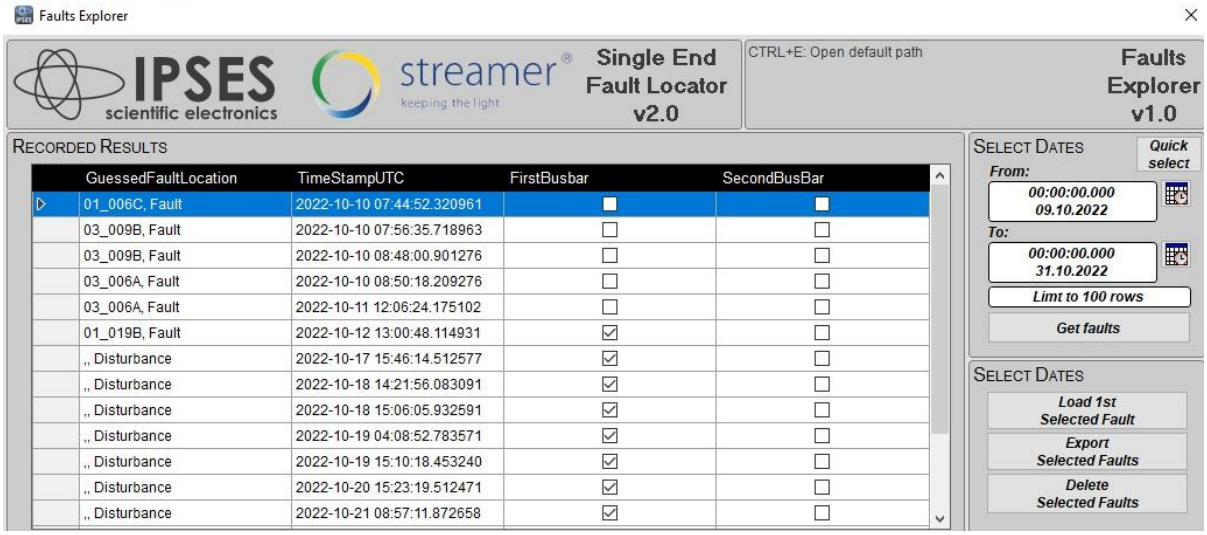

Figure 41: Event log in SEFL software for the second pilot test

4.1.1.2 Fault classifier

Except the triggering system, that classifies events, a fault classifier is integrated to the algorithm with the determination of fault type: phase-to-ground or short-circuit fault. As described in Section 3.2.5 the digital outputs from the protection system are integrated into our system by physical connection through the additional module in the controller. Alternatively, the information can be exchanged through the SCADA. The algorithm of fault classification works based on the received values, as shown in the flow chart in Figure 38.

Monitoring phase: the data exchange and the algorithm were tested during the monitoring phase and offline sessions. For instance, there was an event in October 2022 on the line where the list of actual SCADA output signals was downloaded by SEFL. Signals, their addresses and values related to the

event are presented in Table 9, where protection Démarrage Terre[3] signalizes about directional earth fault protection, Démarrage IMAX stands for directional overcurrent protection and Etat disjoncteur means that the shunt circuit-breaker operated. It can be noticed from the table that the earth fault protection of the feeder Rainoz signalized together with the signal of shunt of phase A. Based on this the algorithm qualified the event as a phase-to-ground fault and calculated the result only for faulty feeder, i.e. feeder Rainoz. In Figure 42 the screenshots of SEFL software HMI with the digital values provided by SCADA are presented, where “Line” means the address of the protection used in SEFL. The outcome of calculation based on the exchanged information proves the correct work both of the data exchanges and the algorithm.

However, the event also indicated an issue that allowed to calibrate the function and was successfully solved by the software developer. The specific of the issue is mentioned in Section 3.2.11 WP7: evaluation and adjustment of the software development.

Table 9: List of signals for the information exchange between the SCADA and the SEFL SEU

Source	Device	Relay protection name	Address IEC	Address SEFL	Value
SCADA	RAINOZ	Démarrage Terre	46000	40	1
SCADA	RAINOZ	Démarrage IMAX	46001	41	0
SCADA	SHUNT_L1	Etat disjoncteur	48011	54:55	0:1

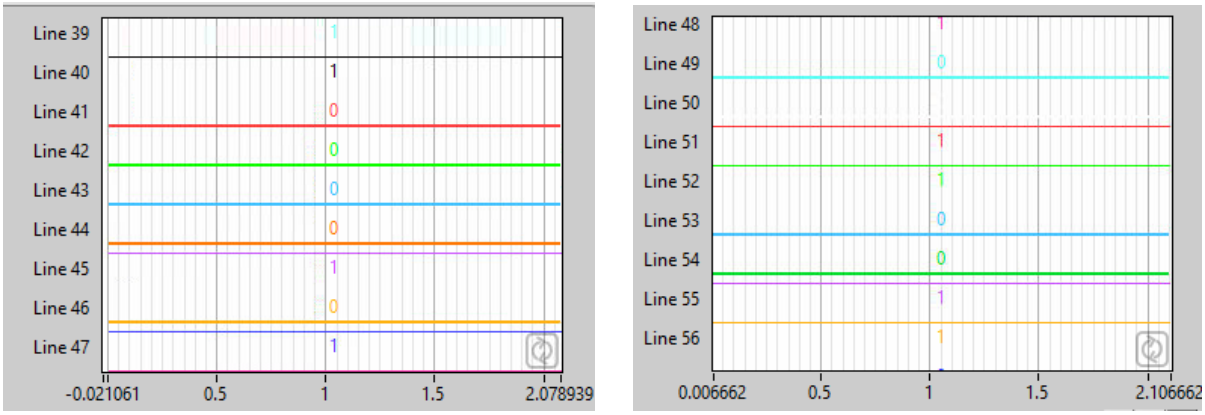

Figure 42: Digital values provided by SCADA

4.1.1.3 Second busbar or current measurement

Even if not foreseen in the framework of this SFOE project, we decided to develop an additional part of the code that allows the prototype to be connected to a second set of sensors, by using an additional digitizer. The user can select if the additional acquired signals are voltages or currents. As known, primary substations have usually two busbars supplied by two different HV/MV transformers. At the moment the prototype is connected only to one busbar, but this part of code would allow the connection to the second busbar, which means, in term of hardware, the duplication of the set of sensors and the digitizer only (instead of having a second prototype). This part of the software allows, as an alternative,

[3] As Groupe E is located in French-speaking part of Switzerland, the names of relay protections are mentioned in the original language, as it is in used by the company.

also to connect the SEFL to current sensors: this could be useful for research purposes to check if current measurements could improve the fault-locating algorithm.

4.1.2 WP2: Integration of SEFL results in the SCADA system

4.1.2.1 Information exchange with the SCADA

SEFL should be able to communicate the result of the information regarding the fault location if a fault occurs. Section 3.2.6 outlines the activities conducted on this matter. The verification of this functionality was done thanks to offline test and pilot test.

Offline test: In October 2021, a test was carried out in order to test the signal exchange between the SEFL and the Groupe E's SCADA in compliance with the IEC 60870-5-104 transmission protocol. The info exchange was successful.

Pilot test: In addition to offline testing, information exchange with the SCADA is successfully verified during the second pilot test, as shown in Section 3.2.10. Thus, SEFL sends the information regarding fault location to SCADA system and such information as faulty feeder (a), fault alarm (b), name of faulty section (c) and the location on the line map (d) is visualized in SCADA HMI (Figure 43).

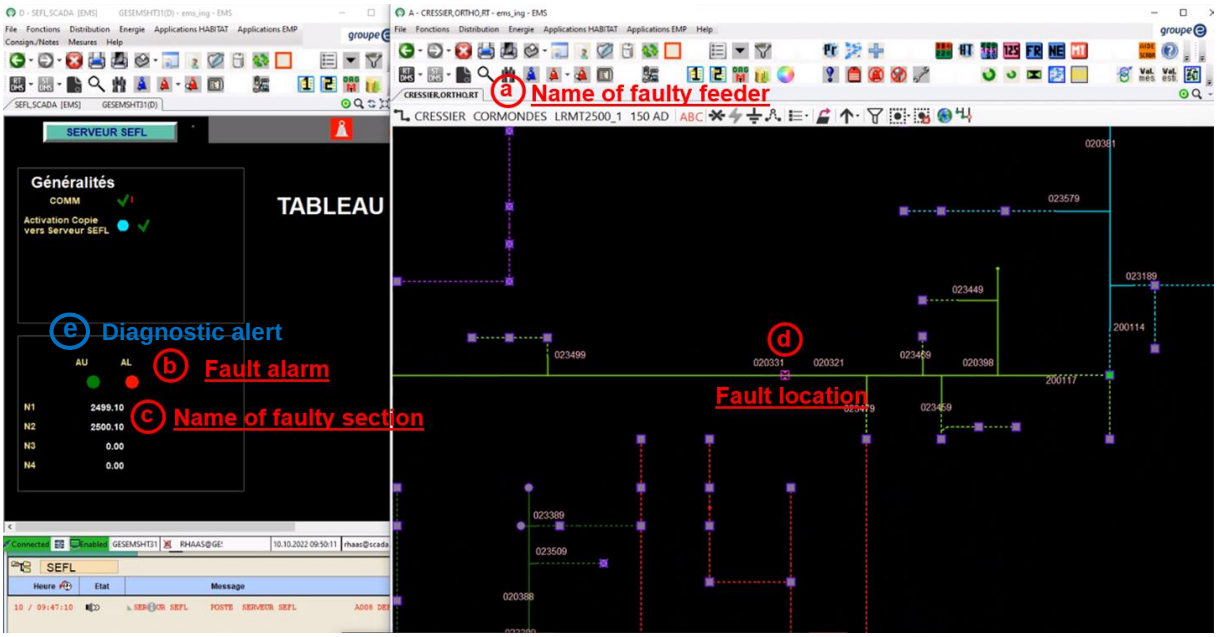

Figure 43: SCADA interface with the information about fault

In further development in order to ensure the reliable operation of the system the functionality of diagnostic alert indication (e) in Figure 43 will be taken into consideration.

4.1.2.2 Real-time grid topology from the SCADA

The real-time topology of the network can be inferred by connecting to the SQL database of Groupe E to get the status of the switches along the line. This part of the software development was carried out specifically for Groupe E, where the information is stored in SQL database, other utilities may contain this information in SCADA system or in protection system. However, the aim was to make it as flexible and adaptable as possible to other utilities. For the utilities that do not record such information, the qualified personnel at the substation should make the appropriate changes in the digital model.

A service has been implemented in LabVIEW that every few minutes updates the EMTP-RV[4] file containing the topological and electrical description of the network. This developed part can be used for each utility. For Groupe E, specifically, the mentioned EMTP-RV file is updated every time the database is queried and there is an update of the switch status. In addition, a translation strategy has been implemented between the name of the switches in the customer's database and in the EMTP-RV file containing the topological and electrical description of the network. In the specific case of Groupe-E, a mapping of the switches in their database is carried out and at the same time, a mapping of the switches in the EMTP-RV file done. If there is a difference between the two, the status is aligned and then logged in the SEFL software console. Figure 44 reports the result of the default query to the SQL database of Groupe E to get the status of the switches along the line.

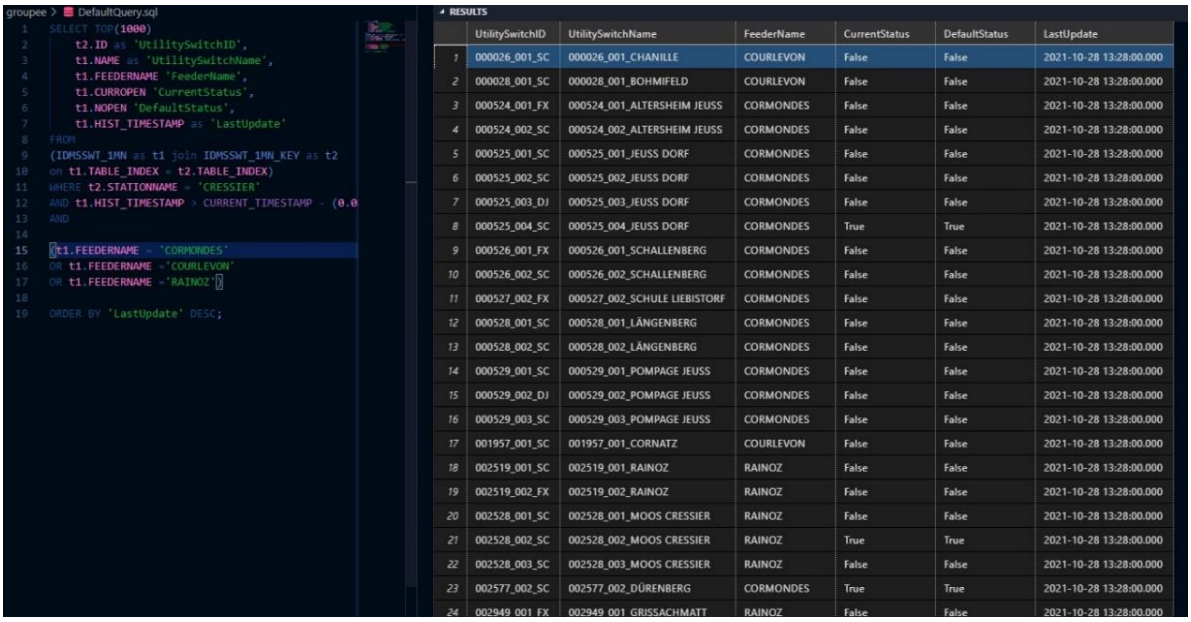

```
groupee > DefaultQuery.sql
SELECT TOP(1000)
    t2.ID as 'UtilitySwitchID',
    t1.NAME as 'UtilitySwitchName',
    t1.FEEDERNAME 'FeederName',
    t1.CURROPEN 'CurrentStatus',
    t1.NOPEN 'DefaultStatus',
    t1.HIST_TIMESTAMP as 'LastUpdate'
FROM
(IDMSSWT_1MN as t1 join IDMSSWT_1MN_KEY as t2
on t1.TABLE_INDEX = t2.TABLE_INDEX)
WHERE t2.STATIONNAME = 'CRESSIER'
AND t1.HIST_TIMESTAMP > CURRENT_TIMESTAMP - (0.0
AND

(t1.FEEDERNAME = 'CORMONDES'
OR t1.FEEDERNAME ='COURLEVON'
OR t1.FEEDERNAME ='RAINOZ')

ORDER BY 'LastUpdate' DESC;
```

RESULTS

	UtilitySwitchID	UtilitySwitchName	FeederName	CurrentStatus	DefaultStatus	LastUpdate
1	000026_001_SC	000026_001_CHANILLE	COURLEVON	False	False	2021-10-28 13:28:00.000
2	000028_001_SC	000028_001_BOHMIFELD	COURLEVON	False	False	2021-10-28 13:28:00.000
3	000524_001_FX	000524_001_ALTERSHEIM JEUSS	CORMONDES	False	False	2021-10-28 13:28:00.000
4	000524_002_SC	000524_002_ALTERSHEIM JEUSS	CORMONDES	False	False	2021-10-28 13:28:00.000
5	000525_001_SC	000525_001_JEUSS DORF	CORMONDES	False	False	2021-10-28 13:28:00.000
6	000525_002_SC	000525_002_JEUSS DORF	CORMONDES	False	False	2021-10-28 13:28:00.000
7	000525_003_DJ	000525_003_JEUSS DORF	CORMONDES	False	False	2021-10-28 13:28:00.000
8	000525_004_SC	000525_004_JEUSS DORF	CORMONDES	True	True	2021-10-28 13:28:00.000
9	000526_001_FX	000526_001_SCHALLENBERG	CORMONDES	False	False	2021-10-28 13:28:00.000
10	000526_002_SC	000526_002_SCHALLENBERG	CORMONDES	False	False	2021-10-28 13:28:00.000
11	000527_002_FX	000527_002_SCHULE LIEBISTORF	CORMONDES	False	False	2021-10-28 13:28:00.000
12	000528_001_SC	000528_001_LÄNGENBERG	CORMONDES	False	False	2021-10-28 13:28:00.000
13	000528_002_SC	000528_002_LÄNGENBERG	CORMONDES	False	False	2021-10-28 13:28:00.000
14	000529_001_SC	000529_001_POMPAGE JEUSS	CORMONDES	False	False	2021-10-28 13:28:00.000
15	000529_002_DJ	000529_002_POMPAGE JEUSS	CORMONDES	False	False	2021-10-28 13:28:00.000
16	000529_003_SC	000529_003_POMPAGE JEUSS	CORMONDES	False	False	2021-10-28 13:28:00.000
17	001957_001_SC	001957_001_CORNATZ	COURLEVON	False	False	2021-10-28 13:28:00.000
18	002519_001_SC	002519_001_RAINOZ	RAINOZ	False	False	2021-10-28 13:28:00.000
19	002519_002_FX	002519_002_RAINOZ	RAINOZ	False	False	2021-10-28 13:28:00.000
20	002528_001_SC	002528_001_MOOS CRESSIER	RAINOZ	False	False	2021-10-28 13:28:00.000
21	002528_002_SC	002528_002_MOOS CRESSIER	RAINOZ	True	True	2021-10-28 13:28:00.000
22	002528_003_SC	002528_003_MOOS CRESSIER	RAINOZ	False	False	2021-10-28 13:28:00.000
23	002577_002_SC	002577_002_DÜRENBERG	CORMONDES	True	True	2021-10-28 13:28:00.000
24	002949_001_FX	002949_001_GRISSACHMATT	RAINOZ	False	False	2021-10-28 13:28:00.000

Figure 44: Result of the default query to the SQL database of Groupe E to get the status of the switches along the line.

Pilot test: During pilot test as well as monitoring phase a new function was tested and verified: after changing the position of a switch on the side of Groupe E, the model of the line is updated accordingly to a new position of the switch. Figure 37 shows the interface of SEFL software, where the line in the console confirms the new status registered.

4.1.2.3 SEFL architecture

As said in Section 3.2.6, the main outcome of WP2 is that the software architecture of SEFL has been radically changed, mainly due to the fact that, for security reasons, SEFL was split into two physical locations. This task dealt mostly with the implementation of an increased reliability for data exchange between the SEFL acquisition unit and the SEFL elaboration unit. In the new architecture, the two units are located in different places and connected through internet: the possibility of losing the connection, and therefore fault data, is higher. The software was therefore enhanced in terms of buffer (i.e., download and buffer data from the controller, emergency saving) and archive (i.e., download and flush buffer, medium-term saving, saving simulation results, and network status saving). Furthermore, an additional memory card was added to the controller in the SEFL acquisition unit: if the connection with the SEFL elaboration unit is lost, the measured data are saved on the mentioned card on the SEFL

[4] As said, EMTP-RV is a well-known software for simulation and analysis of power systems, especially for the simulation of electromagnetic and electromechanical transients. This software is used to build the electrical network model and to run electromagnetic transient simulations.

acquisition unit and sent to the SEFL elaboration unit when the connection is available again, before being deleted. The duration of the measured data is usually 20 ms, in case of intermittent faults it can be several waveforms related to the same event.

4.1.3 WP3: Development of the connection to Groupe E cloud database

4.1.3.1 Connection to Groupe E's database

In case of Groupe E, the electrical features of the network are stored in a XML file, which contains detailed information about lines, branches, breakers, switches, fuses, loads, transformers, etc. Each object contains all the information needed to infer the network topology. The access to this file is done using SFTP (File Transfer Protocol), in order to read the relevant data and to update the file if any change occurred.

Monitoring phase: During monitoring phase three XML files were received, that allowed us to be aware about changes in length of some sections on the line. Figure 45 demonstrates the example of changes in XML files.

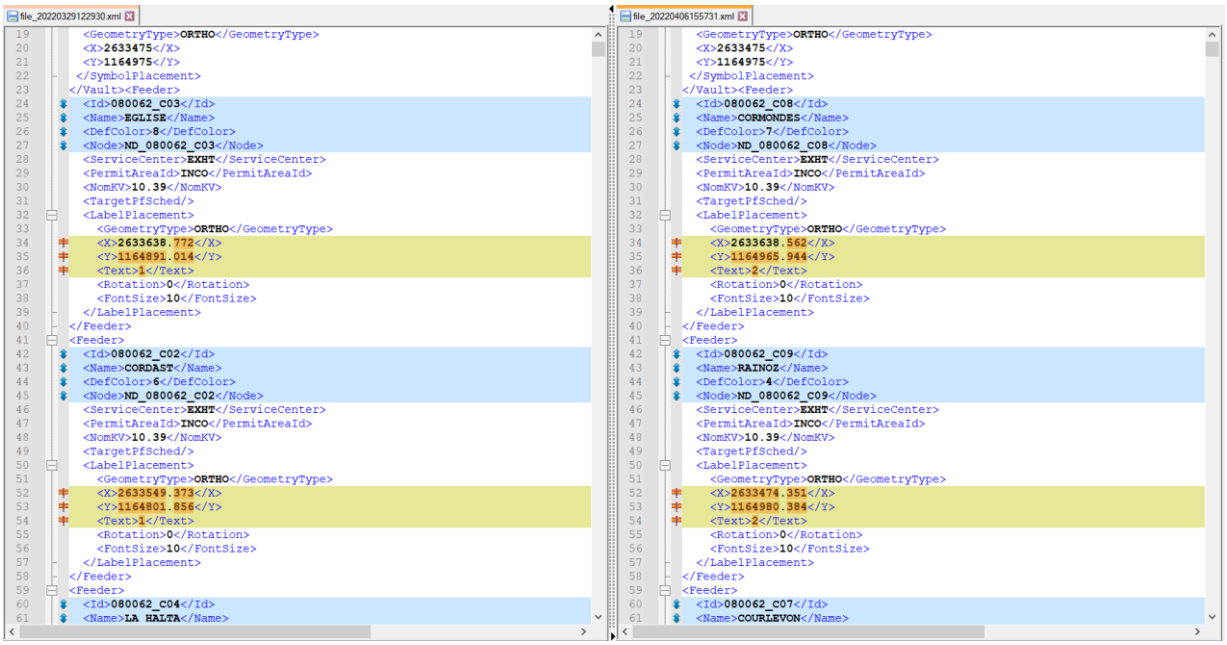

Figure 45: Previous (right) and current (left) XML files comparison

4.1.3.2 Creation of a local database on the SEFL elaboration unit

A local relational database on the SEFL elaboration unit was created in MySQL and linked to the SEFL software. This database contains the main data structure for the whole SEFL software. This is the first step of a more generic task that includes the creation of a more comprehensive database with also network data. The structure of created database is reported in Figure 46.

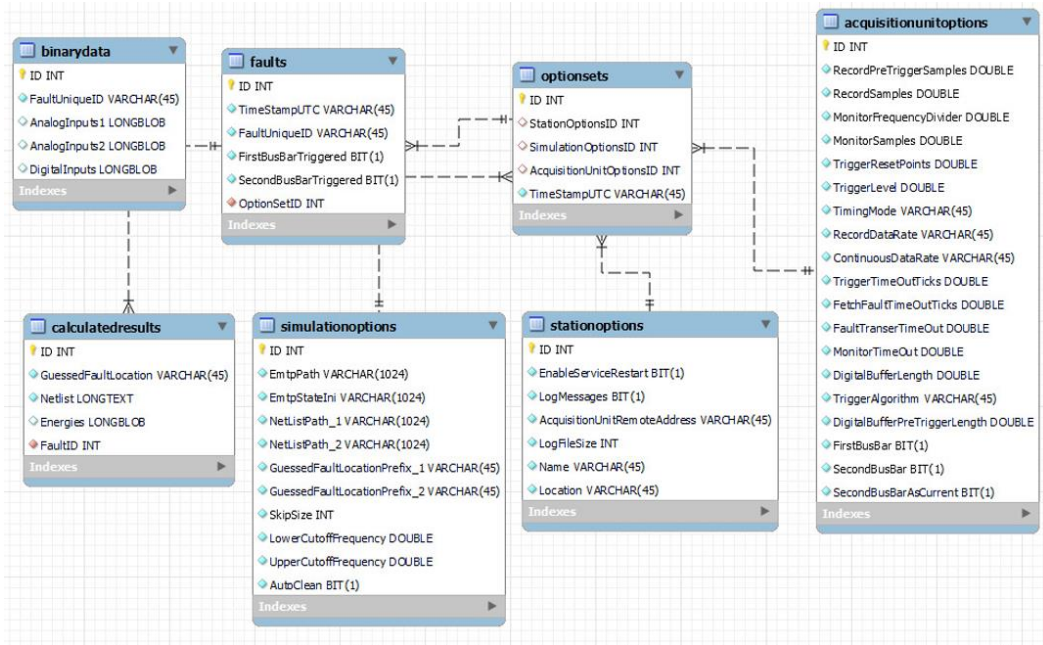

Figure 46: Tables of the relational database created to store SEFL data and updates

4.2 WP4: Improving the accuracy of the fault location

The section describes the methods and studies on fault location accuracy. Thus, phase-to-phase method demonstrated better accuracy of fault localization compared with conventional EMTR methodology and was implemented to the new software release as an additional functionality of the calculation.

Phase-to-phase method

Comparison between the phase-to-phase methodology and the conventional EMTR methodology

Since there was no short-circuit fault during the monitoring nor the pilot tests, the applicability and robustness of the phase-to-phase methodology is assessed occurred in the Russian network using both pilot test data and data of real faults (a short presentation of the project is presented in Section 7). Table 10 reports the results of the comparison between the two methodologies and shows the improvement in terms of accuracy that can be achieved by the phase-to-phase methodology.

Table 10: Comparison between the conventional EMTR method and the method for phase-to-phase faults.

Fault case				**Conventional method**		**Phase-to-phase method**	
Cause of the phase-to-phase faults		**Fault location**	**Distance to the substation**	**Result**	**Error**	**Result**	**Error**
Pilot test		EK_044	5325 m	EK_037	763 m	EK_040	382 m
		EK_099	9000 m	EK_083	2019 m	EK_091	638 m
		EK_037	3932 m	EK_044	1393 m	EK_034	300 m
		BG_142	5190 m	BG_094	4700 m	BG_142	250 m
Real fault	Tree branches on wires	EK_034	4093 m	EK_042	1050 m	EK_034	100 m
	Strong wind	EK_034	4093 m	EK_064	2500 m	EK_034	100m

Line/Cable data in the line model

Comparison between the constant parameter and frequency dependent models of line/cable data

Additional functionality, capable of processing and calculating different types of line models, has been implemented for the SEFL software. As mentioned in 3.2.2 two types of models are available in EMTP-RV for the calculations and they both were applied to the Groupe E model in order to compare the their impact on the model and the algorithm. Thanks to the data from the pilot test the fault events were calculated in order to compare the mentioned models. Table 11 demonstrates that none of models gives the stable good accuracy for each fault case. As the constant parameter model is the basic one and has higher computational speed, we decided to stay at this type of model for further calculations.

Table 11: Comparison between constant parameter and frequency dependent models of line/cable data

#	Number of feeders	Fault distance from substation	Fault type	Constant Parameter model		Frequency Dependent model	
				Result: distance from substation	Error**	Result: distance from substation	Error**
# E_1	3 feeders	3086 m, branch	P-G*, $R = 0\,\Omega$	2635 m, main feeder	450 m	5586 m, main feeder	>2000 m
# E_2			P-G, $R = 34\,\Omega$	2635 m, main feeder	450 m	5586 m, main feeder	>2000 m
# E_3			P-G, $R = 68\,\Omega$	2635 m, main feeder	450 m	5586 m, main feeder	>2000 m
# A_1	1 feeder	2500 m, branch	P-G, $R = 0\,\Omega$	2500 m, branch	0 m	4471 m, main feeder	1971 m
# A_2			P-G, $R = 34\,\Omega$	4251 m, main feeder	1750 m	4471 m, main feeder	1971 m
# A_3			P-G, $R = 68\,\Omega$	4251 m, main feeder	1750 m	4471 m, main feeder	1971 m
# B_1	1 feeder	1668 m, branch	P-G, $R = 0\,\Omega$	1065 m, main feeder	650 m	1668 m, branch	0 m
# B_2			P-G, $R = 34\,\Omega$	1065 m, main feeder	650 m	1368 m, main feeder	360 m
# B_3			P-G, $R = 68\,\Omega$	1065 m, main feeder	650 m	1368 m, main feeder	360 m

*single-phase-to-ground fault

**fault location error is a “bare” error, that is calculated based on the distance from the substation

Network model refinement

The introduction of the network model refinement and methodology of the pilot tests with the pulse generator was described in Section 3.2.8 WP4: improving the performance of the EMTR-based algorithm. Below the pilot test post-processing and its results is presented.

Measurement results

Table 12 shows the recorded voltage signal waveforms at each location. The total duration of the entire voltage signal waveforms is approximately 0.5-1 ms.

Table 12: Voltage signal waveforms recorded by the sensors at the substation

Injection location	Voltage signal waveforms (pulse response)
Point #1 Pole 28 1526 m one line section	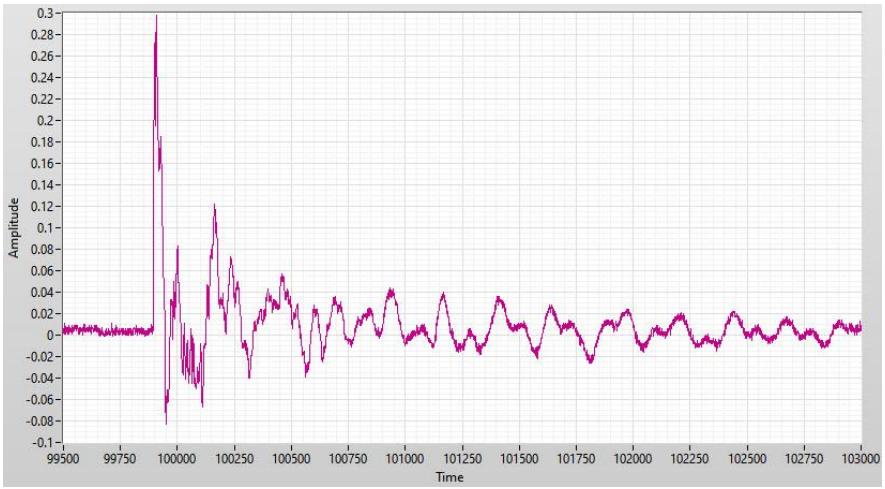
Point #2 Branch 1 (025) 3279 m one line section	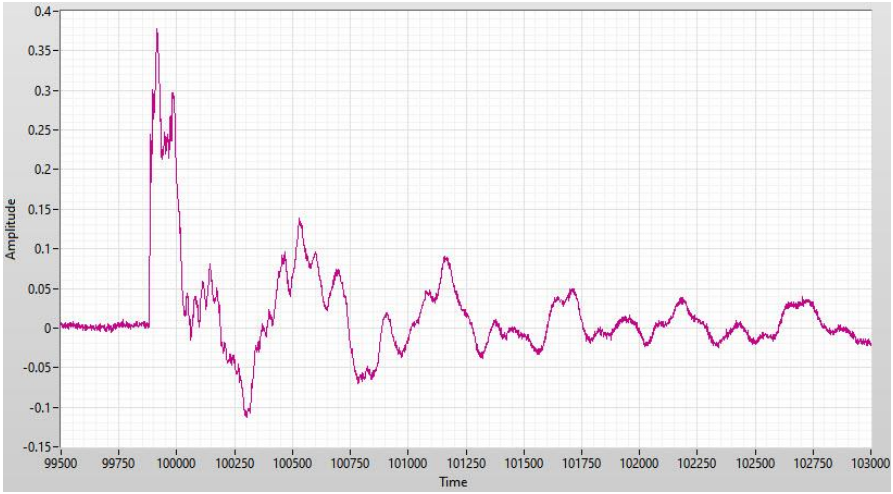

Injection location	Voltage signal waveforms (pulse response)
Point #3 Pole 75 4475 m two line section	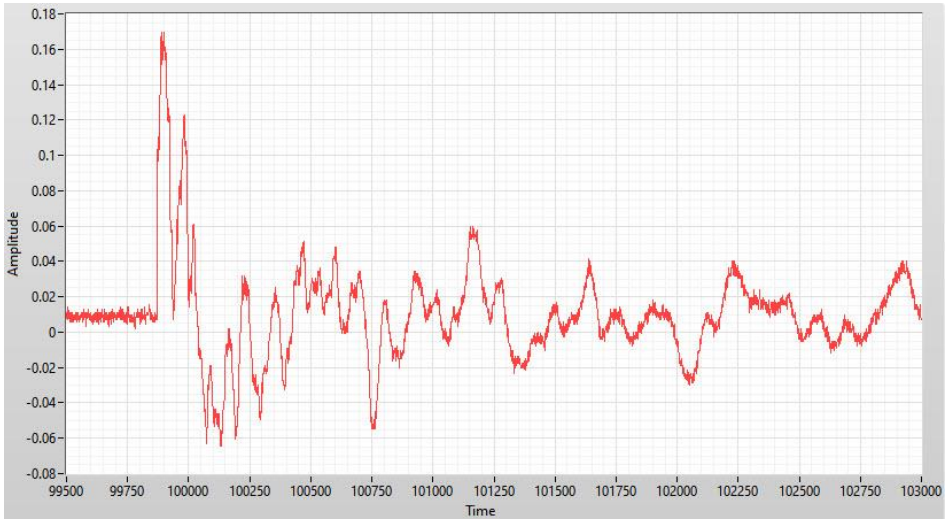
Point #4 Pole 92 5575 m two line section	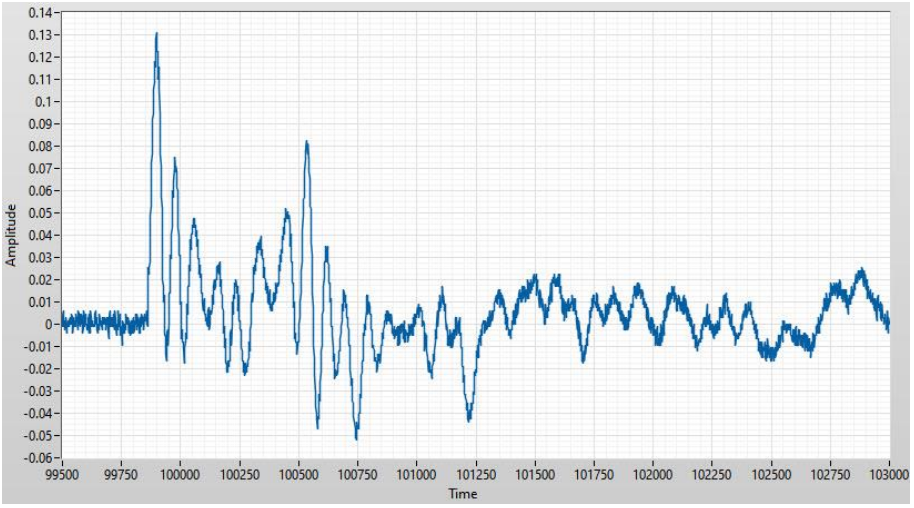

Injection location	Voltage signal waveforms (pulse response)
Point #5 Branch 2 (061) 6355 m two line section	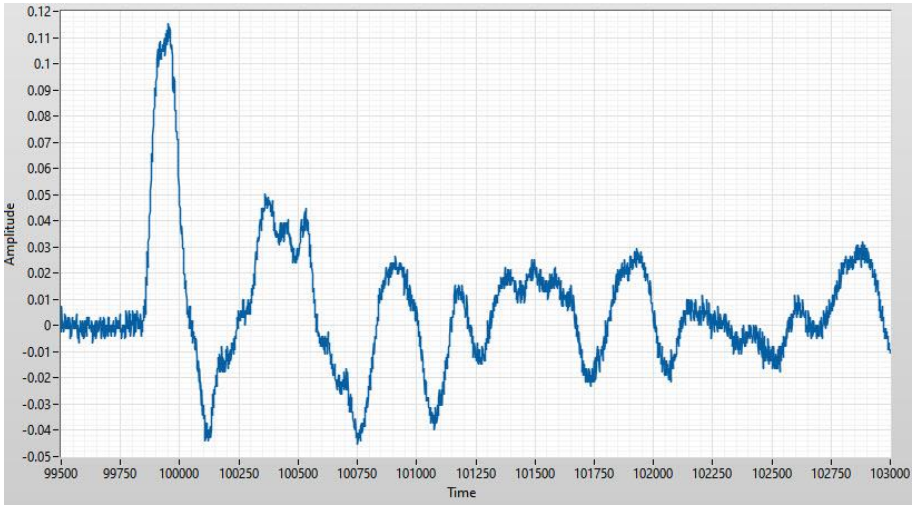
Point #6 Branch 3 (070) 6280 m two line section	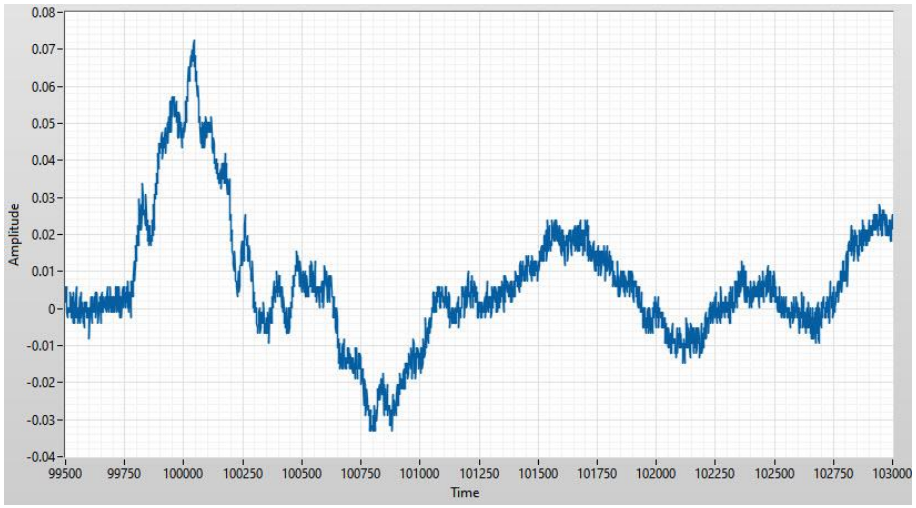

Analysis of the results

To analyze the obtained response waveforms, it is advisable to perform a fast Fourier transform (FFT) and transfer the voltage to the frequency domain. The comparison of the frequency domains will allow to evaluate the obtained results more accurately.

Table 13 shows the frequency spectrograms of the oscillograms for each injection point. The values on the graph show the characteristic frequencies of the spectrogram peaks.

Table 13: Voltage waveform spectrogram of the waveforms for injection points

Injection location	Voltage waveform spectrogram (pulse response)
Point #1 Pole 28 1526 m one line section	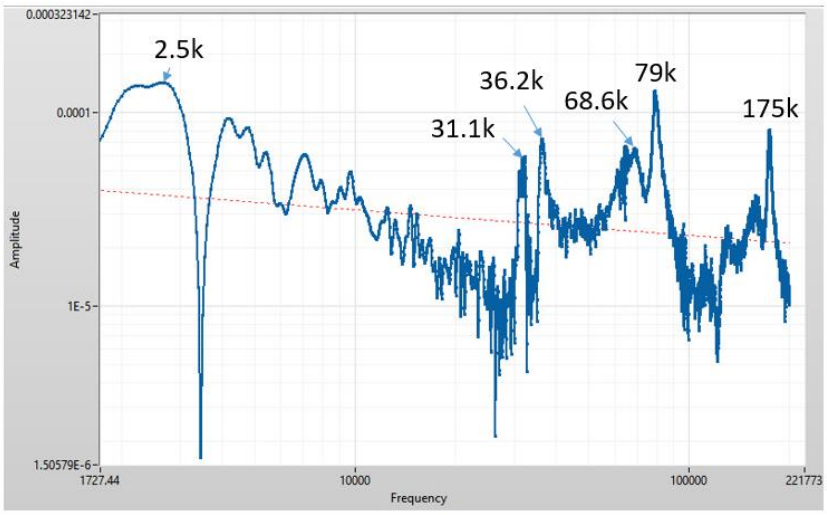
Point #2 Branch 1 (025) 3279 m one line section	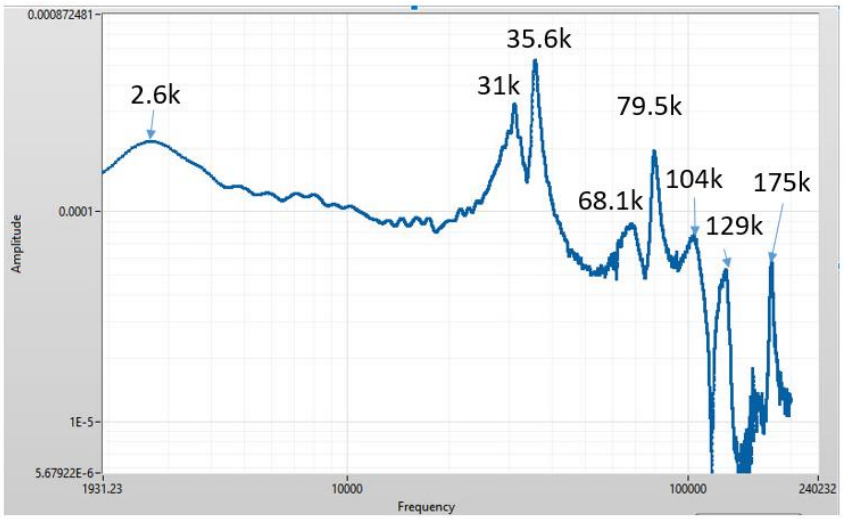

Injection location	Voltage waveform spectrogram (pulse response)
Point #3 Pole 75 4475 m two line section	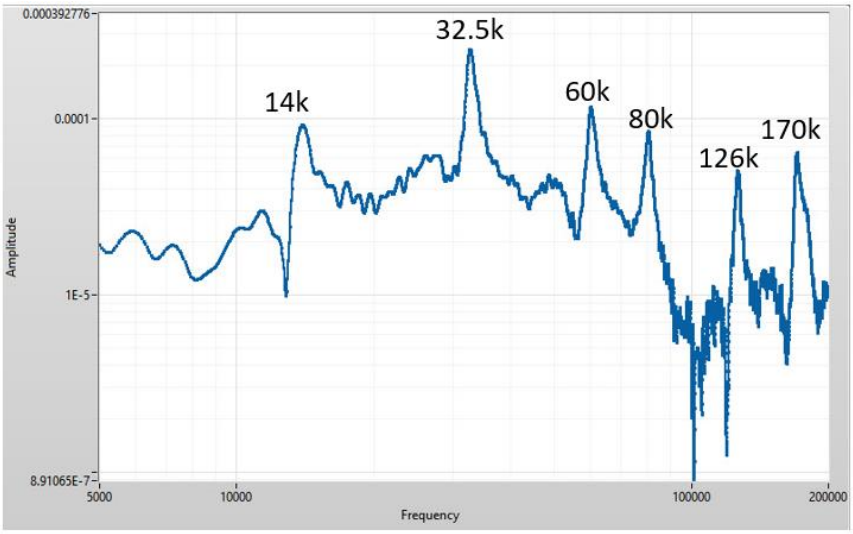
Point #4 Pole 92 5575 m two line section	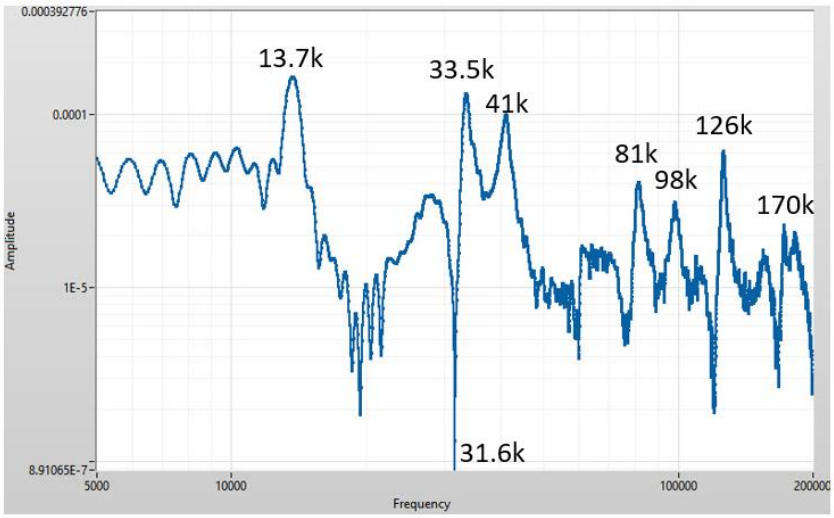

Injection location	Voltage waveform spectrogram (pulse response)
Point #5 Branch 2 (061) 6355 m two line section	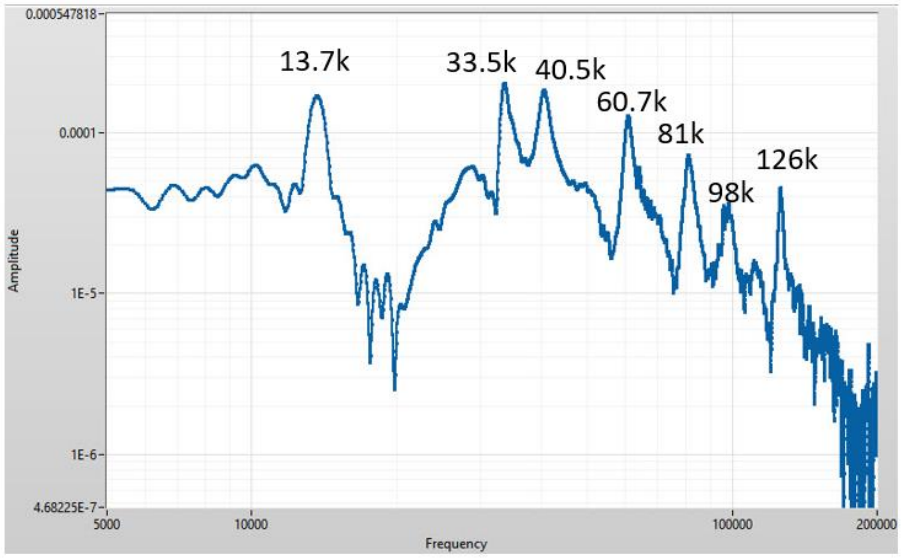
Point #6 Branch 3 (070) 6280 m two line section	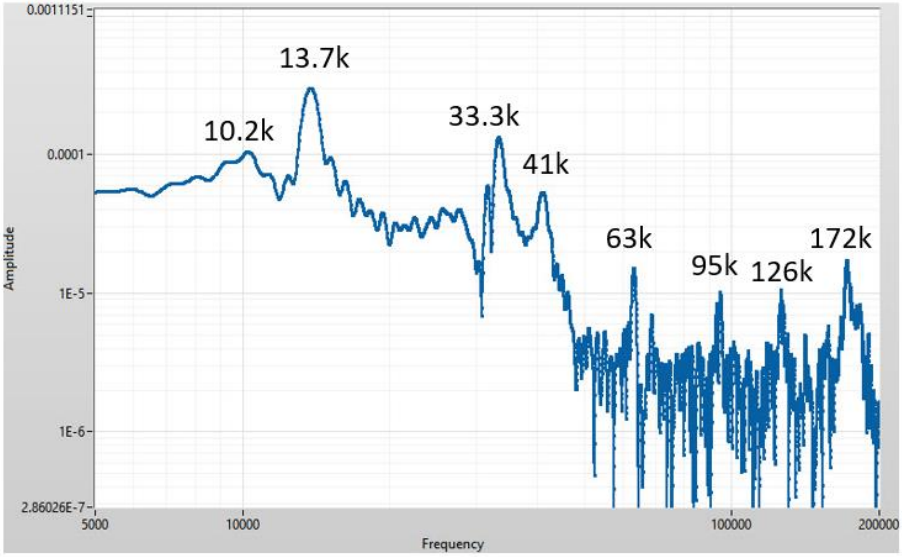

The spectrograms show that most of the characteristic frequencies lie in the region of 30-100 kHz for injection points #1-2 and in the region of 13-125 kHz for injection points #3-6. Let's consider in detail these spectrograms for one graph.

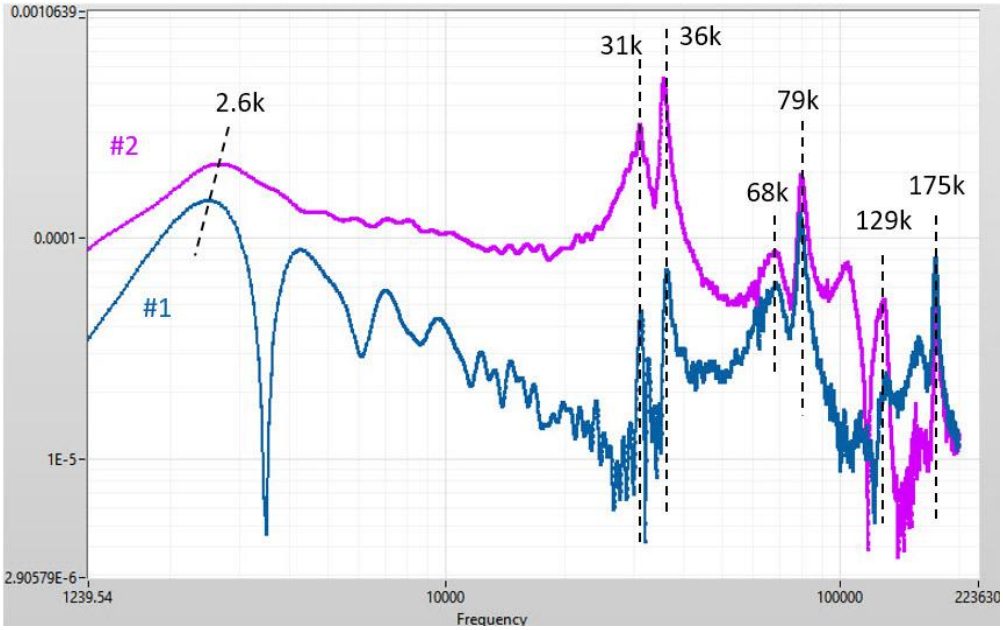

Figure 47: Comparison of FFT of oscillograms from the injection points #1 and #2.

Figure 47 shows the response voltage spectrograms for injection points #1 and #2, where we can clearly see the coincidence of the characteristic frequencies with values of 31 kHz, 36 kHz, 68 kHz, 79 kHz, however with different amplitudes. At point #1, which is at the distance of 1526 m from the measurement unit higher frequencies of 68 kHz and 79 kHz prevail, at point #2, which is further away, at the distance of 3279 m from the measurement, frequencies of 31 kHz and 36 kHz prevail. This is explained by the processes of voltage wave propagation in the line - the closer the distance from the pulse to the place of measurement, the faster and more often the wave reaches it. In general, the picture of both spectrograms coincides because of the same line configuration, and therefore the same boundaries of the pulse wave propagation.

Figure 48 shows the response voltage spectrograms for injection points #3 and #6, where we also observe the coincidence of the characteristic frequencies, especially with the values 13.7 kHz, 33 kHz. A similar tendency is noted that at the near point #3 (4475 m) high frequencies of 30-170 kHz prevail, and at the far point #6 (6280 m) the main frequencies are 13-33 kHz.

Figure 49 shows the response voltage spectrograms for injection points #4 and #5. Point #4 is located at the beginning of branch 2 at the intersection with the main line, and point #5 is at the end of this branch. There is also a coincidence of the characteristic frequencies, especially with values of 13.7 kHz, 33 kHz, 41 kHz, 81 kHz, 126 kHz. At point #4 there are peaks of frequencies 150-300 kHz, which is most likely caused by oscillations of the wave in this branch of the line.

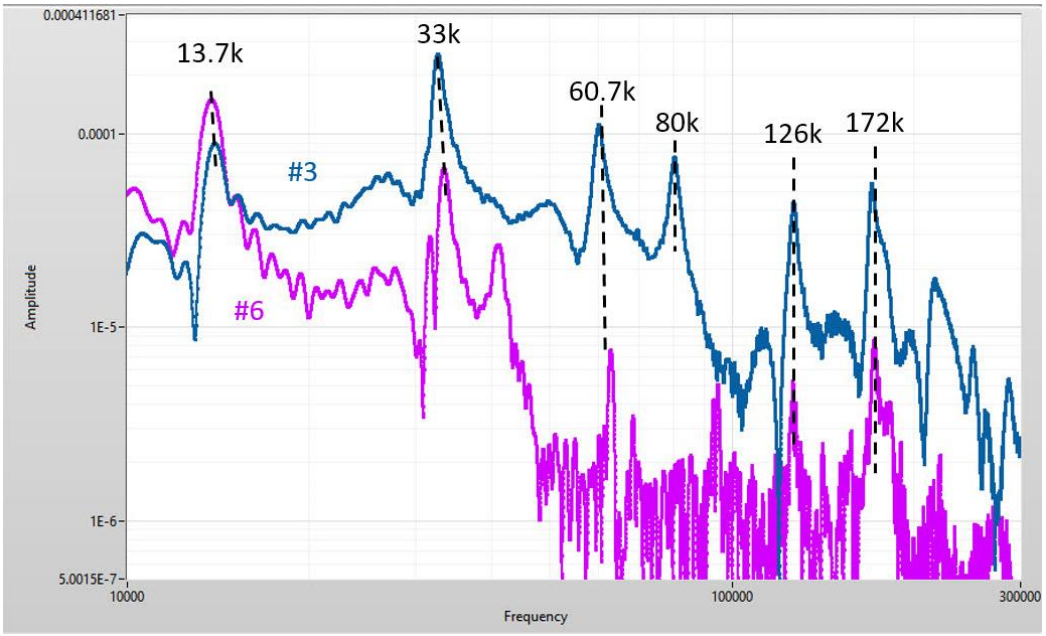

Figure 48: Comparison of FFT of oscillograms from the injection points #3 and #6.

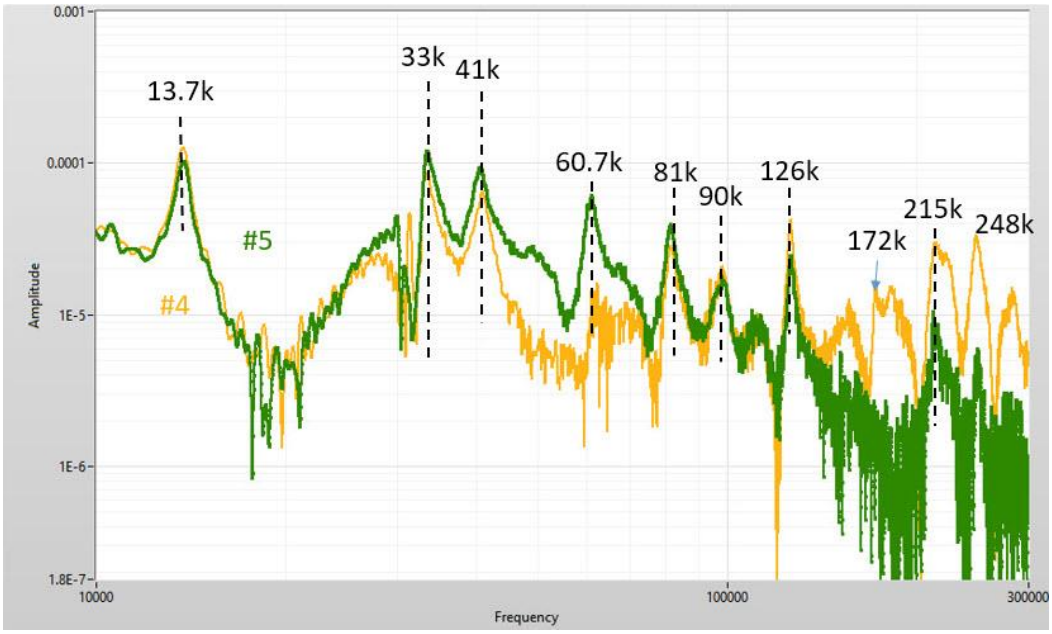

Figure 49: Comparison of FFT of oscillograms from the injection points #4 and #5.

Comparison with the calculations

Table 14 shows the voltage spectrograms for the injection points obtained experimentally and computationally.

Table 14: Comparison table of experimental and computational tests

Injection location	Voltage waveform spectrogram (pulse response)
Point #1 Pole 28 1526 m one line section	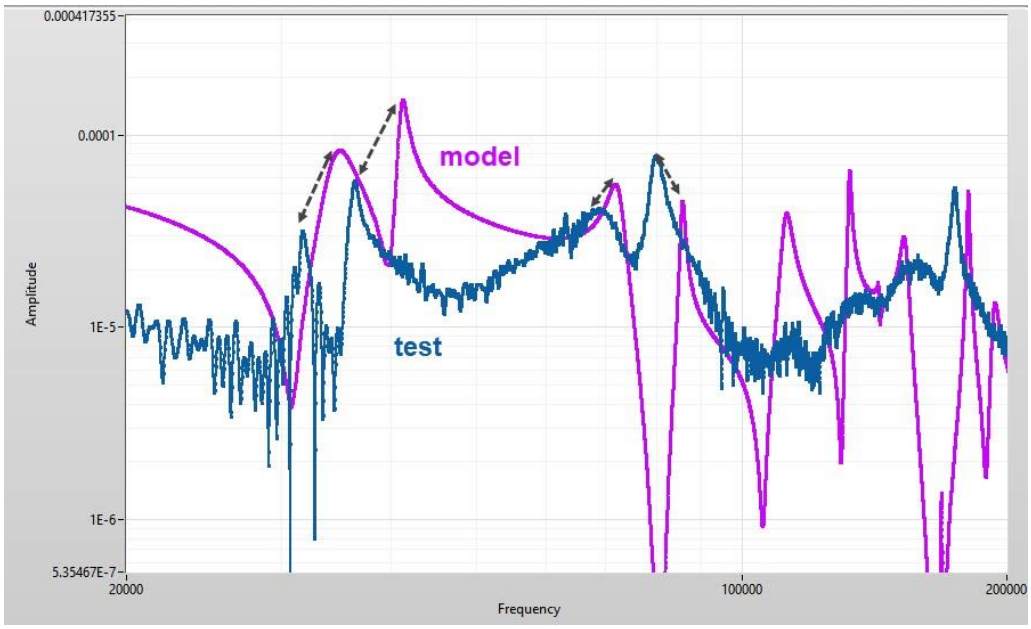
Point #2 Branch 1 (025) 3279 m one line section	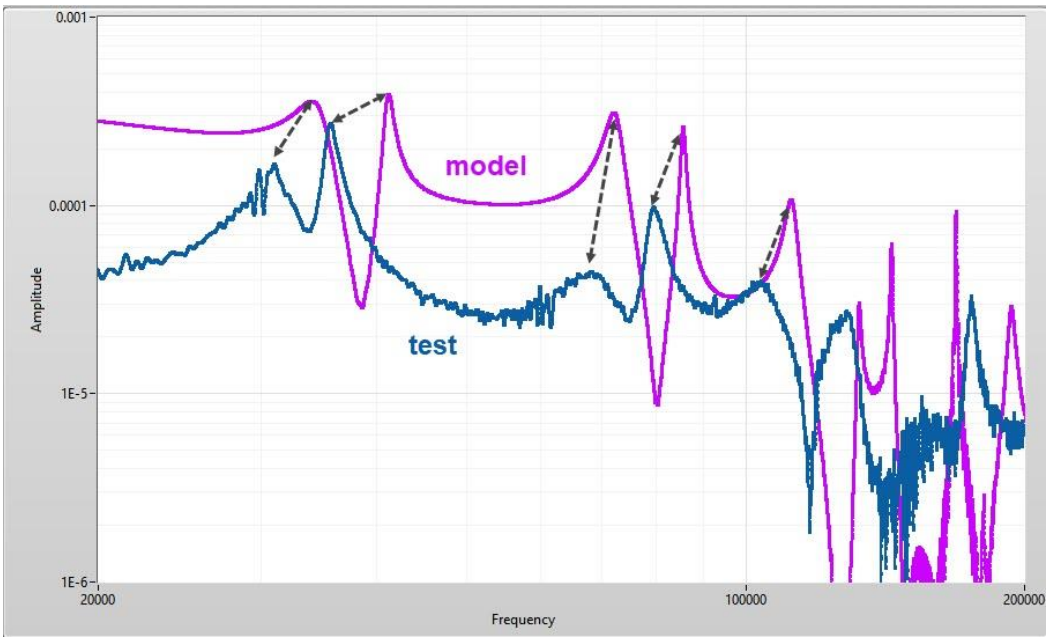

Injection location	Voltage waveform spectrogram (pulse response)
Point #3 Pole 75 4475 m two line section	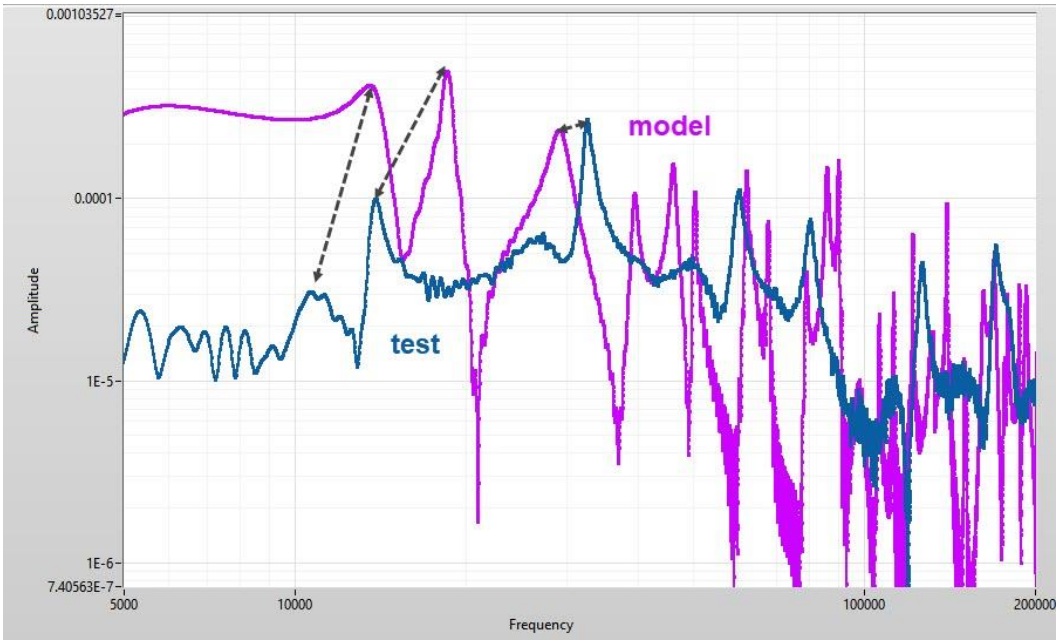
Point #4 Pole 92 5575 m two line section	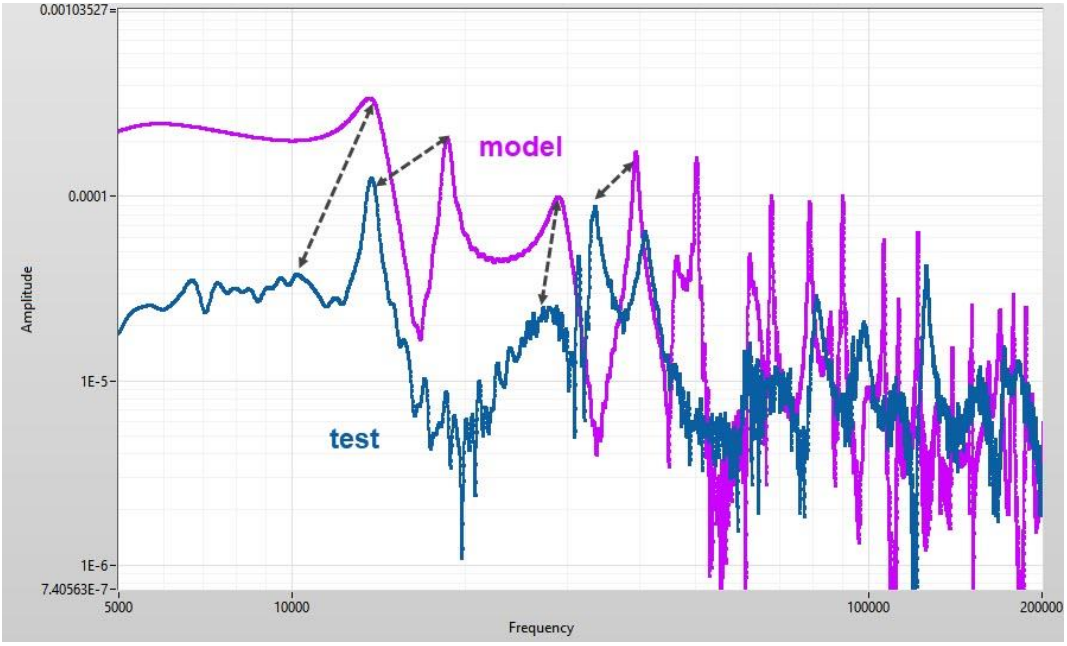

Injection location	Voltage waveform spectrogram (pulse response)
Point #5 Branch 2 (061) 6355 m two line section	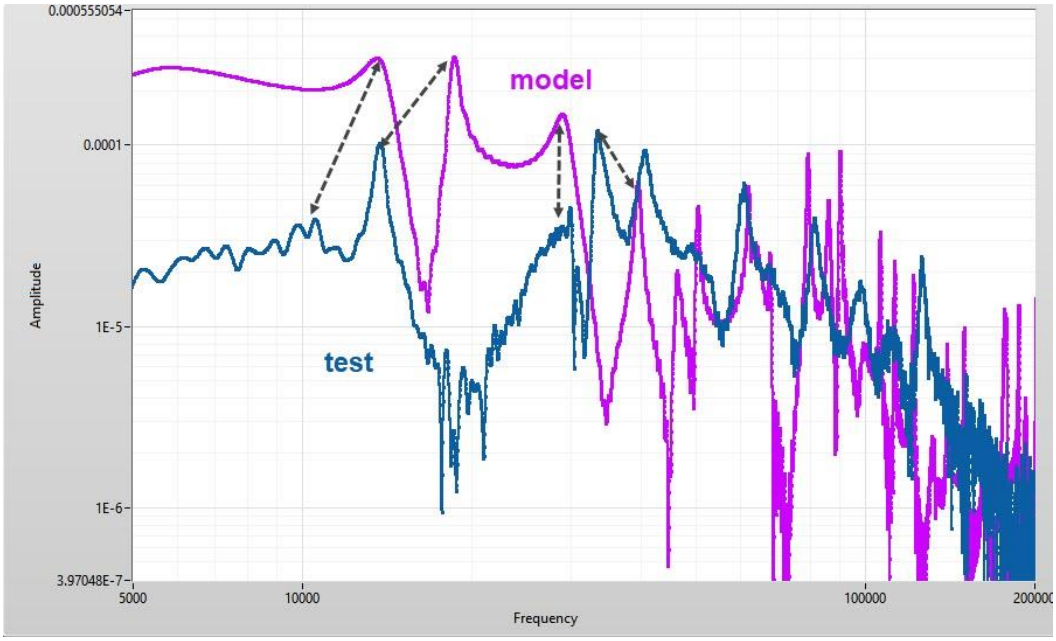
Point #6 Branch 3 (070) 6280 m two line section	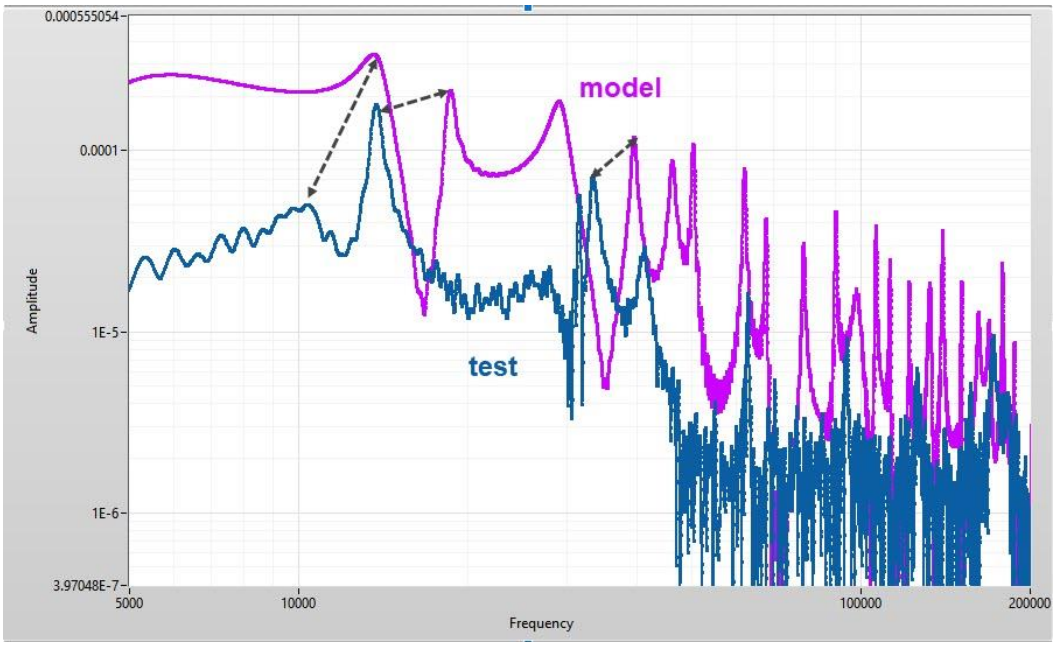

Comparing the results, the following features can be observed:

- The general pattern of the characteristic frequencies is preserved for each location. It means that the configuration of the sections in general is correct. This is especially valid for the injection points 1 and 2 in the frequency range of 10-100 kHz. For the other injection points in the frequency range above 100 kHz, the topological complexity of the line affects.

- There is a shift of frequency peaks to the direction of increasing values on the spectrograms from computations. It indicates that the total capacitance of the overhead line in the mathematical model is less than in reality. Because of this, the voltage wave oscillations have a higher frequency in the mathematical model than in the test measurements.

Sensitivity analysis of line model parameters

As a reference, the test at the injection point #2 was chosen. At this point, the total length of the overhead line was only 3.7 km, the topology of the overhead line has only one branch number 1 with a length of 452 m (see Figure 25). All comparisons of the changed parameters were carried out with the primary model of the line, which is used to determine the fault location in the last SEFL software version.

The influence of such parameters of the line model have been considered:

- Line model type – Frequency Dependent instead of Constant Parameters
- Line and branches length
- Resistivity of wires
- Capacity of the supply substation
- The wave velocity of the zero sequence
- Wave impedance of the positive and zero sequence of wires

Table 15: Comparison table of model parameters influence

#1 Investigated case - **Frequency Dependent line model**
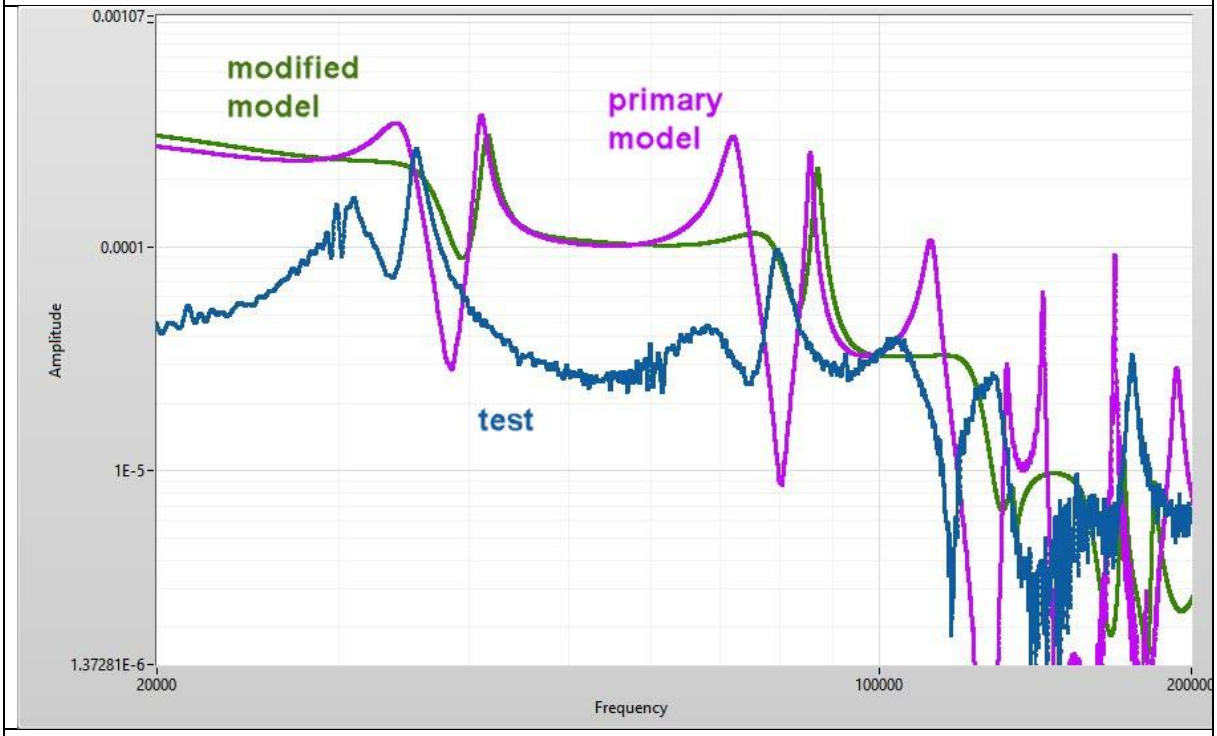
Comment: Frequency peaks are smoothed out, a slight increase in the frequency of the peak of 35 kHz.

#2 Investigated case –**Length of the whole line +10% (+367m)**

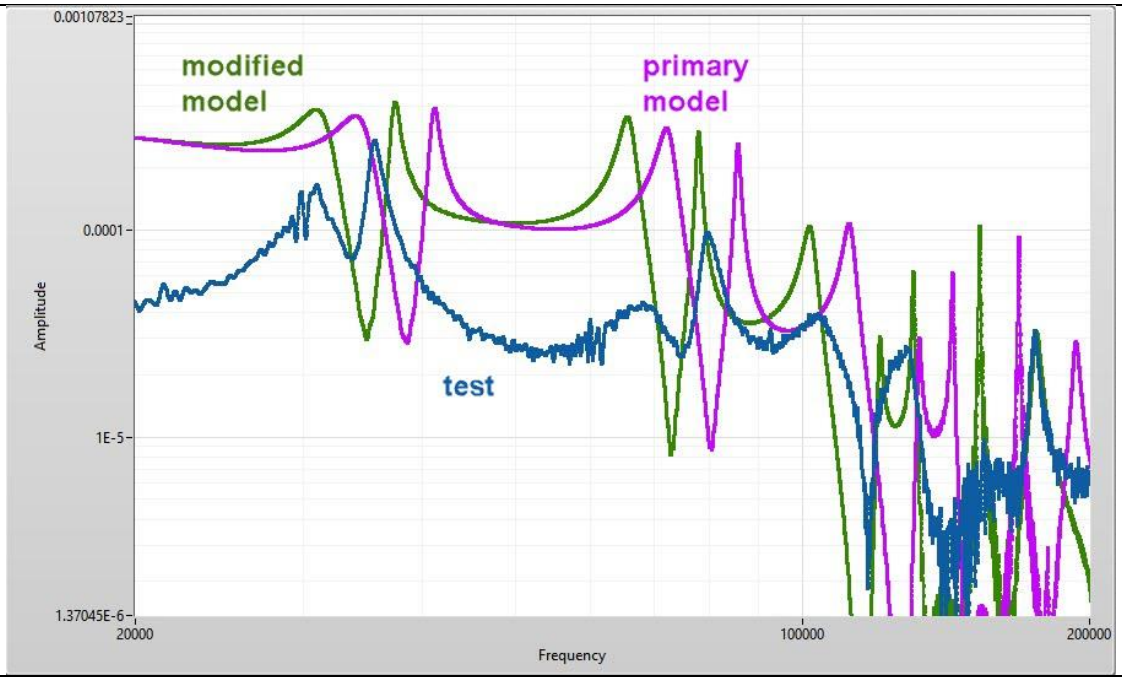

Comment: The increase in the total length of the line leeds to a uniform decrease of all characteristic frequencies, which brings them closer to the required values according to the data from the tests.

#3 Investigated parameter – **Line Resistivity (by 5 times)**

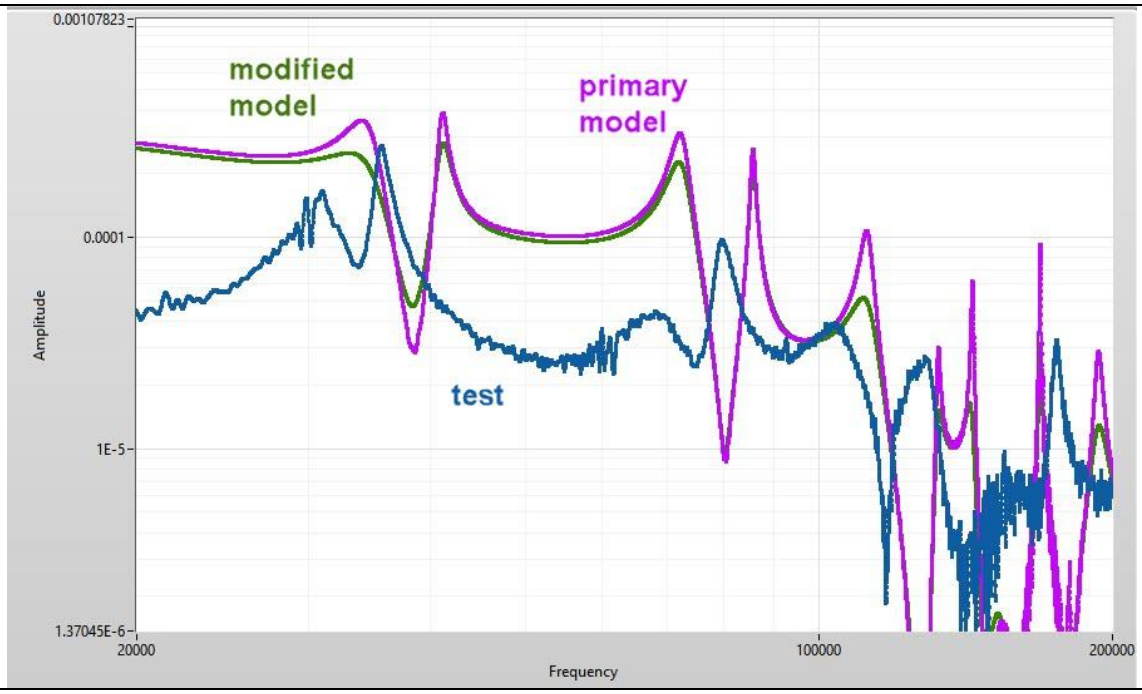

Comment: The characteristic frequencies do not change, they are smoothed out.

#4 Investigated parameter – **Additional capacity at the primary substation (C=1nF)**

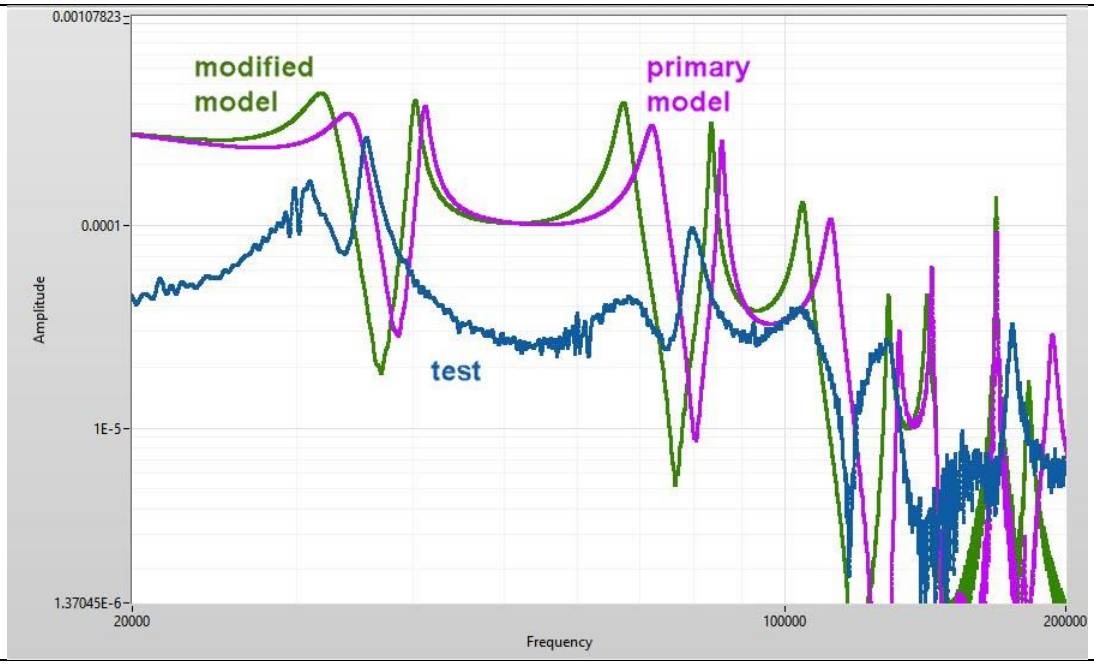

Comment: Adding capacity to a substation uniformly reduces peak frequency values like increasing the length of a line.

#5 Investigated parameter – **Wave velocity of zero sequence voltage (-10%)**

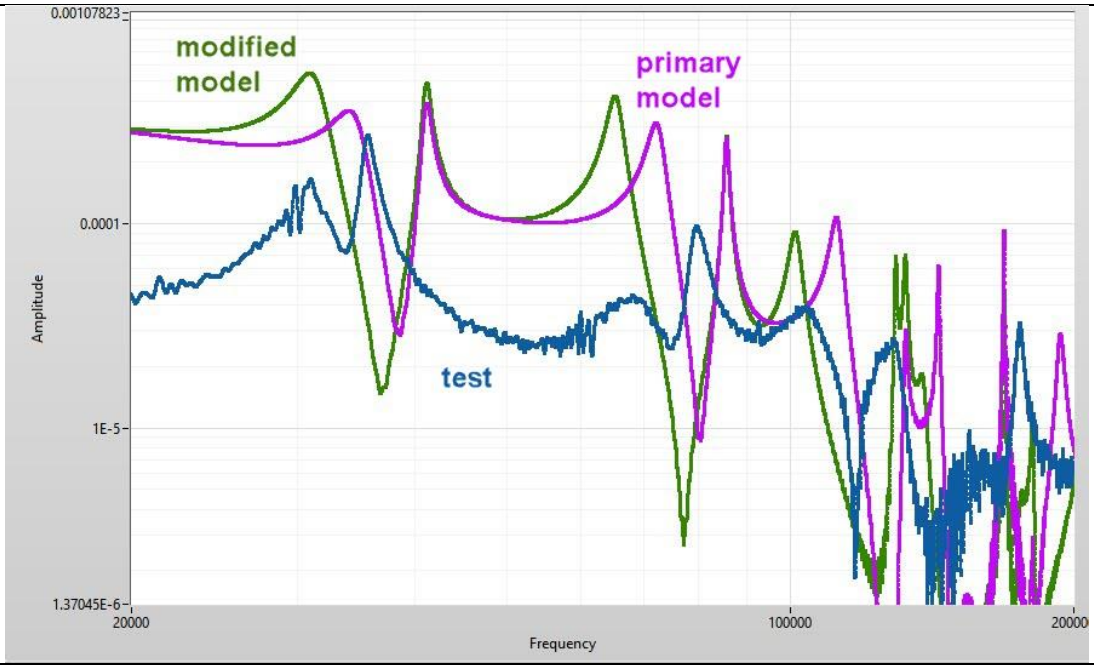

Comment: A decrease in the zero sequence velocity leads to a decrease in only the first characteristic frequency of each pair of peaks. The peak maxima at 30 kHz of the modified model now coincide with the experimental data.

#6 Investigated parameter – **Wave velocity of zero sequence voltage (+10%)**

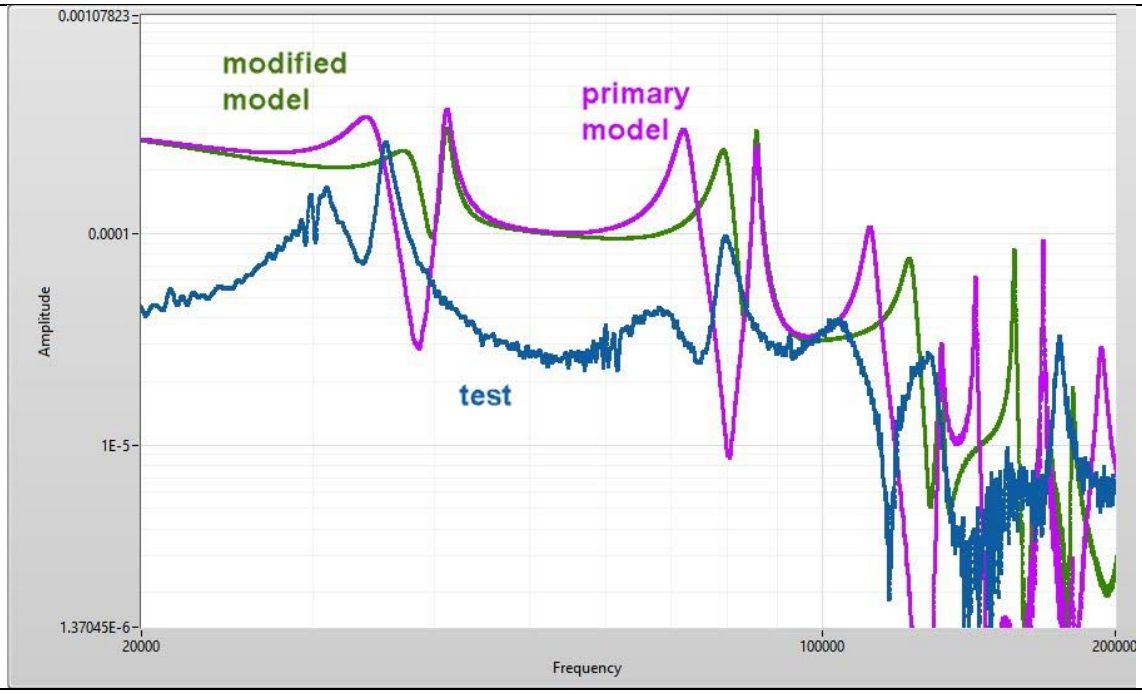

Comment: The reverse situation, the first peak is shifted towards increasing the frequency. The second peak of each frequency pair remains unchanged.

#7 Investigated parameter – **Wave impedance of positive and zero sequence voltage of all wires (+50%)**

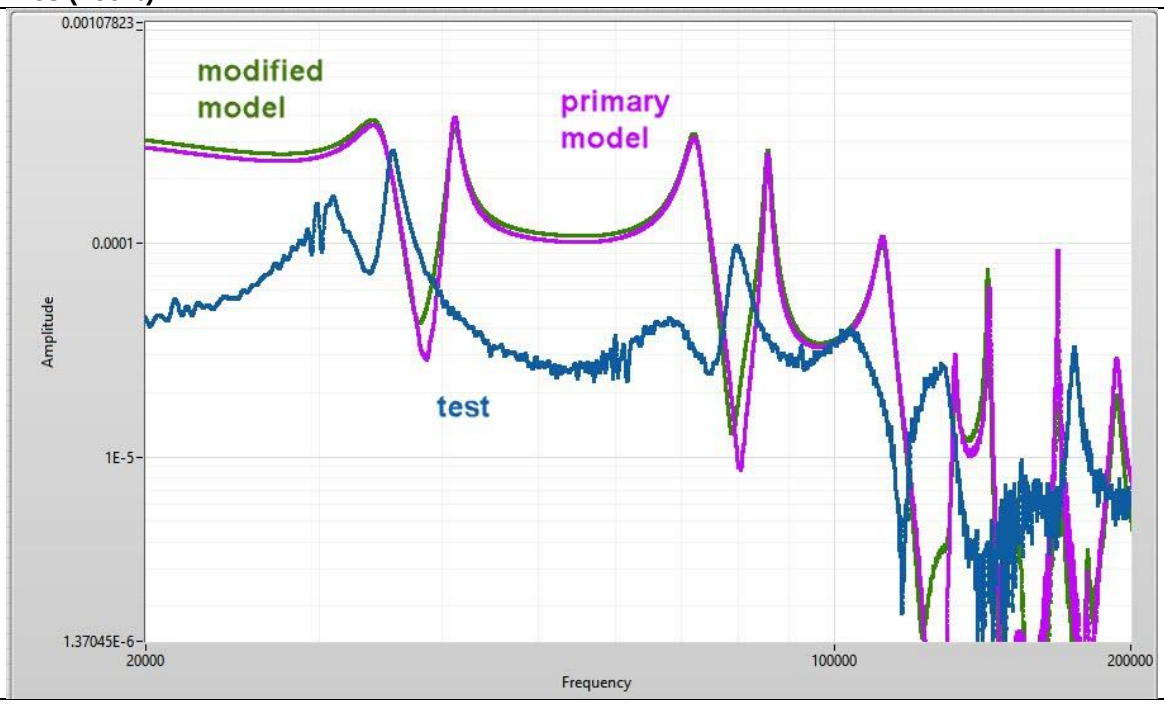

Comment: Modification of all impedances of all types of wires at the same time does not lead to visible changes.

#8 Investigated parameter – **Wave impedance of positive sequence voltage of only 1 wire type (+50%)**

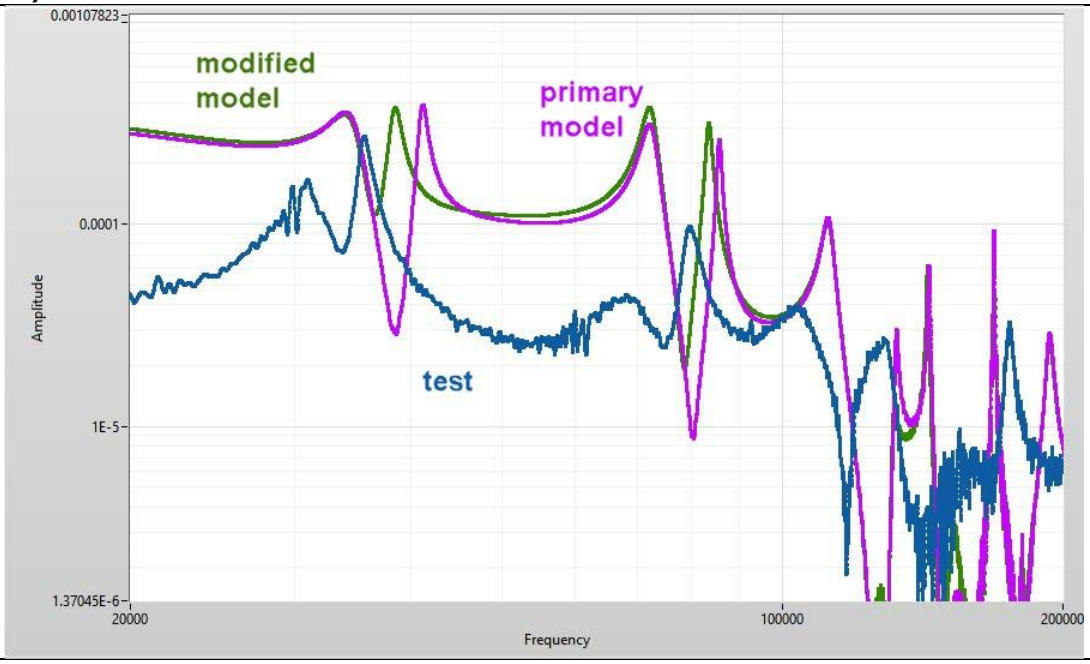

Comment: The initial model contains 3 types of wire of different sizes: wire with a cross section of 35, 50 and 70 mm^2. When changing the wave impedance of the positive sequence of only 70 mm^2 wire (the longest section), there is a decrease in the frequency of every second peak in a pair of characteristic frequencies.

#9 Investigated parameter – **Wave impedance of zero sequence voltage of only 1 wire type (+50%)**

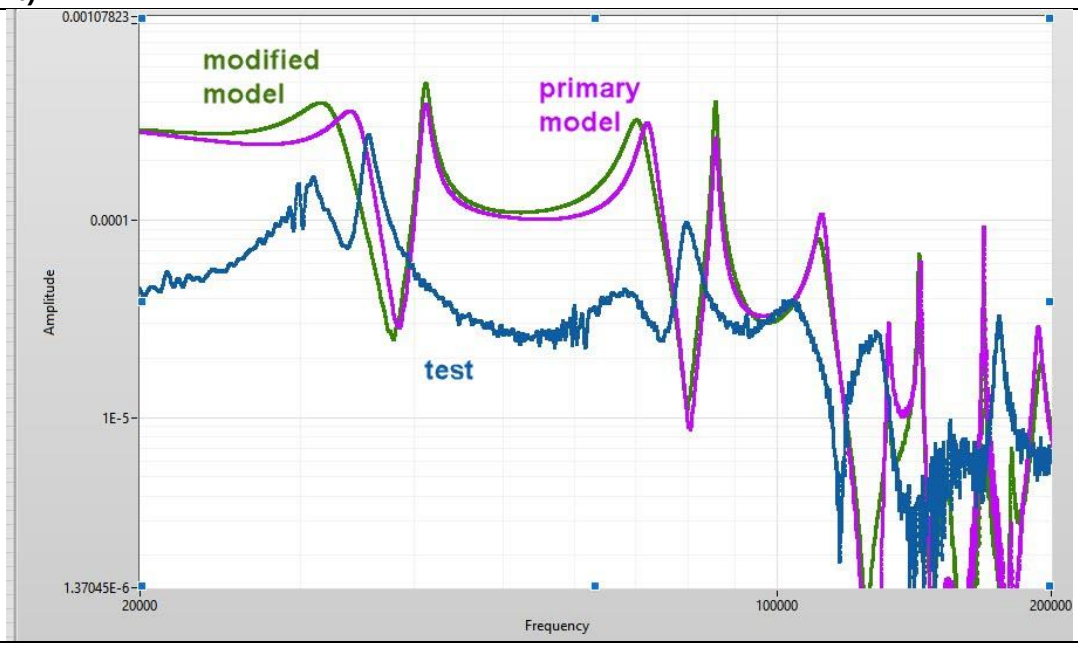

Comment: The situation is similar to the case #8, but the frequency value changes only at the first peak of each pair of characteristic frequencies.

#10 Investigated parameter – **Wave impedance of positive and zero sequence voltage of 1 only wire type (+50%)**

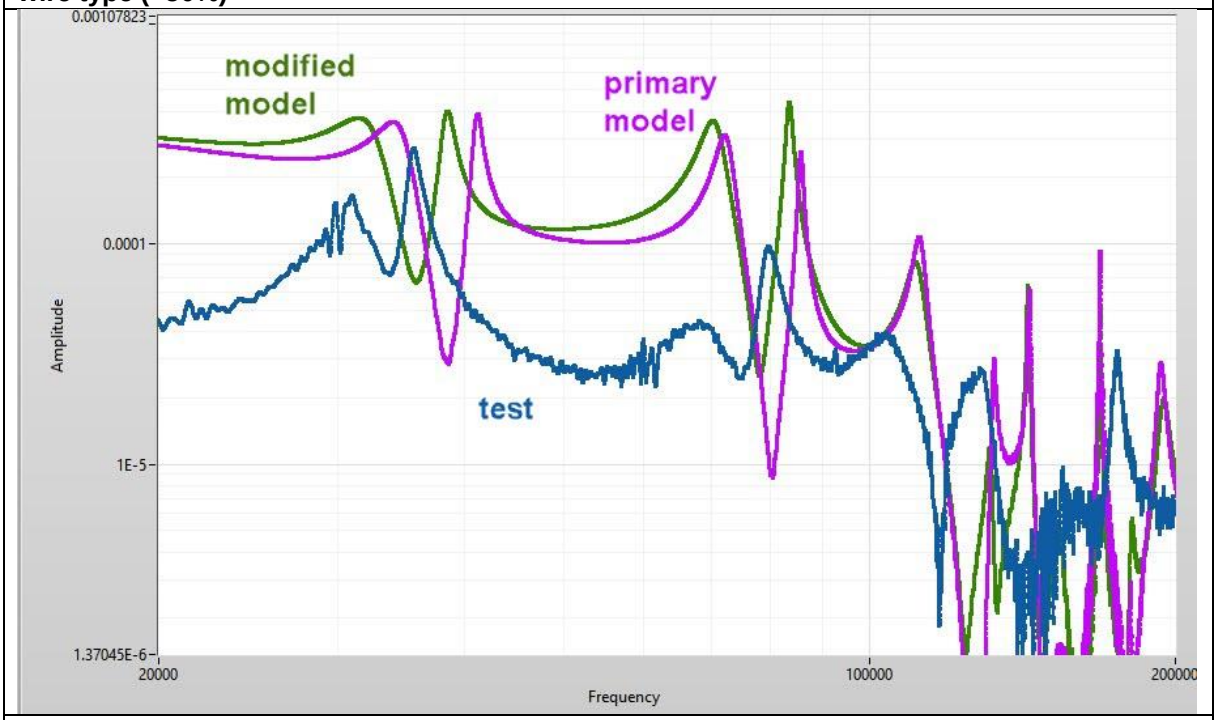

Comment: The total change of both positive and zero sequence wave impedance lead to reducing the value of all characteristic frequencies, especially in the region of about 30 kHz.

A sensitivity analysis with studying how different parameters affect the frequency content showed that such parameters as line length, wave impedance, zero sequence velocity have stronger impact and approximations to experimental data than, for example, changes in resistivity of wires.

The changing of line length, wave impedance, zero sequence has a tendency of the shifting of the main frequency peaks close to the ones from the experiments. As the wave impedance and zero sequence velocity come from such initial data of the network as geometry, height of wires, as well as ground resistivity, their impact indicates about the capacitance in the network. Specifically, the lack of capacitance accelerates the process of wave propagation in the mathematical model. As mentioned in #2 the increase in the total length of the line leeds to a uniform decrease of all characteristic frequencies, which brings them closer to the required values according to the data from the tests.

The investigation #4 showed that the supplementary of lumped capacitance is not enough yet to be close to the reality and the capacitance in the model should be represented as distribution. Cases #7, #8, #9, #10 show the importance of the reflections and refractions in the line between the wires of different types and in the end it impacts the frequency content of the wave. For example, by changing the wave velocity of only type of conductor (#10), the frequencies are able to achieve the reality than the changing the velocity in the whole line, that, obviously, has not led to the changes in the frequencies.

5 Conclusions

Thanks to the SFOE funding, we have made a big step forward in the project. Without this support, we would not have had the possibility to develop SEFL to this point. Thus, for now, the functionality of the software was significantly improved. The software has extended to the version 2.9, which is a more sophisticated software containing many functions, unlike the SEFL v. 1, which, in fact, used to only record and calculate the location of the fault. Now the fault locator is integrated into a modern electrical substation, timely records and classifies events occurring on the line. Important both for the system and the utility, where it is installed – integration of fault location result into their SCADA system as well as receiving the switch status from SCADA for updating the actual network model configuration. The connection to the utility's cloud database containing network parameters has been developed in order to exchange the line data. Furthermore, the system architecture has been changed during the project: two units of the system (acquisition and elaboration units) were split into two different locations and connected through internet.

With reference to the first work package, it should be mentioned the impossibility of proposing an effective strategy for detecting lightning-related events due to the lack of real data, as simulations unfortunately fail to reproduce characteristics similar to real data and therefore cannot be considered completely reliable for our goal. However, thanks to the analysis carried out in the framework of this project and the tools developed, we are confident that a longer monitoring period or an additional installation in a location with a high lightning activity would help in the future with the task completion.

During monitoring phase and pilot tests at different installations, 6 short-circuit faults occurred and recorded by SEFL. The short-circuit methodology has proven to be successful during the years of different installations: 6 short-circuits occurred in the monitoring networks were detected with more precise accuracy, where in 2 cases the fault location error was only 100 m and in 4 cases the error was 200-600 m against 800-4700 m for the conventional method (see Table 10). Now the method is implemented in the fault locator software.

The type of faults that were artificially created on the Groupe E line, i.e. phase-to-ground with small fault current, are identified with unstable accuracy. The fault location results of the pilot tests are presented in Table 9, where two methodologies (constant parameter and frequency parameter models) were applied to the mathematical model that used in the fault location algorithm. From this table it can be followed that the solution of using one methodology for all faults does not work, since in one case it improves the result and make worse in another one. The promising approach to get more stability in the results turned out to be the method of calibrating the mathematical model of the line except the approach of applying CP/FD models. For this realization, tests with voltage pulse injection into the overhead line were done and aimed at calibration and refinement of the mathematical model. It showed wide possibilities of using this method to assess the correspondence of mathematical model of the line to its real form.

Even though the work done on the model has not yet given us a unified strategy for building the model and answering the question of which critical parameter was missing in the model, the data obtained during the pilot tests with the application of a voltage pulse turned out to be very useful. Eventually, we continue to extract data from the tests also for the analysis, which are already outside the scope of the project, however it gives us better understanding of the transient phenomena in the network, specifically, wave attenuation, speed of propagation, frequency content of the signal.

The work carried out during the first year of the project was in line with what planned. The implementation into the LabVIEW software of the waveform classification was done in the end in terms of the software development, as it was more efficient to implement it after the finalization of the data exchange with the SCADA. During the second year of the project, the project manager has left the company that led to the changes on accomplishment of the project. The initial ideas for improving the performance of the EMTR-based algorithm were reconsidered and adapted. Thus, one of the approaches involving the use of artificial intelligence to the problem of fault localization was replaced with the work on the network model

refinement by using a pulse generator on the power line for these purposes. Also, the necessity for further pilot testing has been reconsidered. The first pilot test was done at Groupe E in the beginning of the project, in which we measured and recorded the needed data such as voltage waveforms of the artificial faults created on the line. The change lied in the fact that instead of the performing real faults on the line second time, as was initially applied, we used and processed previously recorded data as fault events and we tested updated SEFL software and subsystems integration.

In more detail, the project has achieved the following results:

1. WP1: The development of an ad-hoc triggering strategy to detect the presence of the fault and its implementation into the SEFL software.
2. WP1: The development of a Matlab tool to analyze the waveforms recorded by the SEFL software, by using several time-domain and frequency-domain features.
3. WP1: The development of a methodology to distinguish faults and disturbances.
4. WP1: The study of a methodology to distinguish faults and lightning-originated event.
5. WP2: The development of the software function devoted to the communication with the SCADA system to integrate the SEFL results of the fault location.
6. WP2: The development of the software function devoted to the communication with the SCADA system to receive the real-time topology of the network.
7. WP3: The development of the function to connect the SEFL to the Groupe E database to automatically input the needed data into the SEFL system.
8. WP4: The development of a methodology and its integration to the software to improve the accuracy of phase-to-phase faults.
9. WP4: The development of an interactive dashboard to analyze the fault location results based on different metrics.
10. WP4: The development of the function to choose the line model with different types of line and cable models.
11. WP5: The installation of the equipment at the substation of Groupe E for the continuous monitoring.
12. WP5: During monitoring phase and pilot test the developed functions, described in WP1÷WP4 were tested and adjusted.

6 Outlook and next steps

During the SFOE project, we have faced the major limitation of fault localization accuracy and relate it, primarily, to the mathematical model of the line, which does not guarantee the stability of fault localization results for each event recorded during the pilot test. The work on the project of fault localization in distributed networks was challenging since the beginning due to a complex topology with numerous branches and small current to ground in case of phase-to-ground faults, as was also described in the Introduction. The work done on the model has not yet led us to an approach that would cover most cases of faults with the accuracy up to ±300 m on different networks with its own characteristics.

Based on current results, the SEFL product is not ready to be commercialized and still requires large investment in order to develop it and solve all issues. Streamer Electric AG might not have to funds to carry one such development. However, the interest from the utility sector and the industry is still there. Groupe E found the technology very innovative and useful. If this would be working flawlessly they would be ready to deploy it on the whole medium voltage network.

The next steps planned to deal with the following tasks:

i) As a sensitivity analysis of line data used in the mathematical model of the line, the study of the influence of the following parameters on the fault location accuracy:

- fault type – single-phase-to-ground fault, short-circuit fault;
- fault resistance;
- ground resistivity;
- remoteness of a fault to the measurement unit;
- pole material;
- pollution and obsolescence of insulation;
- conductor parameters – cross-section, resistance, protective insulation presence;
- geometric parameters of conductors above the ground;
- influence of cable insert and cable parameters – cross-section, resistance, relative permittivity of insulation;
- impact of the equivalent parameters of transformers.

ii) Collaboration with the technical support of EMTP-RV software as experts in power lines transients and developers of the different types line and cable models.

iii) The final fault location accuracy represents the sequence of errors as measurement, transmission, acquisition and line modeling errors. Since a combination of factors can lead to inaccuracies in fault location results, we need to determine what percentage of inaccuracies each factor may contribute. For a more extensive research, two sets of sensors from different manufacturers are ordered. The length of signal cables that transmit the measured voltage to the DAQ will be also tested.

iv) In addition to selecting the measuring unit, it is planned to find an alternative to the DAQ system with the same characteristics and a lower cost. Therefore, the composition of the equipment may change.

7 National and international cooperation

Another installation of SEFL

Additional installation of SEFL system for line monitoring was carried out at the electrical substation of B. Grimm, one of the largest Private Power Producers in Thailand. B. Grimm Power's total installed capacity is currently 3,379 MW. By 2025 the target is to reach 7,200 MW across the ASEAN region.

Fault locator SEFL was installed in a 22 kV electrical substation on 31st December, 2021. The network is operated with solidly grounded neutral system and the substation includes 3 busbars on one of which the high-frequency sensors of the SEFL system are installed. The maximum number of feeders that the system is monitored at the same time is eight The SEFL system monitored a maximum of 8 feeders simultaneously – when all connecting bus ties are closed. However, the most common scheme used at the substation is the one when bus ties disconnected. Therefore, on the average, is the SEFL was monitoring four feeders of 4 km length.

During a year of monitoring, 6 single-phase-to-ground faults were successfully registered. The origins of the faults were predominantly animals, but also short circuits in transformers, partial discharges, tree's branches. Figure 50 shows the waveform of a fault caused by a snake that climbed to a power pole.

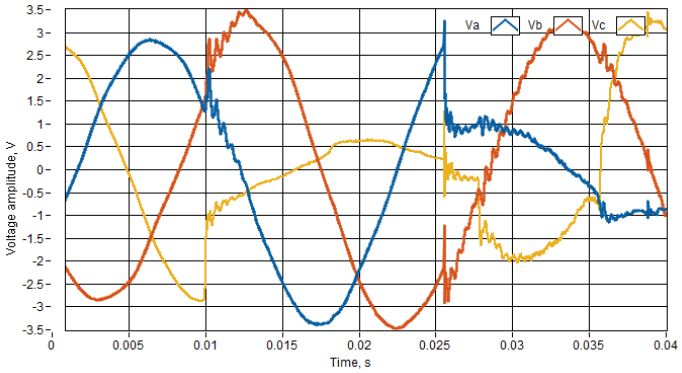

Figure 50: Single-phase-to-ground fault recorded by SEFL

Thanks to the additional installation, we managed to check and adjust functionalities developed in WP1-WP3 functionalities. In the project of B. Grimm, the functionality of the digital inputs monitoring was carried out through RS232 Modbus register interrogation instead of IEC 104 protocol in case of Groupe E. Thus, the operation of the feeder selector was calibrated, digital inputs monitoring and triggering system were successfully tested for the new network. The latter functionality is shown in Figure 51. So, the fault presence on the line was correctly determined, classified and saved to the database.

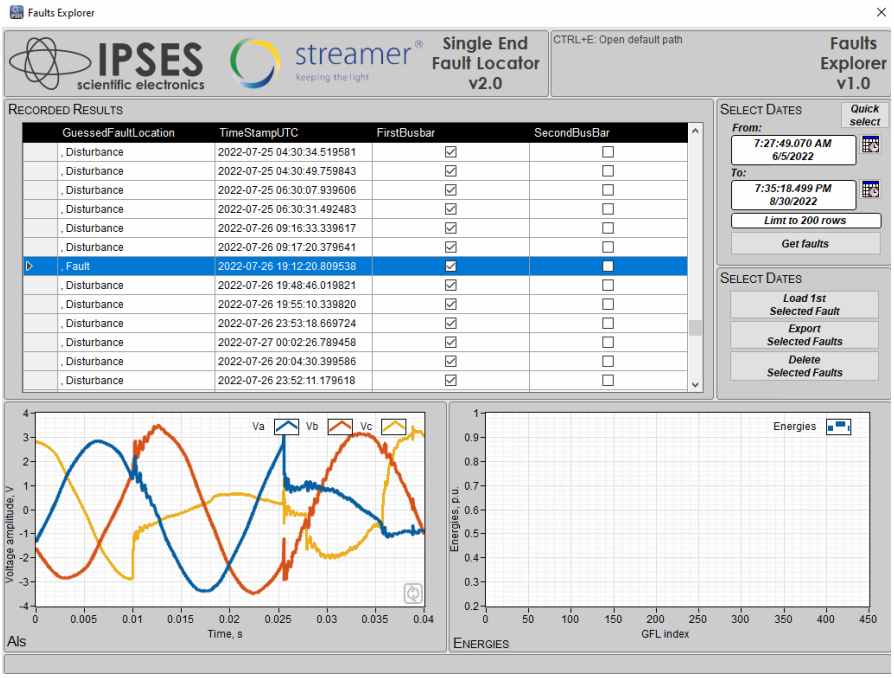

Figure 51: Faults Explorer with the event classification

In 2019, a Single-End Fault Locator (SEFL) CH7000 unit was installed in a 35/10 kV primary substation in Russia. The winter average temperature of the installation area is about -20 degrees Celsius and therefore outdoor equipment was needed. Outdoor sensors were installed at the busbar at the beginning of the line and a computation unit was placed in a climate-controlled server rack (shown in Figure 52).

Figure 52: Outdoor sensors installed at the 35/10 kV primary substation (at the left) and climate-controlled server rack with the computation unit (at the right)

The single-line diagram of the pilot line is shown in Figure 53. The line is composed of four different types of overhead conductors and has three branches departing from the main feeder, for an aggregate length of about 11 km. The grounding system of the network is insulated and, due to the low fault current level for single-line-to-ground faults, the protection strategy does not require the circuit breaker to disconnect the line for single-phase ground faults. The fact that line-to-ground faults are the most common types of faults in MV networks calls for accurate and fast fault locating systems, particularly for ungrounded lines.

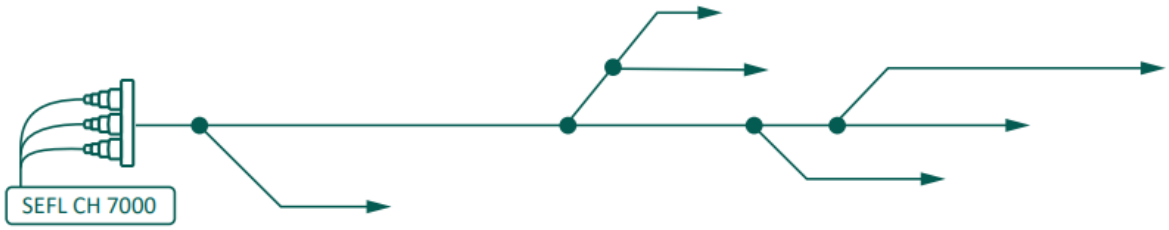

Figure 53: Single-line diagram of the pilot line

During 3.5 years of installation, SEFL helped to localise and indicate the fault location on the line in cases caused by different reasons: damaged insulator on the pole, fallen branch on the line, hurricane, wire fallen on cross-arm. The installation allowed to check how phase-to-phase method works for the real faults happened during the monitoring period. The short-circuit faults were detected with the error of only 100 m (as shown in Table 10).

Testing of SEFL against the state-of-the-art

In order to perform an experimental comparison with the state-of-the-art in terms of performance, the installation of both SEFL and fault indicators (FIs) system at Russian network MRSK Urala was used for analysis.

The parallel monitoring and comparison of the installed products were done during the period from September 2019 to March 2021. From March 2021 until now, the fault indicators are still installed on the line, but technical support for devices is discontinued, therefore the state of FIs can be checked only by visual inspection on site.

After the installation also a pilot test with the creation of artificial faults on the line was carried out. The procedure is identical to the one for the pilot test in Groupe E, described in Section 3.2.10.

One set of fault indication system is composed of 3 fault indicators mounted on overhead conductors and a communication unit mounted on the pole. Communication units are equipped with a solar panel intended to charge the battery inside the unit box. When a fault occurs, indicators switch on a LED light and send the fault signal to the communication unit by radio-frequency connection (TETRA). Communication unit, in its turn, by long range wireless communications transmits the signal to the server with the monitoring software or web-client – the platform that collects the information about all installed fault indicators on the line, such as electrical parameters and event log.

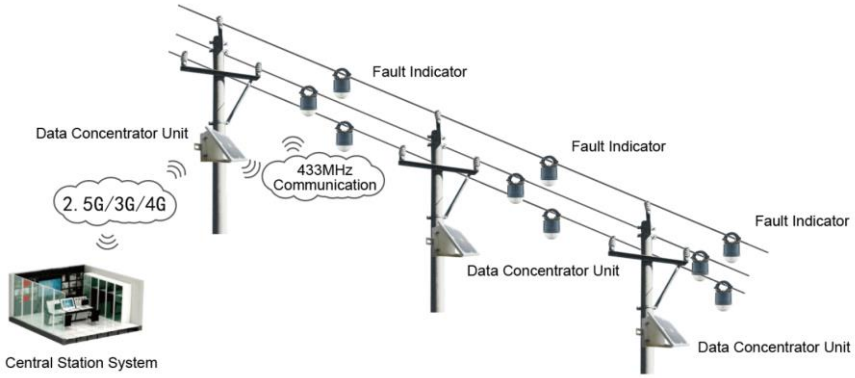

Figure 54: System of fault indicators

Given comparison of the performance was done aiming to check such functionalities as a fault registration for SEFL system and indication presence, as well as sending fault message to the platform (web-client) for fault locators. Table 16 represents the comparison of two systems during pilot test in terms of faults recognition. The comparison in accuracy of fault localization was not performed in this case since the amount of fault indicators mounted on the line does not allow to be objective. To ensure the accuracy of 600 meters, 18 sets of fault indicators would be required. Thus, only 5 sets of fault indicators were mounted on line.

Table 16: the comparison of two location systems performance during the pilot test.

	SEFL		Fault indicators		
	Fault registration	Waveform	Indication	Message to server	Waveform
Phase-to-phase faults	✓	✓	✗	✓	✓
Phase-to-ground faults	✓	✓	✗	✗	6 waveforms of 18 events were recorded

Table 17 reports the criteria that can help in evaluation of the performances of the two technologies. Based on it we followed that the installation and maintenance of SEFL is easier, as the maintenance crew does not need to mount the devices along the live line. The mounting of SEFL sensors is done once, in one location at a primary substation. Due to the advantage of one device in SEFL system, the equipment configuration is also faster. Possible maintenance is needed in one place, instead of the whole line and require less operating staff, as well as number of hours. The power supply of the communication unit for FIs is carried out from batteries or by recharging it from a solar battery, which is inefficient in a number of regions, while SEFL is powered by 220 V at the substation.

Table 17: Criteria to evaluate the performance of Fault indicators versus SEFL

	SEFL		Fault indicators (5 sets)	
	Configuration and mounting	Maintenance	Configuration and mounting	Maintenance
Time spent	8 hours	20 hours	8 hours	30 hours
Convenience and security*	- additional voltage transformers must be installed on the busbar - line should be discharged for the time of transformers installation (2 hours)		- multiple usage of mounting crane or climbing gaffs - live-line maintenance - communication for each set must be configured singly - configuration takes a lot of time	- the solar panel did not charge the battery in the communication unit that led to manual charge - in case of issues with indicator, disassembly and reassembly is necessary - subscriber service of SIM-cards
Required number of people of the operating staff	4 people	1 person	4 people	3 people

*the disadvantages of convenience and security are described in the table.

After testing in the laboratory and 6 months of monitoring the following issues in different areas such as fault localization, connection, data transferring and the user interface operation were registered with the fault indicators:

- phase-to-ground faults have been detected unsatisfactorily during the pilot test and the monitoring phase. The indicators were updated by the supplier and new sets, as well as 2 more, were installed on the overhead line;
- problems with battery charging. Some sets are not able to be charged from the power line as it is supposed to be;
- platform with the web-client is not always available;

- doubling of fault location messages at the platform with the same time stamp, but different values of electrical parameters;
- translation failures in the platform;
- sometimes there is no record in the event log when there is an alarm;
- system errors when configuring indicators by the configuration tool;
- difficulties with opening and uploading waveforms at the platform;
- connection between the web-client and the indicators can be lost;
- constant firmware update is required.

The testing of FIs on site were performed, in the first place, because of checking the feasibility of adding FIs to the product line of Streamer and further commercial usage. 2 years of installation has not shown any improvements and adjustments from the supplier in terms of technical issues of both hardware and software parts, as well as detection and therefore localization of phase-to-ground faults in the networks with insulated grounding system, i.e. the main goal of indicators testing, has not met the expectations. As the time spent on the project of FI system has not led to a visible and stable progress, it was decided to close the project and thereby stop the technical support of the product, although the indicators remained on the line for a possible visual indication of a fault.

It is important to note that this test has been done with a single brand of Fault Indicators and we cannot therefore draw a conclusion on the efficiency of this solution in general. However, there are multiple factors common to all manufacturers of FIs that lead to a more complex installation and heavier maintenance than for a SEFL installation: battery supply of indicators and communication box, management of modem with SIM card for each communication box, dependency of communication network availability.

8 Publications

1. R. Razzaghi, G. Lugrin, H. Manesh, C. Romero, M. Paolone, and F. Rachidi, “An efficient method based on the electromagnetic time reversal to locate faults in power networks,” IEEE Transactions on Power Delivery, vol. 28, pp. 1663–1673, July 2013.
2. F. Rachidi and M. Rubinsein, “Time reversal of electromagnetic fields and its application to lightning location,” in Proc. Int. Symp. Lightning Protection, Oct. 2013, pp. 378–383.
3. A. Codino, Z. Wang, R. Razzaghi, M. Paolone, F. Rachidi, “An Alternative Method for Locating Faults in Transmission Line Networks Based on Time Reversal”, Sept. 2017

9 References

[1] M. M. Saha, J. J. Izykowski, and E. Rosolowski, Fault location on power networks. Springer Science & Business Media, 2009.

[2] M. Saha, K. Wikström, J. Izykowski, and E. Rosolowski, “Fault location techniques,” Department of Electrical Engineering Wroclaw, Poland & Department TTD ABB Automation Products AB SE-721 59 Vasteras, Sweden, 2006.

[3] M. Sant and Y. Paithankar, “Online digital fault locator for overhead transmission line,” in Proceedings of the Institution of Electrical Engineers, vol. 126, pp. 1181–1185, IET, 1979.

[4] L. J. Lewis, “Traveling wave relations applicable to power-system fault locators” Transactions of the American Institute of Electrical Engineers, vol. 70, no. 2, pp. 1671–1680, 1951.

[5] R. Razzaghi, G. Lugrin, H. Manesh, C. Romero, M. Paolone, and F. Rachidi, “An efficient method based on the electromagnetic time reversal to locate faults in power networks,” IEEE Transactions on Power Delivery, vol. 28, pp. 1663–1673, July 2013.

[6] N. Mora, F. Vega, G. Lugrin, F. Rachidi, and M. Rubinstein, “Study and classification of potential IEMI sources”, SDAN, vol. 41, 2014.

[7] N. Mora, B. Daout, M. Nyffeler, C. Romero and F. Rachidi, "Revisiting the Calculation of the Early Time HEMP Conducted Environment", IEEE Transactions on Electromagnetic Compatibility, vol. 63, no. 1, pp. 111-124, 2021.

[8] E. de Raemy, and J. Dutoit, “Réduction des interruptions de fourniture grâce au disjoncteur shunt, ” Bulletin.ch, 2009.

[9] C.A. Nucci, "Lightning-induced voltages on overhead power lines. Part II: Coupling models for the evaluation of the induced voltages", Electra, vol. 162, pp.120-145, 1995

[10] S. He et al., “Norm Criteria in the Electromagnetic Time Reversal Technique for Fault Location in Transmission Lines,” IEEE Trans. Electromagn. Compat., vol. 60, no. 5, pp. 1240–1248, Oct. 2018.

[11] S. He, A. Cozza, and Y. Xie, “Electromagnetic Time Reversal as a Correlation Estimator: Improved Metrics and Design Criteria for Fault Location in Power Grids,” IEEE Trans. Electromagn. Compat., vol. 62, no. 2, pp. 598–611, Jun. 2020.

[12] Z. Wang, R. Razzaghi, M. Paolone, and F. Rachidi, “Electromagnetic Time Reversal Applied to Fault Location: On the Properties of Back-Injected Signals,” 2018.

[13] Z. Wang, R. Razzaghi, M. Paolone, and F. Rachidi, “Electromagnetic Time Reversal Similarity Characteristics and Its Application to Locating Faults in Power Networks,” IEEE Trans. Power Deliv., vol. 35, no. 4, pp. 1735–1748, Aug. 2020.

[14] X. Zhang, N. Tai, P. Wu, C. Fan, X. Zheng, and W. Huang, “A New Theory for Locating Line Fault in Power System: Theoretical Part,” IEEE Access, vol. 7, pp. 91337–91346, Jul. 2019.

[15] D. Liu, S. Vasudevan, J. Krolik, G. Bal, and L. Carin, “Electromagnetic Time-Reversal Source Localization in Changing Media: Experiment and Analysis,” IEEE Trans. Antennas Propag., vol. 55, no. 2, pp. 344–354, Feb. 2007.

[16] A. Codino, Z. Wang, R. Razzaghi, M. Paolone, and F. Rachidi, “An Alternative Method for Locating Faults in Transmission Line Networks Based on Time Reversal,” IEEE Trans. Electromagn. Compat., vol. 59, no. 5, pp. 1601–1612, Mar. 2017.

[17] Z. Wang, A. Codino, R. Razzaghi, M. Paolone, and F. Rachidi, “Using Electromagnetic Time Reversal to Locate Faults in Transmission Lines: Definition and Application of the ‘Mirrored Minimum Energy’ Property,” 2017.

Acknowledgements

The completion of this project could not have been possible without the participation and assistance of a lot of individuals contributing to this project. However, we would like to express our deep appreciation and indebtedness to Prof. Farhad Rachidi, as an ideological inspirer, the project has got the opportunity to develop the product based on the innovative method for locating faults in power networks. Dr. Asia Codino, project leader and the main engine of the practical implementation of the fault location system. With the departure of Dr. Codino, during the second year of the project, a significant reorganization of the structure of the project management has been made. Thus, the responsibilities have been divided between Ms. Polina Gonina, Mr. Jean-Baptiste Frain and Mr. Matthieu Zinck. Also, thanks to Mr. Jonathan Zahnbrecher and Mr. Dmitriy Belko the project has been taken up and got new ways of the development.

We would like to extend our sincere thanks to our industrial partner Groupe E, namely Mr. Yves Fritsché, Mr. Richoz Frédéric and Mr. Romain Haas, which provided a platform for practical testing of the system.

In general, the project had to be reorganized into several work packages which led to an increase in cost, this additional costs have been taken in charge by Streamer Electric AG.